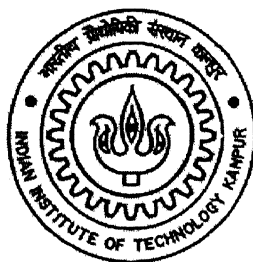


SUPPRESSION OF FLOW-INDUCED INTERFACIAL INSTABILITIES BY SOFT SOLID LAYER COATINGS

A Thesis Submitted
In Partial Fulfillment of the Requirements
for the Degree of
Master of Technology

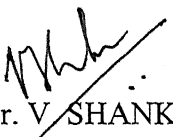
by
Akhilesh Kumar Sahu



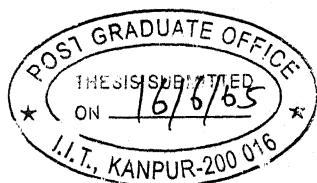
to the
DEPARTMENT OF CHEMICAL ENGINEERING
INDIAN INSTITUTE OF TECHNOLOGY KANPUR
INDIA
June 2005

CERTIFICATE

This is to certify that the present work contained in the thesis entitled "**Suppression of Flow-Induced Interfacial Instabilities by Soft Solid Layer Coatings**" has been carried out by Mr. Akhilesh Kumar Sahu under my supervision and that this has not been submitted elsewhere for a degree.


Dr. V. SHANKAR
Assistant Professor,
Department of Chemical Engineering,
Indian Institute of Technology,
Kanpur- 208016.

June'05



8 J111 2005/CHE
पुस्तक
भारतीय ... संस्थान ...
पुस्तक क्र० A 151945

TH
CHE/2005/M
Sa 198



A151945

ACKNOWLEDGEMENT

At the very beginning I would like to thank the authority of IIT Kanpur for providing high-class facilities and the ambience necessary to carry out research work. During the research work, my thesis guide Dr. V. Shankar has helped me immensely with his ingenious ideas and valuable guidance. I am highly grateful to him for motivating and encouraging me during all the stages of my thesis work. By working under his guidance I have come to know the intricate details of research work. It was my privilege to have worked under him.

I shall always cherish the sweet memories attached with my lab mates Gaurav, Pavan, Janakiram, Sameer and Lalit. They have always helped to maintain a friendly atmosphere in our lab. More than this, they have always been a constant source of inspiration.

The time spent with Parimal, Manoj, Satyam, Ravi, Seenu, Abhijit, Alok and Saurabh has been a major recreation for me. The memories associated with them will surely be cherished forever. They were always there to give me moral support in every situation in my life here.

At the end I would like to convey my regards to my parents and all other family members for their endless love, encouragement and endurance during my stay at IIT Kanpur. Their silent presence behind my all achievements cannot be properly expressed.

Finally, I am grateful to the almighty for what I am today.

Akhilesh Kumar Sahu

Abstract

The stability of a single layer Newtonian fluid flow down an inclined plane lined with soft solid layer and pressure-driven two-layer plane Poiseuille flow through a channel lined with soft solid layers are studied. The flow down an inclined plane system consists of a Newtonian fluid of density ρ , viscosity μ and thickness R flowing adjacent to a soft solid layer of density ρ , modulus of elasticity E , viscosity μ_g and thickness HR which is fixed onto a inclined rigid plane having inclination angle of θ . The linearized Navier-Stokes equations for the fluid and the elasticity equations for the soft solid layer are solved numerically, and the characteristic equation is obtained using the boundary conditions. The characteristic equation for the growth rate is a nonlinear equation, so analytical solutions cannot be obtained in general. Numerical solutions are obtained by a procedure using the solution from low wavenumber asymptotic analysis as the starting guess. It is found that soft solid layer has a stabilizing effect when the liquid flow down an inclined rigid plane exhibits instability. The stabilization is strongly affected by the nondimensional elasticity parameter $\Gamma = \frac{\mu v_a}{ER}$, the nondimensional solid layer thickness

H , the ratio of viscosities $\eta_r = \frac{\mu_g}{\mu}$ and wavenumber k .

The two-layer flow system consists of two layers of linear viscoelastic solid of thickness H_1R and H_2R , shear modulus E_1 and E_2 , and viscosity μ_{g1} and μ_{g2} fixed onto rigid surfaces at $z = -H_1R$ and $z = (1+H_2)R$ respectively, a layer of Newtonian fluid (fluid B) of thickness βR in the region $0 < z < \beta R$ with viscosity μ_b , and another

Newtonian fluid (fluid A) of thickness $(1-\beta)R$ in the region $\beta R < z < R$ with viscosity μ_a . Similar to the previous analysis in this case also the Navier Stokes equations for the fluid layers and the elasticity equations for the solid layers are solved numerically, and the characteristic equation for each layer is obtained using the boundary conditions. The existence of interfacial instability in two-layer flow through rigid channel depends on viscosity ratio μ_r and thickness ratio β of fluid layers. Asymptotic results predict the soft solid layer has a stabilizing effect on the interfacial instability between two Newtonian fluids. Asymptotic results are valid only in the low wavenumber limit; we use a numerical procedure to continue the results to finite wavenumber. Numerical results reveal that two fluid interface can be completely stabilized by choosing appropriate values of parameter $\Gamma_\varphi = \frac{\nu_c \mu_b}{E_\varphi R}$, solid layer thickness H_φ , viscosities of solid layers η_r^φ and interfacial tension between two-fluids Σ ($\varphi = 1$ and 2 are indices for solid layers).

Contents

Abstract	i
List of Figures	iv
List of Tables	viii
Nomenclature	ix
1 Introduction	1
2 Stability of Liquid Flow down an Inclined Plane Lined with Soft Solid Layer	7
2.1 Problem Formulation	8
2.1.1 Dimensional Governing Equation	8
2.1.2 Base state	10
2.1.3 Nondimensional Governing Equation	11
2.1.4 Linear Stability Analysis	12
2.2 Numerical Method	16
2.3 Results and Discussion	18
2.4 Conclusion	24
3 Stability of Pressure-Driven Two-Layer Plane Poiseuille Flow in a Channel Lined with Soft Solid Layer	37
3.1 Problem Formulation	38
3.1.1 Dimensional Governing Equation	38
3.1.2 Nondimensional Governing Equation	40
3.1.3 Base State	43
3.1.4 Linear Stability Analysis	43
3.2 Asymptotic Results	47
3.3 Numerical Method	50
3.4 Results and Discussion	53
3.5 Conclusion	57
4 Conclusion and Scope for Future Work	82
References	84

List of Figures

Figure 2.1: Schematic diagram of liquid flow down an inclined plane coated by soft solid layer.....	25
Figure 2.2: Instability in flow down an inclined rigid plane: variation of c_i with k for $\theta = 45^\circ$ and $\Sigma = 0$	26
Figure 2.3: Instability in flow down a vertical rigid plane: variation of c_i with k for $\theta = 90^\circ$, $\Sigma = 0$ and $\Gamma = 0$	26
Figure 2.4: Instability in flow down a inclined rigid plane: effect of surface tension on c_i vs k	27
Figure 2.5: Instability in liquid flow down vertical plane lined by soft solid layer: variation of c_i with k for $H = 2, Re = 0.1, \theta = 90^\circ, \eta_r = 0$ and $\Sigma = 0$	28
Figure 2.6: Instability in liquid flow down an inclined plane lined by soft solid layer: variation of c_i with k for $H = 0.8(<1), Re = 1, \theta = 45^\circ, \eta_r = 0$ and $\Sigma = 0$	29
Figure 2.7: Effect of solid layer deformability: c_i vs k for $H = 2, Re = 1, \theta = 45^\circ, \eta_r = 0$ and $\Sigma = 0$	30
Figure 2.8: Effect of solid layer deformability: c_i vs k for $H = 2, Re = 5, \theta = 45^\circ, \eta_r = 0$ and $\Sigma = 0$	31
Figure 2.9: Effect of Reynolds number on c_i vs k for $H = 2, \Gamma = 0.1, \eta_r = 0, \Sigma = 0$ and $\theta = 45^\circ$	32

Figure 2.11: Neutral stability curves: Γ vs k for $H=2, Re=1, \eta_r=0, \Sigma=0$ and $\theta=45^\circ$	33
Figure 2.12: Neutral stability curves: Γ vs k for $H=2, Re=1, \eta_r=0.5, \Sigma=0$ and $\theta=45^\circ$	33
Figure 2.13: Neutral stability curves: Γ vs k for $H=2, Re=3, \eta_r=0, \Sigma=0$ and $\theta=45^\circ$	34
Figure 2.14: Neutral stability curves: Γ vs k for $H=2, Re=1, \eta_r=0$ and $\theta=45^\circ$	34
Figure 2.15: Neutral stability curves: Γ vs k for $H=3, Re=1, \eta_r=0, \Sigma=0$ and $\theta=45^\circ$	35
Figure 2.16: Effect of viscosity of soft solid layer on Γ vs k for $Re=1, \theta=45^\circ, \Sigma=0$ and $H=3$	35
Figure 2.17: Effect of thickness of soft solid layer on Γ vs k for $Re=1, \theta=45^\circ, \eta_r=0$ and $\Sigma=0$	36
Figure 3.1: Schematic diagram of two-layer plane Poiseuille flow in a channel lined with soft solid layers.	68
Figure 3.2: Neutral stability diagram for two-layer Plane Couette flow for long-wavelength disturbances.....	69
Figure 3.3: Neutral stability diagram for two-layer Plane Poiseuille flow for long-wavelength disturbances.....	69

Figure 3.4: Interfacial instability in the rigid channels: variation of imaginary part of wavespeed c with wavenumber k for two-layer Plane Poiseuille flow in rigid channels ($\Gamma_1 = 0$ and $\Gamma_2 = 0$).	70
Figure 3.5: Effect of solid layer deformability on fluid-fluid interfacial mode: variation of c_i with k for different values of thickness H_1 when the solid layer is placed only at bottom plate.	71
Figure 3.6: Effect of solid layer deformability on fluid-fluid interfacial mode: variation of c_i with k for different values of thickness H_2 when the solid layer is placed only at top plate.	72
Figure 3.7: Effect of solid layer deformability on fluid-fluid interfacial mode: variation of c_i with k for different values of parameter Γ_1 when the solid layer is placed only at bottom plate.	73
Figure 3.8: Effect of solid layer deformability on fluid-fluid interfacial mode: variation of c_i with k for different values of thickness Γ_2 when the solid layer is placed only at top plate.	74
Figure 3.9: Effect of solid layer deformability on fluid-fluid interfacial mode: variation of c_i with k when the solid layer is placed at both plates.	75
Figure 3.10: Effect of interfacial tension when solid layers are placed on both the plates.	76
Figure 3.11: Effect of Reynolds number when solid layers are placed on both the plates.	77

Figure 3.12: Effect of viscosity of solid layers when solid layers are placed on both the plates.....	78
Figure 3.13: Neutral stability curves for fluid-fluid interfacial mode: variation of Γ with k	79
Figure 3.14: Effect of interfacial tension on neutral stability curves for fluid-fluid interfacial mode: variation of Γ with k	80
Figure 3.15: Effect of Reynolds number on neutral stability curves for fluid-fluid interfacial mode: variation of Γ with k	81

List of Tables

TABLE 3.1: Summary of results from low wavenumber analysis when solid layer is placed only at bottom plate for $\mu_r = 2.0$	60
TABLE 3.2: Summary of results from low wavenumber analysis when solid layer is placed only at top plate for $\mu_r = 2.0$	61
TABLE 3.3: Summary of results from low wavenumber analysis when solid layer is placed only at bottom plate for $\mu_r = 0.25$	62
TABLE 3.4: Summary of results from low wavenumber analysis when solid layer is placed only at top plate for $\mu_r = 0.25$	63
TABLE 3.5: Summary of results from low wavenumber analysis when solid layer is placed only at bottom plate for $\mu_r = 4.0$	64
TABLE 3.6: Summary of results from low wavenumber analysis when solid layer is placed only at top plate for $\mu_r = 4.0$	65
TABLE 3.7: Summary of results from low wavenumber analysis when solid layer is placed only at bottom plate for $\mu_r = 0.5$	66
TABLE 3.8: Summary of results from low wavenumber analysis when solid layer is placed only at top plate for $\mu_r = 0.5$	67

Nomenclature

General

c	Complex wavespeed, $c_r + i c_i$
v_i	Velocity field in fluid
u_i	Displacement field in soft solid layer
T_{ij}	Total stress field in fluid
Π_{ij}	Total stress field in soft solid layer
p_f	Pressure field in fluid
p_g	Pressure field in soft solid layer
k	Wavenumber
G	Pressure gradient in fluid
E	Shear modulus of the soft solid layer
H	Nondimensional thickness of the soft solid layer
R	Dimensional thickness of fluid
Re	Reynolds number, $\frac{\rho v R}{\mu}$

Greek Symbols

β	Ratio of thickness of fluid layers
γ	Dimensional interfacial tension
Γ	Nondimensional elasticity parameter of soft solid layer, $\frac{v\mu}{E R}$

η_r	Ratio of soft solid layer to fluid viscosity, $\frac{\mu_g}{\mu}$
μ_r	Ratio of viscosities of fluid layers
Σ	Nondimensional interface tension between two fluids, $\gamma/(\mu v)$
θ	Angle of inclination
τ_{ij}	Deviatoric stress tensor in fluid
σ_{ij}	Deviatoric stress tensor in soft solid layer

Chapter 1

Introduction

Fluid flow adjacent to a flexible surface is often encountered in biological systems and biotechnological processes. The flow of blood and other biological fluids in the body takes place through tubes whose walls are made of elastic materials such as tissues and membrane, and more recently, in microfluidic devices where soft elastomers are used in the fabrication of microchannels. A clear understanding of fluid flow past soft solid surfaces, and the way in which the solid interacts with the flow, will help in the accurate design and development of these applications. Such flows are also encountered in industrial applications which often involve fluid flow near polymer matrices or membranes. Recent experimental and theoretical studies indicate that the characteristics of the fluid flow in these systems could be very different from that in a rigid-walled channel due to the effect of the elasticity of the wall. In particular, the transition from laminar to turbulent flow in a flexible walled channel is qualitatively different from that in a rigid channel. A good understanding of the transition from laminar to turbulent flow in flexible channels could be important in technological applications because laminar and turbulent flows have very different transport coefficients. In applications where high heat or mass transfer rates are desired, it would be necessary to operate the system in the turbulent regime where the transfer rates are three to four orders of magnitude greater than that in the laminar regime. In processes where low drag forces are desirable the system could be operated in the laminar regime. The dynamics of fluid flow past soft

solids is very different from that of flow past rigid surfaces due to the deformability of the solid surface, which couples the dynamics of the fluid with the deformation of the solid. In particular, this coupling could lead to interfacial instabilities between the fluid and the solid, as first theoretically predicted by Kumaran *et al.* [5] and experimentally demonstrated by Kumaran and Muralikrishnan [6,9]. An interesting feature concerning these instabilities is that they can occur even in the creeping flow limit, in the absence of fluid and solid inertia.

The problem of maintaining stable interfaces in two-fluid viscous flows is of considerable interest to many modern engineering flow processes. Interface stability is of critical importance in coextrusion processes in the plastics industry where multilayer flows are relevant. The coextrusion operation consists of combining several melt streams in a feedblock. The combined melt stream then flows to the die where the layers take their final dimensions. Under certain operating conditions, interfacial instabilities arise with detrimental effects on mechanical, optical, and barrier properties of the final product. Efficient and robust control of the flow and suppression of instabilities is then of paramount importance in maintaining stable operating states.

In the petroleum industry, for example, pumping costs in pipeline operations may be reduced considerably by adding a low viscosity fluid into the system. Experimental investigations of two-fluid pipe flow indicate that low viscosity fluids eventually encapsulate the more viscous fluids in both high and low Reynolds number flows [4]. Interfacial instabilities in two-layer shear flows have been investigated by various authors. In his pioneering work, Yih [17] studied the stability of the interface using a long-wave asymptotic technique and showed that viscosity stratification alone can cause

instability even at vanishingly small Reynolds numbers. Subsequent to the study of Yih, a large number of studies (for an extensive review, see Joseph and Renardy [4]) have focused on the theoretical understanding of interfacial instabilities in two-layer and multilayer flows of Newtonian and viscoelastic fluids.

Free surface flow of fluids is of great importance in many industrial applications where solids are coated with polymeric films. For example, in slide coating operations the flow of liquid flow down an inclined plane is a fundamental step in production of multilayer products [2]. It is well-known that the rectilinear flow of multiple fluid layers down an inclined plane can be unstable. The predominant application of the inclined plane flow geometry is in the manufacture of multilayer products such as photographic films, where the inclined plane provides a means by which individual fluid layers can be stacked on top of one another. At the end of the plane, these layers are then deposited simultaneously on a moving substrate [15].

In the present work, we consider gravity flow of a single layer Newtonian fluid down an inclined plane (shown in Fig 2.1) and pressure-driven two-layer plane Poiseuille Newtonian flow (shown in Fig 3.1).

Linear stability of two superposed fluids in plane Poiseuille and Couette flow was first studied theoretically by Yih [17], who presented an analysis for two-dimensional, long-wavelength perturbations. Yih [17] derived a general expression for the complex wavespeed and showed that viscosity stratification can give rise to an interfacial mode depends on the geometric and physical parameters of the flow systems, notably the viscosity ratio μ_r and thickness ratio β of fluid layers. In the analysis for two-layer Couette flow Yih [17] showed that even in the presence of a vanishingly small Reynolds

number, the interface becomes unstable in the long-wave limit due to viscosity stratification when the thickness of the more viscous fluid is smaller than the thickness of the less viscous fluid. The interface is stable when the thickness of the more viscous fluid is larger than that of the less viscous fluid. In the analysis for Poiseuille flow, Yih [17] did not discuss explicitly how the growth rate depends on the parameters β and μ_r , and gave the numerical results only for the case fluids having same density and $\beta = 0.5$, thereby demonstrating effect of viscosity stratification alone is sufficient to cause instability. Yiantsios and Higgins [16] extended Yih's [17] results for small wavenubers to large wavenumbers and accounted for differences in density and thickness ratios, as well as the effects of interfacial tension and gravity. Yiantsios and Higgins gave a relation between β and μ_r for a stable two-layer plane Poiseuille flow configuration. Papanastasiou *et al.* [10] performed the linear stability analysis of n -layer plane Poiseuille flow and had presented the asymptotic solutions for long and short wavelengths and numerical solutions for wavelengths of $O(1)$. Papanastasiou *et al.* [10] suggested that nonsymmetric arrangements, with thinner material in the outer layer and thicker material in the middle layer, tend to more unstable than symmetric arrangements of the same material. Recently Pinarbasi [10] presented the interface stabilization by surface heating and cooling. He did the analysis for two set of immiscible liquids silicone/water and oil/water (water at the bottom layer in both cases) and showed that an imposed wall temperature difference can be stabilizing or destabilizing depending on the disturbance wavenumber and layer thickness ratio.

The onset of instability of a liquid film flow down a stationary inclined plane was theoretically analyzed by Benjamin [1] and Yih [18]. In particular, they showed that the film on the vertical plate is always unstable and the Reynolds number is greater than $\frac{5}{6} \cot \theta$ where θ is inclination angle then only instability exists. When the inclined plane has zero angle of inclination, the horizontal layer of liquid is stable. Lin *et al.* [7] carried out the stability analysis of viscous liquid film flow down an inclined plane that oscillates in the direction parallel to the flow. They showed that the onset of instability in a liquid film flowing down a stationary inclined plane can be suppressed by imparting an oscillation to the plane in a direction parallel to the flow. For a given liquid film, more than one band of frequency of oscillation may exist for the stabilization. Recently Lin *et al.* [8] carried out a similar analysis for two-layer film and demonstrated that the instability in a stratified film flow can be stabilized by imparting appropriate plate oscillation.

Kumaran *et al.* [5] studied the stability of the plane Couette flow of a Newtonian fluid past a deformable wall of finite thickness, which was modeled as an incompressible linear viscoelastic solid of fixed to a rigid substrate at zero Reynolds number. They showed that the plane Couette flow past a deformable solid is a finite wavenumber instability, and is stable for perturbations with very large and very small wavelengths at zero Reynolds number. Srivatsan and Kumaran [14] studied the same flow system but at nonzero Reynolds number. They used a numerical procedure and showed that the instability predicted by Kumaran *et al.* [5] at $Re=0$ extends to finite and large Re . Shankar and Kumar [13] studied the stability of the two-layer plane Couette flow of Newtonian fluids past a deformable wall of finite thickness. They found that when the

two fluids are arranged so that they undergo low- k instability in rigid channels due to viscosity stratification ($\mu_r > 1$ & $\beta > 0.5$ or $\mu_r < 1$ & $\beta < 0.5$), the solid layer invariably has a stabilizing effect on two-fluid interfacial mode. When the two fluids are arranged such that the two-fluid interfacial mode is stable ($\mu_r < 1$ & $\beta > 0.5$ or $\mu_r > 1$ & $\beta < 0.5$), the solid layer could have both destabilizing and stabilizing effects, depending on its thickness.

We want to explore the possibility of stability of stabilizing flow down an inclined plane, and two-layer pressure-driven Poiseuille flow using soft solid layers, following the previous work of Shankar and Kumar [13].

The outline of this thesis is as follows. In this work we first intend to study the problem of stability of liquid flow down an inclined plane lined with a soft solid layer in Chapter 2 and then in the next chapter we present the stability analysis of pressure-driven two-layer plane Poiseuille flow in a channel lined with soft solid layers. Both the chapters consist of formulation of the linear stability analysis followed by presentation of asymptotic results and discussion of numerical method used to solve the governing stability equations. Results are then presented in successive sections primarily in terms of plots between imaginary part of wavespeed and wavenumber and secondarily in terms of neutrally stability diagram. Conclusions are given in last section.

Chapter 2

Stability of Liquid Flow down an Inclined Plane Lined with Soft Solid Layer

In this chapter, we consider the stability of the Newtonian fluid flow past a soft, deformable solid layer which is fixed onto an inclined plane. Such a configuration might be relevant in the manufacturing of multilayer products such as photographic films [15]. The onset of instability of a liquid film flow down an inclined plane was analyzed by Benjamin [1] and Yih [18]. In particular, they showed that the film on the vertical plate is always unstable and when the inclined plane has zero angle of inclination, the horizontal layer of liquid is stable. In this chapter we are interested in studying how the instability of a liquid film flow down an inclined plane can be influenced by soft solid layer coatings. In particular, we explore the possibility of suppression of the instability by the soft solid layer.

The organization of this chapter is as follows. The governing equations, base state and the linearized stability equations are presented in Sec. 2.1. In Sec. 2.2, we briefly discuss the numerical method used to solve the linearized stability equations, and in Sec. 2.3 we provide representative results for the complex wavespeed as a function of the wavenumber, and secondarily in the form of neutral stability diagram. Conclusions are given in Sec. 2.4.

2.1. Problem Formulation

The system configuration consists of a Newtonian fluid of density ρ , viscosity μ and thickness R , flowing past a deformable wall (soft solid layer) having density ρ_g , viscosity μ_g , coefficient of elasticity E and thickness HR , fixed onto a inclined rigid plane at $z = (1+H)R$, in the region $0 < z < R$ as shown in Figure 2.1. The liquid has a free surface at $z = \eta(x)$. The soft solid layer is modeled as an incompressible linear viscoelastic solid, similar to that used in previous studies [5,13,14]. The soft solid wall is at rest in the unperturbed state but there is a strain in the soft solid due to fluid stress at the fluid-solid interface. The base velocity profile in the fluid is a parabolic function of z . Small perturbations to the flow are induced by spontaneous fluctuations, and we study the effect of wall deformability on the stability of these perturbations.

2.1.1. Dimensional Governing Equations

With the origin of Cartesian coordinates (shown in Fig. 2.1) at the free surface and with v_i , u_i , p_f and p_g characterizing the velocity field in the fluid, displacement field of viscoelastic solid, pressure field in fluid and the pressure in viscoelastic solid respectively, the dimensional governing mass and momentum conservation equations are as follows.

Equation of continuity

$$\partial_i v_i = 0. \quad (2.1)$$

Equation of motion [Navier-Stokes equation]

$$\rho(\partial_t + v_j \partial_j) v_i = -\partial_i p_f + \mu \partial_j^2 v_i + \rho g_i. \quad (2.2)$$

The elastic medium (soft solid layer) is considered to be incompressible, so that the displacement field satisfies the following incompressibility condition

$$\partial_i u_i = 0. \quad (2.3)$$

Equation of motion [Linear viscoelastic model]

$$\rho_g (\partial_t^2 u_i) = -\partial_i p_g + E \partial_j^2 u_i + \mu_g \partial_i \partial_j^2 u_i + \rho_g g_i. \quad (2.4)$$

In this equation, the first term on the right side is gradient of the pressure, the second term on the right side is the elastic stress due to strain, and the third term is the usual viscous stress due to gradient in the velocity.

Boundary conditions used to solve these equations are as follows. At free surface $z = \eta(x)$ the normal and tangential stresses in the fluid must vanish i.e.

$$t_i T_{ij} n_j = 0, \quad (2.5)$$

$$n_i T_{ij} n_j = 0. \quad (2.6)$$

The viscoelastic solid is fixed to a rigid surface so, it satisfies the zero displacement condition at the rigid surface $z = (1+H)R$:

$$u_i = 0. \quad (2.7)$$

The conditions at the interface ($z=R$) are continuity of velocities and continuity of stresses.

$$v_i = \partial_t u_i, \quad (2.8)$$

$$t_i T_{ij} n_j = t_i \Pi_{ij} n_j, \quad (2.9)$$

$$n_i T_{ij} n_j = n_i \Pi_{ij} n_j, \quad (2.10)$$

where T_{ij} and Π_{ij} are total stress tensor inside the fluid and viscoelastic solid respectively and these can be written as

$$T_{ij} = -p_f \delta_{ij} + \tau_{ij}, \quad (2.11)$$

$$\tau_{ij} = \mu (\partial_i v_j + \partial_j v_i), \quad (2.12)$$

where τ_{ij} is deviatoric stress tensor in fluid, and

$$\Pi_{ij} = -p_g \delta_{ij} + \sigma_{ij}, \quad (2.13)$$

$$\sigma_{ij} = (E + \mu_g \partial_i) (\partial_i u_j + \partial_j u_i), \quad (2.14)$$

where σ_{ij} is deviatoric stress tensor in soft solid layer.

2.1.2. Base State

With reference to Figure. 2.1, the base flow assumed steady, is parallel to x -axis, with a flat free surface the velocity varying only with z . Since the pressure gradient the x direction and velocity component parallel to z is zero, the Navier-Stokes equations are simply

$$\rho g \sin \theta + \mu \frac{d^2 \bar{v}_x}{dz^2} = 0, \quad (2.1)$$

$$\frac{d\bar{p}_f}{dz} = \rho g \cos \theta. \quad (2.1)$$

These equations can be integrated with the boundary conditions $\bar{v}_x = 0$ at $z = 0$ and

$\frac{d\bar{v}_x}{dz} = 0$ at $z = R$. The result is

$$\bar{v}_x = (\rho g \sin \theta / 2\mu)(R^2 - z^2), \quad (2.1)$$

and the average velocity is given by

$$\bar{v}_a = \rho g R^2 \sin \theta / 3\mu. \quad (2.18)$$

2.1.3. Nondimensional Governing Equations

It is useful to nondimensionalize the various physical quantities at the outset and the following scales are used for this purpose: R for length, average velocity \bar{v}_a for velocity, $\frac{R}{\bar{v}_a}$ for time and $\frac{\mu \bar{v}_a}{R}$ for stresses and pressure. This gives the following nondimensional equations. From this point onwards, all the variables are nondimensional unless it is explicitly stated that they are dimensional.

Base velocity profile for fluid:

$$\bar{v}_x = \frac{3}{2}(1 - z^2), \quad (2.19)$$

$$\bar{v}_z = 0. \quad (2.20)$$

Equation of continuity for fluid and solid layer:

$$\partial_i v_i = 0, \quad (2.21)$$

$$\partial_i u_i = 0. \quad (2.22)$$

Equation of motion:

Fluid:
$$Re(\partial_t + v_j \partial_j) v_i = -\partial_i p_f + \partial_j^2 v_i + \frac{\rho g_i R^2}{\mu \bar{v}_a}. \quad (2.23)$$

Soft solid layer:
$$Re(\partial_t^2 u_i) = \partial_j \Pi_{ij} + \frac{\rho g_i R^2}{\mu \bar{v}_a}. \quad (2.24)$$

The scaled stresses in fluid and soft solid are

$$T_{ij} = -p_f \delta_{ij} + (\partial_i v_j + \partial_j v_i), \quad (2.25)$$

$$\Pi_{ij} = -p_g \delta_{ij} + \left(\frac{1}{\Gamma} + \eta_r \partial_i\right)(\partial_j u_i + \partial_i u_j). \quad (2.26)$$

where the various non-dimensional quantities are defined as:

$$\Gamma = \frac{\mu \bar{v}_a}{E R}, \quad Re = \frac{R \bar{v}_a \rho}{\mu} \quad \text{and} \quad \eta_r = \frac{\mu_g}{\mu}.$$

Nondimensional boundary conditions are

at $z = \eta(x)$ [perturbed free surface]

$$T_{zx} = 0, \quad (2.27)$$

$$T_{zz} = 0, \quad (2.28)$$

at $z = 1 + H$ [rigid surface]

$$u_x = 0, \quad (2.29)$$

$$u_z = 0, \quad (2.30)$$

at $z = 1$ [fluid-solid interface]

$$v_z = \partial_t u_z, \quad (2.31)$$

$$v_x = \partial_t u_x, \quad (2.32)$$

$$T_{zx} = \Pi_{zx}, \quad (2.33)$$

$$T_{zz} = \Pi_{zz}. \quad (2.34)$$

2.1.4. Linear Stability Analysis

In this section we use a linear stability analysis to calculate the complex wave speed of perturbations to the interface between the elastic medium and fluid. In the analysis the velocity and displacement fields are expressed as a sum of mean and perturbation terms, i.e.

$$v_i = \bar{v}_i + v'_i, \quad u_i = \bar{u}_i + u'_i. \quad (2.35)$$

All the perturbation quantities are expanded in the forms of Fourier modes in the x direction, and with an exponential dependence in time:

$$v'_i = \tilde{v}_i(z) \exp[ik(x - ct)], \quad u'_i = \tilde{u}_i(z) \exp[ik(x - ct)], \quad (2.36)$$

where k is wave number, c is wave speed and $\tilde{v}_i(z)$ and $\tilde{u}_i(z)$ are the eigenfunctions, determined by solving the conservation equations. Substituting Eqs. (2.35) and (2.36) in the conservation equation for the fluid, Eqs. (2.21) and (2.23), we obtain the linearized equation for the fluid as:

$$d_z \tilde{v}_z + ik \tilde{v}_x = 0, \quad (2.37)$$

$$Re\{ik(\bar{v}_x - c)\tilde{v}_x + (d_z \bar{v}_x)\tilde{v}_z\} = -ik\tilde{P}_f + [d_z^2 - k^2]\tilde{v}_x, \quad (2.38)$$

$$Re\{ik(\bar{v}_x - c)\tilde{v}_z\} = -d_z \tilde{P}_f + [d_z^2 - k^2]\tilde{v}_z. \quad (2.39)$$

The above equations can be combined to give a single fourth-order, Orr-Sommerfeld-like equation for \tilde{v}_z :

$$ik Re\{(\bar{v}_x - c)[d_z^2 - k^2] + (d_z^2 \bar{v}_x)\} \tilde{v}_z = [d_z^2 - k^2]^2 \tilde{v}_z. \quad (2.40)$$

The linearized equations for the soft solid layer are obtained by inserting (2.35) and (2.36) in (2.22) and (2.24):

$$d_z \tilde{u}_z + ik \tilde{u}_x = 0, \quad (2.41)$$

$$-Re k^2 c^2 \tilde{u}_x = -ik \tilde{p}_g + \left(\frac{1}{\Gamma} - \eta_r i k c\right) [d_z^2 - k^2] \tilde{u}_x, \quad (2.42)$$

$$-Re k^2 c^2 \tilde{u}_z = -d_z \tilde{p}_g + \left(\frac{1}{\Gamma} - \eta_r i k c\right) [d_z^2 - k^2] \tilde{u}_z. \quad (2.43)$$

These equations can be reduced to a single fourth-order differential equation for \tilde{u}_z :

$$Re k^2 c^2 [d_z^2 - k^2] \tilde{u}_z + \left(\frac{1}{\Gamma} - \eta_r i k c\right) [d_z^2 - k^2]^2 \tilde{u}_z = 0. \quad (2.44)$$

The linearized equations for perturbations to stress fields in the fluid and soft solid layer are derived from (2.25) and (2.26):

$$\tilde{T}_{zx} = d_z \tilde{v}_x + i k \tilde{v}_z, \quad \tilde{T}_{zz} = -\tilde{p}_f + 2 d_z \tilde{v}_z, \quad (2.45)$$

$$\tilde{\Pi}_{zx} = \left(\frac{1}{\Gamma} - i k c \eta_r\right) (d_z \tilde{u}_x + i k \tilde{u}_z), \quad \tilde{\Pi}_{zz} = -\tilde{p}_g + \left(\frac{1}{\Gamma} - i k c \eta_r\right) 2 d_z \tilde{u}_z. \quad (2.46)$$

Now turning to the boundary conditions, the free surface condition must be applied at $z = \eta$ not at $z = 0$. These conditions are obtained by Taylor-expanding about the flat interface position in the base state. Because the gradient of shear stress of the pressure in the base flow is not zero at $z = 0$, additional terms appear as a result of the linearization about $z = 0$. Hence (2.27) and (2.28) can be written in the forms

$$(\tilde{T}_{zx})_{z=\eta} = -3\tilde{\eta} + (d_z \tilde{v}_x + i k \tilde{v}_z)|_{z=0} = 0, \quad (2.47)$$

$$(\tilde{T}_{zz})_{z=\eta} = -\tilde{p}_f|_{z=0} - 3\tilde{\eta} \cot \theta + 2 d_z \tilde{v}_z|_{z=0} - k^2 \Sigma \tilde{\eta} = 0, \quad (2.48)$$

where $\tilde{\eta}$ the Fourier expansion coefficient for the free-surface position $\eta = \tilde{\eta} \exp[ik(x - ct)]$, and $\Sigma = \gamma / (\mu \bar{v}_a)$ is the nondimensional surface tension for fluid.

The linearized kinematic condition at $z = 0$ (free surface) is given by

$$ik[\bar{v}_x(z=0) - c]\tilde{\eta} = \tilde{v}_z. \quad (2.49)$$

Linearized boundary conditions in terms of perturbed quantities at $z = (1 + H)$ are

$$\tilde{u}_x = 0, \quad (2.50)$$

$$\tilde{u}_z = 0. \quad (2.51)$$

Interfacial conditions for the perturbations at fluid-solid interface, $z = h(x)$ Eqs. (2.31)-(2.34) reduces to

$$\tilde{v}_z = -ikc\tilde{u}_z, \quad (2.52)$$

$$\tilde{v}_x + (d_z \tilde{v}_x)_{z=1} \tilde{u}_z = -ikc\tilde{u}_x, \quad (2.53)$$

$$\tilde{T}_{xz} = \tilde{\Pi}_{xz}, \quad (2.54)$$

$$\tilde{T}_{zz} = \tilde{\Pi}_{zz}. \quad (2.55)$$

In these equations, the height of interface, $h(x)$, is approximated by \tilde{u}_z at $z=1$; this approximation is valid for small perturbations. The second term in left side of equation (2.53) represents the nontrivial contribution that arises as a result of the Taylor expansion of mean flow quantities about the unperturbed fluid-solid interface. This additional term is responsible for the instability of interface between the fluid and deformable solid wall [13].

The differential system governing the stability problem consists of Eqs. (2.40), (2.44), (2.47), (2.48), (2.50), (2.51), (2.52), (2.53) and (2.55). It defines an eigenvalue problem for the complex wave speed c . The problem at hand is to determine c as a function of $\Gamma, \eta_r, Re, \Sigma, \theta, k$ and H . It is not possible to solve this differential eigenvalue problem analytically. However, for long waves, it is possible to carryout an asymptotic analysis in the small parameter k , and this procedure yields analytical solution to c as a series in k . The asymptotic analysis was carried out by Shankar [12] and this gives an analytical expression for complex wave speed, but is valid only for long waves ($k \ll 1$):

$$c = c^0 + kc^1, \quad (2.56)$$

where c^0 is purely real and c^1 is purely imaginary. From Shankar's [12] analysis

$$c^0 = 3.0, \quad (2.57)$$

$$c^1 = i \{ (1.2 Re - \cot \theta) - 9 \Gamma H \}. \quad (2.58)$$

The asymptotic results shows that in the $k \rightarrow 0$ limit, the parameters Σ and η_r do not appear in c^0 and c^1 . In the Eq. (2.58), first term proportional to Reynolds number and inclination angle θ is inertial contribution while the second term proportional to ΓH is soft solid layer's contribution. Stability of liquid flow down an inclined rigid plane depends upon the Reynolds number as well as on the inclination angle. The asymptotic results show that the soft solid layer's contribution is always stabilizing in the limit of long waves. However, the long-wave analysis does not address the issue of whether the soft solid layer is stabilizing at all k . To answer this question, we undertake a numerical study of the stability problem which is valid at all wavelengths.

We use the asymptotic result as an initial guess for the numerical method through which we can continue up to finite values of wavenumber. The flow is unstable, neutrally stable, or stable according to whether c^1 is positive, zero or negative.

2.2. Numerical Method

We first briefly outline the method to solve the governing equations described in the previous section. There are two fourth-order differential equations for the fluid layer in the terms of \tilde{v}_z and for solid layer in terms of \tilde{u}_z . We use a fourth-order Runge-Kutta integrator with adaptive size control to obtain the solution. To solve a fourth-order differential equation we must know the function's value and its first three derivatives at any particular value of independent variable. For the solid layer at $z=1+H$, we have from Eqs. (2.50) and (2.51)

$$\tilde{u}_z = 0, \quad d_z \tilde{u}_z = 0. \quad (2.59)$$

We use two different sets of higher derivatives $d_z^2 \tilde{v}_z$ and $d_z^3 \tilde{v}_z$ at $z = 1 + H$, which will yield two linearly independent solutions to the displacement field in solid layer [14]:

$$\tilde{u}_z = 0, d_z \tilde{u}_z = 0, d_z^2 \tilde{u}_z = 1, d_z^3 \tilde{u}_z = 0, \quad (2.60)$$

$$\tilde{u}_z = 0, d_z \tilde{u}_z = 0, d_z^2 \tilde{u}_z = 0, d_z^3 \tilde{u}_z = 1. \quad (2.61)$$

Using these conditions at $z = 1 + H$, we use the Runge-Kutta method to integrate the ODE [Eq. (2.44)] in solid layer up to $z = 1$. The displacement field in soft solid is then obtained as a linear combination of these two solutions.

$$\tilde{u}_z = A_1 \tilde{u}_z^{(1)} + A_2 \tilde{u}_z^{(2)}, \quad (2.62)$$

$$d_z \tilde{u}_z = A_1 d_z \tilde{u}_z^{(1)} + A_2 d_z \tilde{u}_z^{(2)}, \quad (2.63)$$

$$d_z^2 \tilde{u}_z = A_1 d_z^2 \tilde{u}_z^{(1)} + A_2 d_z^2 \tilde{u}_z^{(2)}, \quad (2.64)$$

$$d_z^3 \tilde{u}_z = A_1 d_z^3 \tilde{u}_z^{(1)} + A_2 d_z^3 \tilde{u}_z^{(2)}. \quad (2.65)$$

Here A_1 and A_2 are constants which have to be determined by the boundary conditions.

Now we evaluate the velocity field of fluid \tilde{v}_z , and its higher derivatives, in terms of same constants A_1 and A_2 with the help of boundary conditions at fluid-solid interface i.e. Eqs. (2.52)-(2.55). Using these two set of values at $z = 1$, we integrate the ODE [Eq. (2.40)] in the fluid up to $z = 0$ and the velocity field \tilde{v}_z in the fluid is then obtained as a linear combination of these two set of solutions. At $z = 0$ fluid velocity field must satisfy the boundary conditions (2.47) and (2.48). We can write the equations in matrix form as:

$$\begin{bmatrix} \tilde{T}_{zx}^{(1)} & \tilde{T}_{zx}^{(2)} \\ \tilde{T}_{zz}^{(1)} & \tilde{T}_{zz}^{(2)} \end{bmatrix} \begin{bmatrix} A_1 \\ A_2 \end{bmatrix} = 0. \quad (2.66)$$

In this matrix, the subscripts 1 and 2 over the quantities refer to the solutions for the stress field in the liquid at gas-liquid interface calculated using the first and second set of boundary conditions respectively. For nontrivial solution of A_1 and A_2 , determinant of matrix is set to be zero, which gives the characteristic equation. The characteristic equation is non-linear in c , so it is not possible to solve for c analytically. A Newton-Raphson iteration technique is used to solve the characteristic equation and obtain the complex wave speed, for specified values of Γ , η_r , Re , Σ , θ , k and H .

We use the low- k asymptotic results as starting guess for the numerical procedure, and continue the low- k results numerically to finite values of k . We have compared the results from numerical code for the low values of k with Shankar's [12] asymptotic results and found that numerical code is agreeing with the asymptotic results for small values of wavenumber.

2.3. Results and Discussion

It is instructive to briefly summarize the results of Yih [18] for the case of stability of liquid flow down in an inclined rigid plane. Yih's [18] solution for long-waves shows that for the configuration where $Re > \frac{5}{6} \cot \theta$ long-wave disturbances will be amplified. Also the free-surface flow down a vertical plane ($\theta = 90^\circ$) is unstable for all finite Reynolds numbers. Using the numerical procedure described above, it is possible to recover the case of flow down an inclined rigid channel, by setting the parameters $\Gamma = 0$ or $H = 0$. Here, by setting $\Gamma = 0$ we achieve the conversion of the soft solid layer in to rigid solid layer, which has very high values of shear modulus (shear

modulus $G \propto \frac{1}{\Gamma}$) and $H = 0$ signifies the disappearance of soft solid layer, which is fixed onto the rigid surface at $z = (1 + H)$. The results of the low wavenumber asymptotic analysis are used as starting guess for this numerical solution. In Figure 2.2 the imaginary part of wave speed is plotted as a function of wavenumber, for different values of Reynolds number. Figure 2.2 validates Yih's [18] result and shows that the configurations is stable if $Re < \frac{5}{6} \cot \theta$ ($Re = 0.1, \theta = 45^\circ$), while in opposite case where $Re > \frac{5}{6} \cot \theta$, exhibits instability for the low and intermediate k . Reynolds number has a destabilizing effect at perturbations with long as well as intermediate wavelengths, as shown in the same figure. In both cases ($Re < \frac{5}{6} \cot \theta$ and $Re > \frac{5}{6} \cot \theta$) short waves are stable even in the absence of gas-liquid interfacial tension. Figure 2.3 shows that free-surface flow down a vertical plate ($\theta = 90^\circ$) is unstable for all finite Reynolds number. Similar to previous figure, here also increase in Re has a destabilizing effect at long and intermediate wavelengths and short waves are stable even with zero values of gas-liquid interfacial tension. Shankar and Kumar [13] showed that, in the case of two-layer flow only the presence of a sufficiently strong nonzero interfacial tension only can stabilize the short wave unstable modes. Variation of c_i with k for $\Sigma \neq 0$ is presented in Figure 2.4. On comparison of Figure 2.4(a) ($\Sigma = 0.1$) with Figure 2.2 ($\Sigma = 0$), we find that the interfacial tension has no significant effect in the growth rate for the perturbations having long wavelengths, while in the case of short and intermediate waves it quantitatively affects the growth rate. From Figure 2.4(b) it is more clear that interfacial tension

decreases the growth rate at high- k but in this region the flow is already stable. So we can conclude that, for the present case interfacial tension does not qualitatively affect the instability of flow down an inclined plane.

Now we examine the effect of soft solid layer on the interfacial instability of a liquid flow down an inclined plane. No work has been reported in literature related to free surface flow past a deformable wall. This effect was analyzed in the limit of long waves by Shankar [12] and the results are given in Eq. (2.56)-(2.58). That analysis showed that as $k \rightarrow 0$, at leading order the wave speed is purely real and is identical to Yih's [18] result. The destabilizing effect of fluid inertia appears at $O(k)$. And the effect of the solid layer also appears at the same order, which is always stabilizing in the long-wave limit.

In the present study we wish to examine whether the stabilization persists for intermediate wavelengths as well. Before we discuss the present results, it must be mentioned that shear flow past a soft solid layer in the creeping flow limit could become unstable when solid layer become sufficiently soft or when it is sufficiently thick. Srivatsan and Kumaran [13] showed that this instability is not present for nondimensional thickness $H < 1$. So, if we choose soft solid layers with nondimensional thickness $H < 1$, we will not excite the instability of the interface between the fluid and the soft solid. Also, the instability of Kumaran *et.al* [5,14] exists only for $\Gamma \sim O(1)$ values. We will show below that for free surface flow the stabilizing effect of the solid layer occurs at value of $\Gamma \sim O(10^{-2})$, which is much smaller than the critical value required to destabilizing the fluid-solid interface in case of shear flow.

Here we present the cases where flow down an inclined rigid plane is unstable and study the effect of the soft solid layer. We first discuss the effect of solid layer on the

liquid flow down a vertical plane and this is presented in Figure 2.5. Figure 2.5(a) and Figure 2.5(b) shows the variation of c_i with k for $\theta = 90^\circ$ and $Re = 0.1$ for different values of Γ . The soft solid layer is stabilizing only when the parameter Γ exceeds a critical value. In Figure 2.5(a), the solid layer with $\Gamma = 0.001$ has no significant effect on instability because here Γ is less than the critical value, while free surface is stable for $\Gamma = 0.1$ and 0.5 in low- k limit. However value of c_i at $k \approx 1$ for $\Gamma = 0.1$ and 0.5 is larger than c_i for the case when $\Gamma = 0$. So the soft solid layer has destabilizing effect at finite- k , while short waves are always stable regardless of the parameter Γ . In Figure 2.5(b), we show the effect of increasing Γ further. From this figure we conclude that complete stabilization (at all k) of the free surface in the case of vertical plane can be achieved by making the solid layer sufficiently soft. Figure 2.6 shows that for stabilization it is not essential to have nondimensional thickness $H > 1$. Figure 2.6(a) and Figure 2.6(b) shows the variation of c_i with k for $H = 0.8$, $\theta = 45^\circ$ and $Re = 1$ for different values of Γ . Figure 2.6(a) shows that while short waves are still stabilized, increase in Γ has a destabilizing effect on finite wave length fluctuations which is similar to the case of flow down a vertical plane discussed earlier. In the Figure 2.6(b), we show the effect of increasing Γ further. Indeed, compare with the rigid results show that the range of unstable k for $\Gamma = 5$ are stable in the case of rigid plane. Therefore, increase in Γ introduces new unstable modes for finite values of k . Therefore, if one were to choose the shear modulus of the solid layer, it is advantageous to have $\Gamma < 1$ for the present configuration. On comparing Figure 2.5(b) and Figure 2.6(b) we find that in case of liquid flow down an inclined plane, high values of Γ has destabilizing effect at finite- k while there is no such destabilizing effect in case of vertical plane. Figure 2.7 shows the

variation of c_i with k for $H = 2$, $\theta = 45^\circ$ and $Re = 1$ for different values of Γ . In Figure 2.6(a) for $\Gamma = 0.5$ c_i values at all k are negative while in Figure 2.7(b) c_i values are positive at finite- k . So increase in H has a destabilizing effect on finite- k modes. On comparing Figure 2.7(a) and Figure 2.7(b), we find that for the same value of $Re = 1$, increase in Γ has a destabilizing effect on growth rate at finite- k . So, if we were to use soft solids for stabilizing the interfacial mode it is necessary to have nonzero ΓH , but there is an optimum value of ΓH , and beyond this optimum value of ΓH the soft solid layer has a destabilizing effect on the free surface at finite wavenumber as well as on the fluid-solid interfacial instability. Figure 2.8(a) and 2.8(b) shows that at $Re = 5$ the soft solid layer can not stabilize the instability at all wavenumbers: There is always there is a possibility of finite wavenumber instability. On comparing Figure 2.8(a) and Figure 2.7(a) we can conclude that Re has destabilizing effect on finite-wavelengths fluctuations. This is further illustrated in Figure 2.9 where the parameter $\Gamma = 0.1$ is sufficient for stabilization of free surface at $Re = 1$ while it is less than the critical value at $Re = 3$ and 5. Nonzero value of gas-liquid interfacial tension has no significant effect on the instability at finite wavenumbers, as shown in Figure 2.10.

It is useful to construct neutral stability curves demarcating stable and unstable regions in the $\Gamma - k$ plane, for fixed values of $\eta_r, Re, \Sigma, \theta$ and H . Such plots allow us to select the parameter Γ (i.e. the shear modulus of the solid layer), for complete stabilization at all wavelengths. Neutral curves are provided in Figure 2.11-Figure 2.15. When Γ is increased beyond the neutral curve, there is transition from unstable to stable perturbations and an additional unstable region is identified when Γ is increased beyond a critical value for the finite wavenumber fluctuations. There are two neutral curves

separated by a stable region between them, where the flow is stabilized for perturbations with all wavelengths. The upper neutral curve corresponds to finite wavenumber instability that is absent in flow down a rigid plane. This finite wavenumber instability arises due to the soft solid layer only. Gas-liquid interfacial tension does not qualitatively affect the neutral stability curve. However, there is a qualitative change in the neutral stability curve due to variation in the ratio of viscosities of the fluid and soft solid layer (η_r). In Figure 2.11 where $\eta_r = 0$ the region where flow is completely stabilized ranges from $\Gamma \sim 10^{-2}$ to $\Gamma \sim 10^{-1}$ while in Figure 2.12 where $\eta_r = 0.5$ it is from $\Gamma \sim 10^{-2}$ to $\Gamma \sim 10^0$. So viscosity of the deformable wall is always stabilizing on the finite wavenumber instability of the free surface due to which the stable region between the two neutral curves increases with η_r . Figure 2.13 is for same set of parameters as in Figure 2.11 but for $Re = 3$ where the gap between the neutral curves has been reduced very much. This agrees with our previous conclusion that, Reynolds number has destabilizing effect on finite wave length fluctuations. Gas-liquid interfacial tension has no significant effect on neutral stability curve. This is illustrated in Figure 2.14. Figure 2.15 is for same data set as in Figure 2.11 but for $H = 3$, in this figure the upper neutral curve which is due to soft solid layer, starts appearing at $\Gamma = 0.26$ while for $H = 1$ it appears after $\Gamma = 0.44$. Hence increase in H also has destabilizing effect at finite wave length modes. It is also useful here to estimate the dimensional value of shear modulus that would be required to realize the present prediction. We consider the Figure 2.11 where $Re = 1$ and $\theta = 45^\circ$ and the region where the modes are definitely stable ranges from $\Gamma \sim 10^{-2}$ to $\Gamma \sim 10^{-1}$. To estimate E we use $\rho = 1000 \text{ kg m}^{-3}$ and

$\mu = 10 \text{ kg m}^{-1} \text{ sec}^{-1}$. By using $Re = 1$ thickness of film comes out to be $O(10^{-2}) \text{ m}$ and in the mentioned range of Γ , we conclude that E should be in the range $10^4 - 10^3 \text{ Pa}$ in order for all modes to be stable. Figure 2.16 and Figure 2.17 more clearly demonstrate the stabilizing effect of viscosity ratio η_r and destabilizing effect of nondimensional thickness H at finite wavenumber instability.

2.4. Conclusion

According to Yih's [18] solution in the small wave number limit, liquid flow down an inclined rigid plane is unstable, even in the limit of small Reynolds number. The condition for instability is Re should be greater than $\frac{5}{6} \cot \theta$, where θ is the angle with respect to horizontal. Our study concerning the stability of flow down an inclined plane lined with soft solid layer shows that it is possible to stabilize this type of free surface flow instabilities by soft solid layer coatings. The asymptotic analysis for long waves shows that the deformable wall contribution is always stabilizing. The results of the low wave number asymptotic analysis were continued to finite and higher values of k using a numerical solution of the governing stability equations. We have found that, in the case of perturbations with finite wavelengths, the soft solid layer has a destabilizing effect, while it is always stabilizing for the perturbation with very large wave lengths. The present configuration is always stable to short waves, regardless of soft solid layer coating. The nondimensional parameter Γ required to achieve the stabilization is typically very small compared to unity. The interfacial instability at the fluid-solid interface occurs at $\Gamma \sim O(1)$ [5,14] therefore it is possible to choose a "band" of Γ value

in which fluid-solid interfacial instability is not excited. Surface tension of liquid-gas interface has negligible effect on the instability. Viscosity of soft solid layer is always stabilizing. Stability depends on the parameters, viz., Γ (elasticity parameter of soft solid), H thickness of soft solid layer and η_r (soft solid layer's viscosity parameter). Neutral stability curves were presented which help in tuning the solid properties so as to achieve complete stabilization at all wave-numbers.

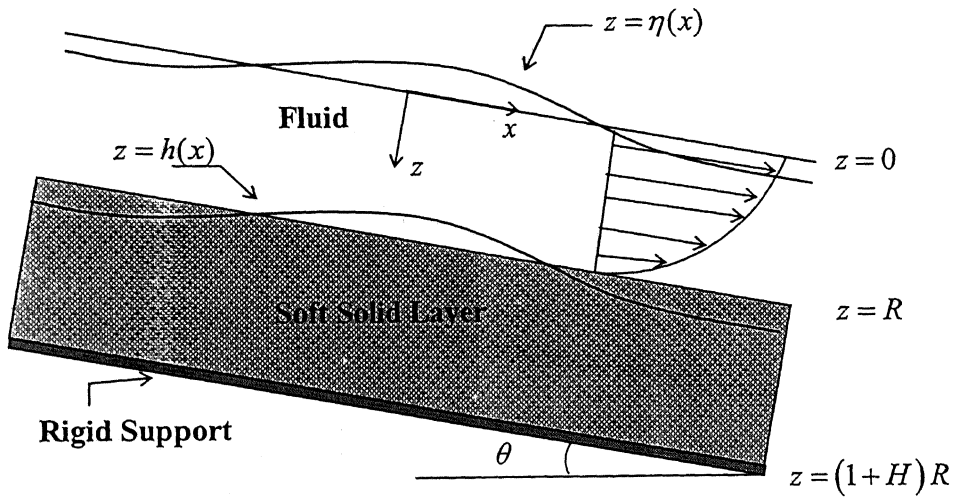


Figure 2.1. Schematic diagram of liquid flow down an inclined plane coated by soft solid layer (All the quantities are dimensional in the figure)

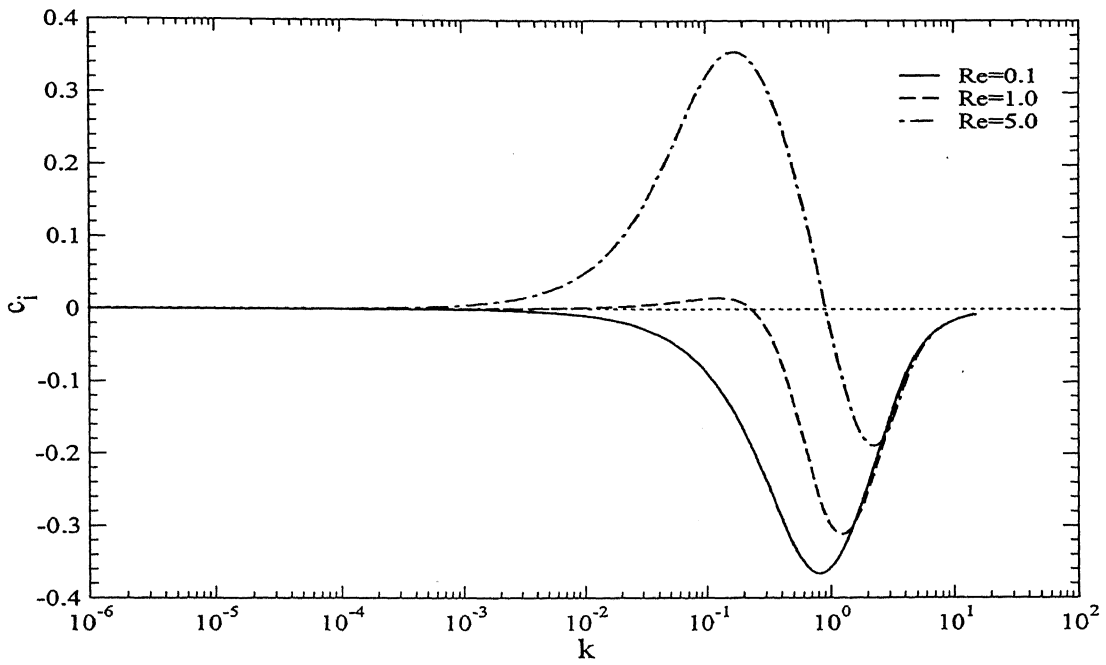


Figure 2.2 Instability in flow down an inclined rigid plane: variation of c_i with k for $\theta = 45^\circ$ and $\Sigma = 0$.

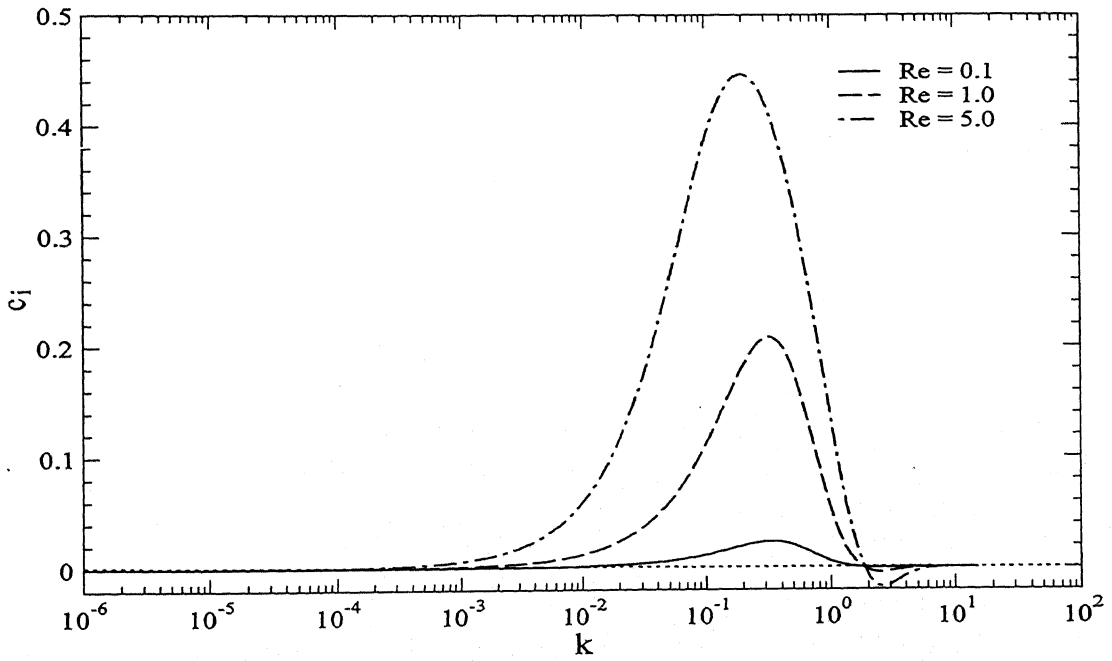
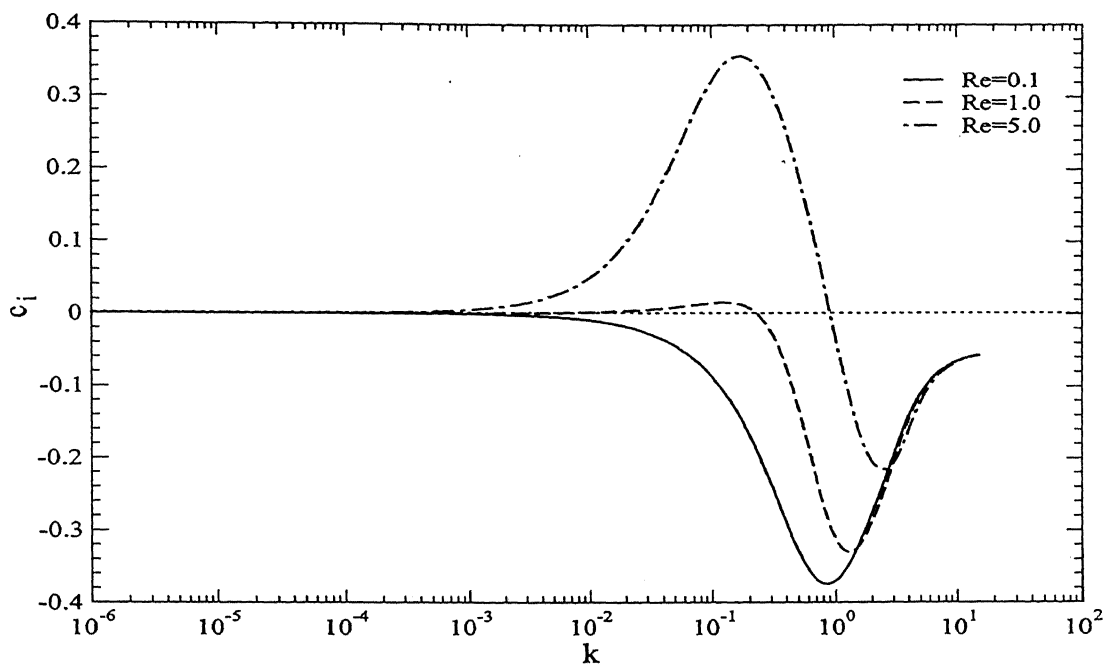
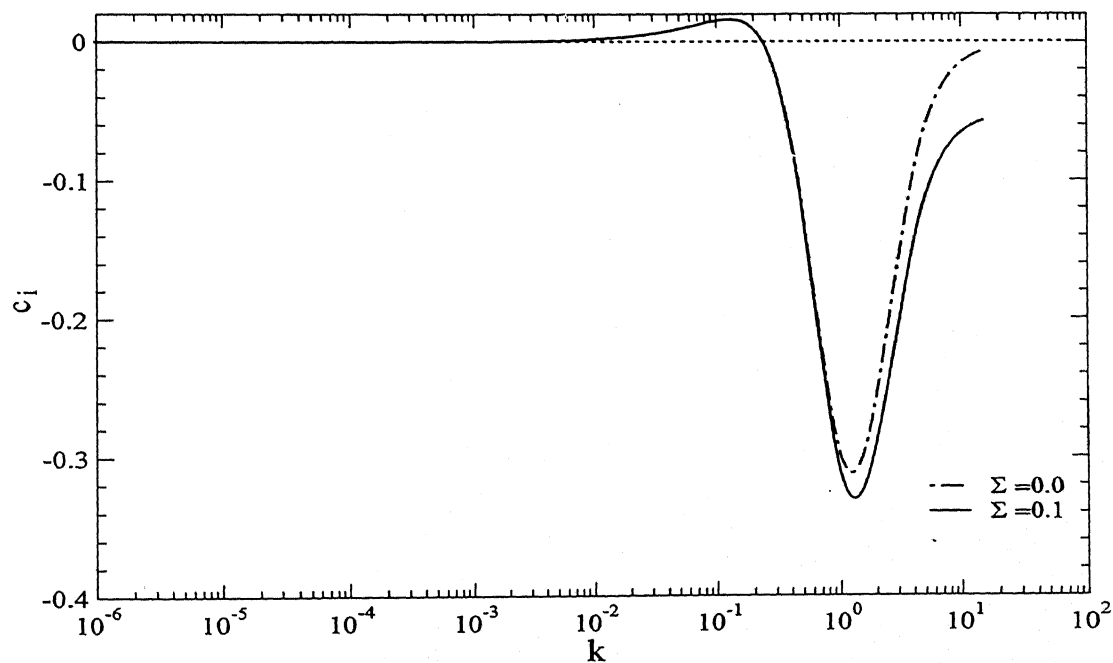


Figure 2.3 Instability in flow down a vertical rigid plane: variation of c_i with k for $\theta = 90^\circ$, $\Sigma = 0$ and $\Gamma = 0$.



(a) Variation of c_i with k for $\theta = 45^\circ$, $\Gamma = 0$ and $\Sigma = 0.1$



(b) Variation of c_i with k for $\theta = 45^\circ$, $\Gamma = 0$ and $Re = 1$

Figure 2.4 Instability in flow down a inclined rigid plane: effect of surface tension on c_i vs k

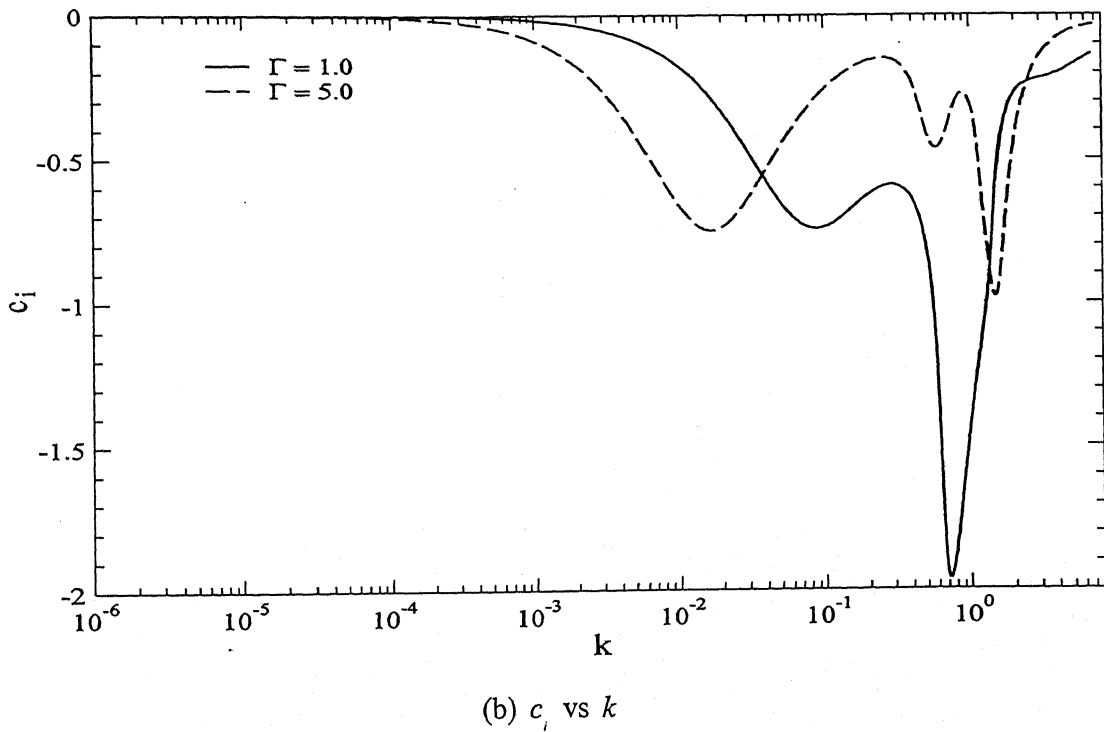
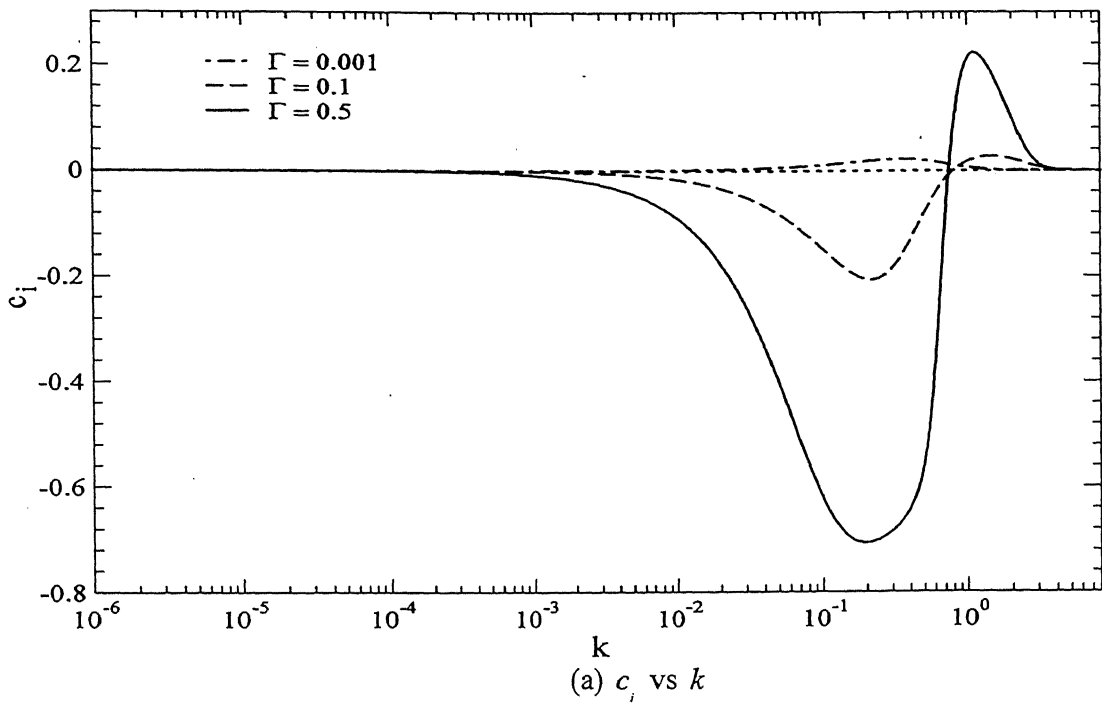
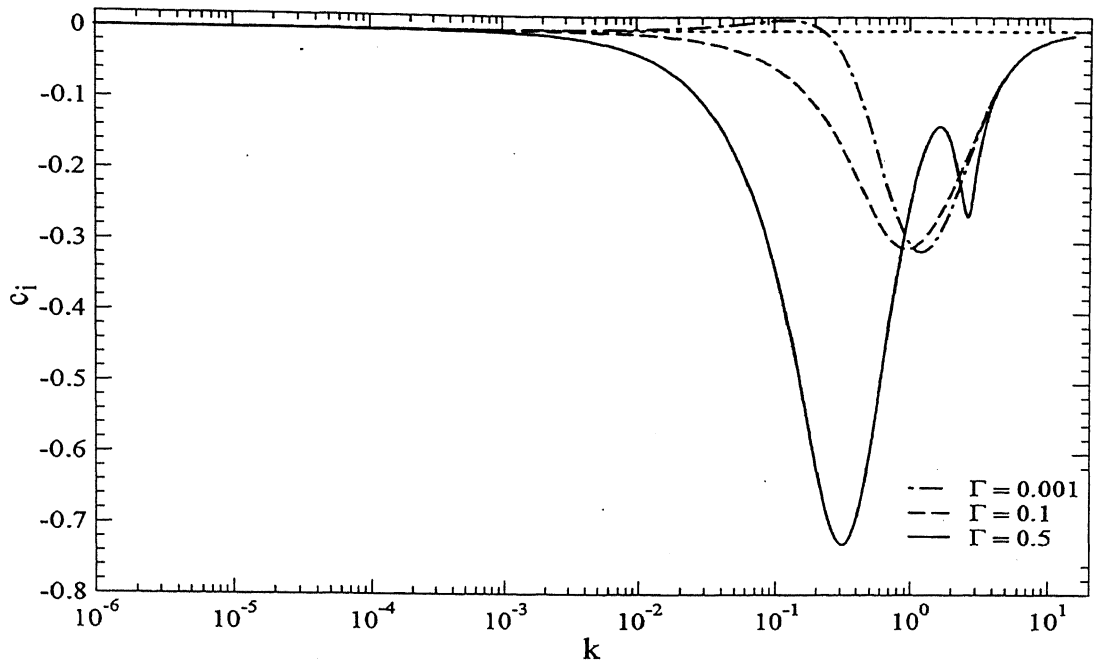
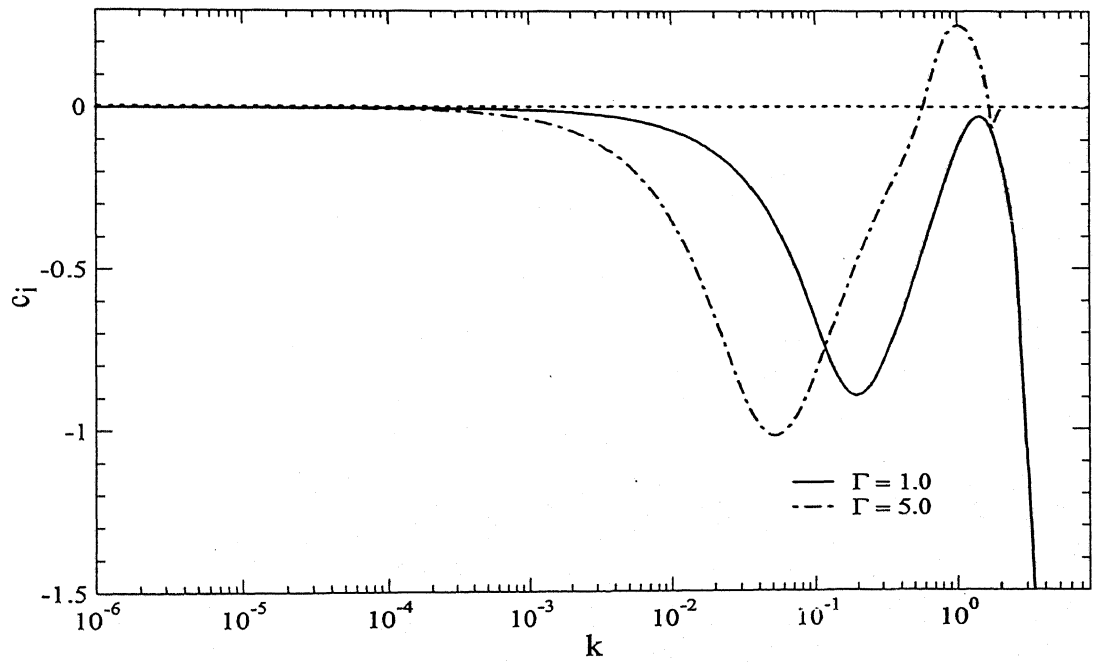


Figure 2.5 Instability in liquid flow down vertical plane lined by soft solid layer: variation of c_i with k for $H = 2, Re = 0.1, \theta = 90^\circ, \eta_r = 0$ and $\Sigma = 0$.

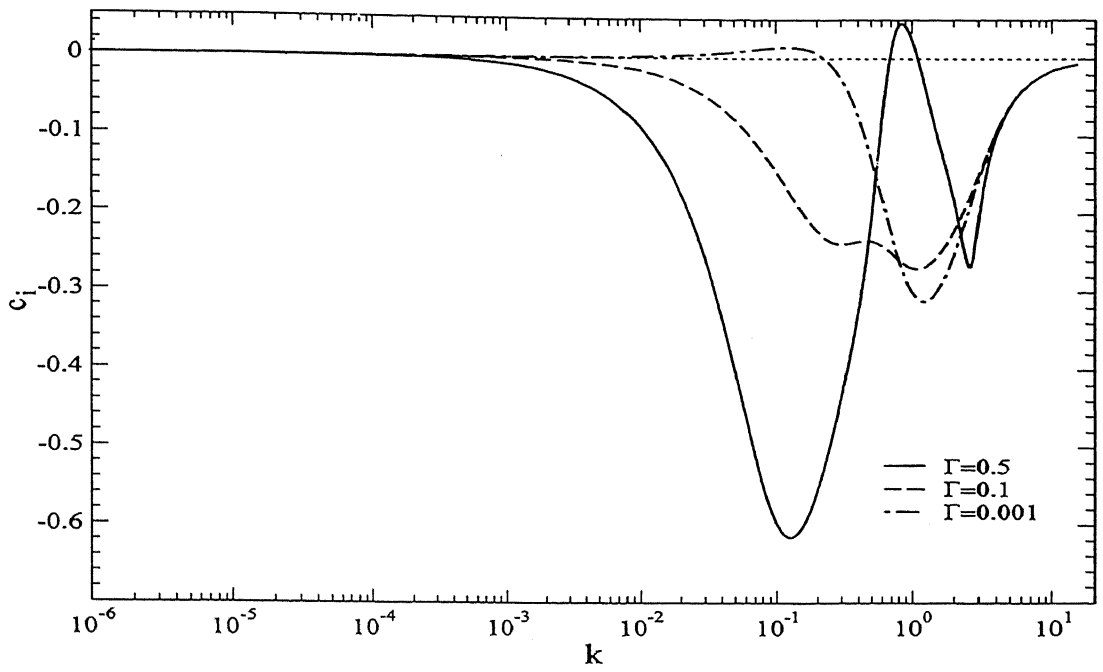


(a) c_i vs k

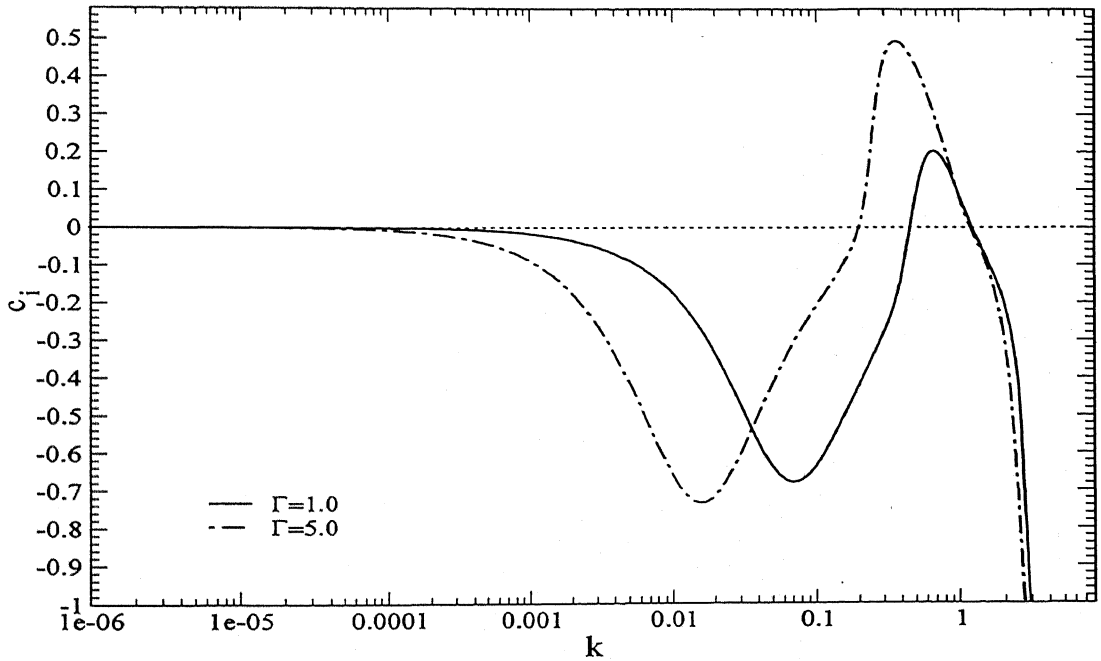


(b) c_i vs k

Figure 2.6 Instability in liquid flow down an inclined plane lined by soft solid layer: variation of c_i with k for $H=0.8(<1)$, $Re=1$, $\theta=45^\circ$, $\eta_r=0$ and $\Sigma=0$.

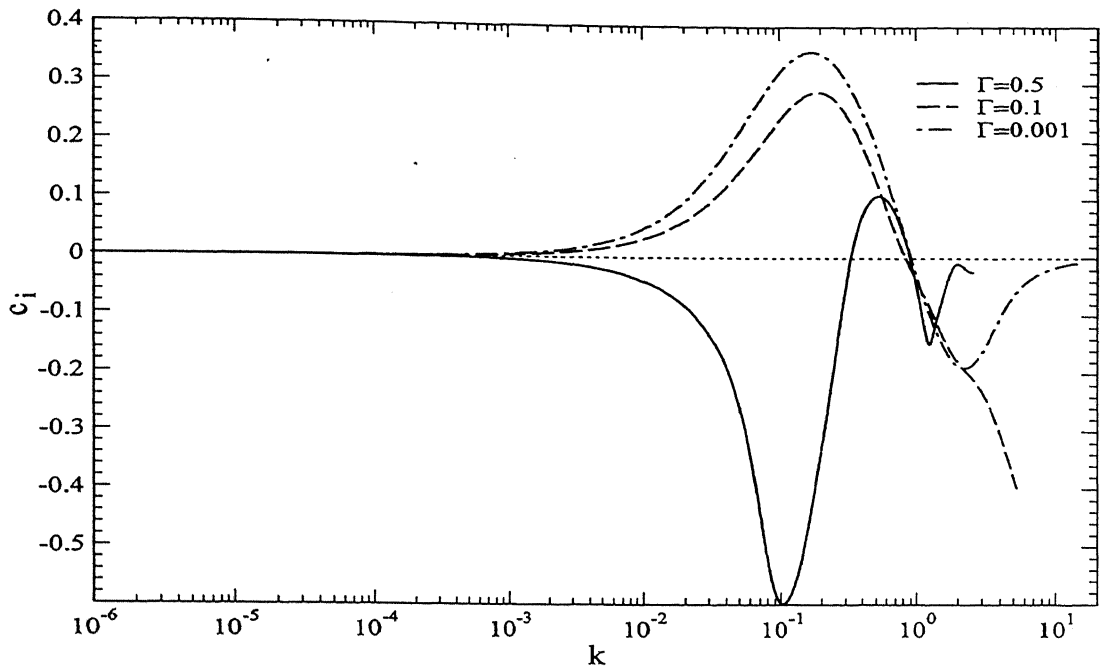


(a) c_i vs k

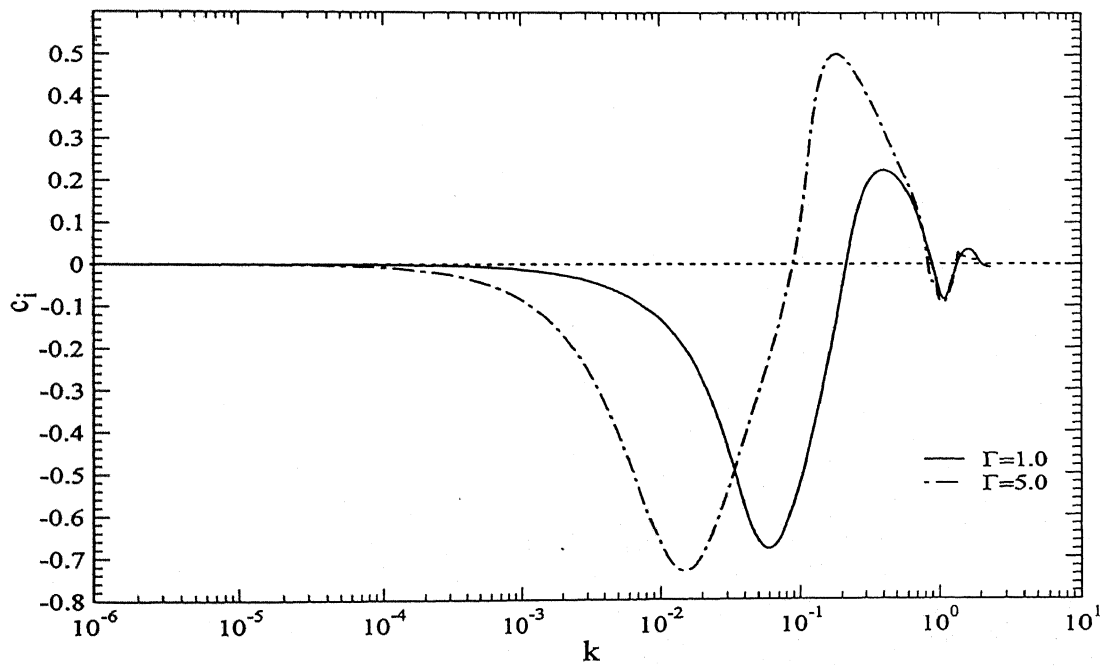


(b) c_i vs k

Figure 2.7 Effect of solid layer deformability: c_i vs k for $H=2$, $Re=1$, $\theta=45^\circ$, $\eta_r=0$ and $\Sigma=0$.



(a) c_i vs k



(b) c_i vs k

Figure 2.8 Effect of solid layer deformability: c_i vs k for $H=2$, $Re=5$, $\theta=45^\circ$, $\eta_r=0$ and $\Sigma=0$.

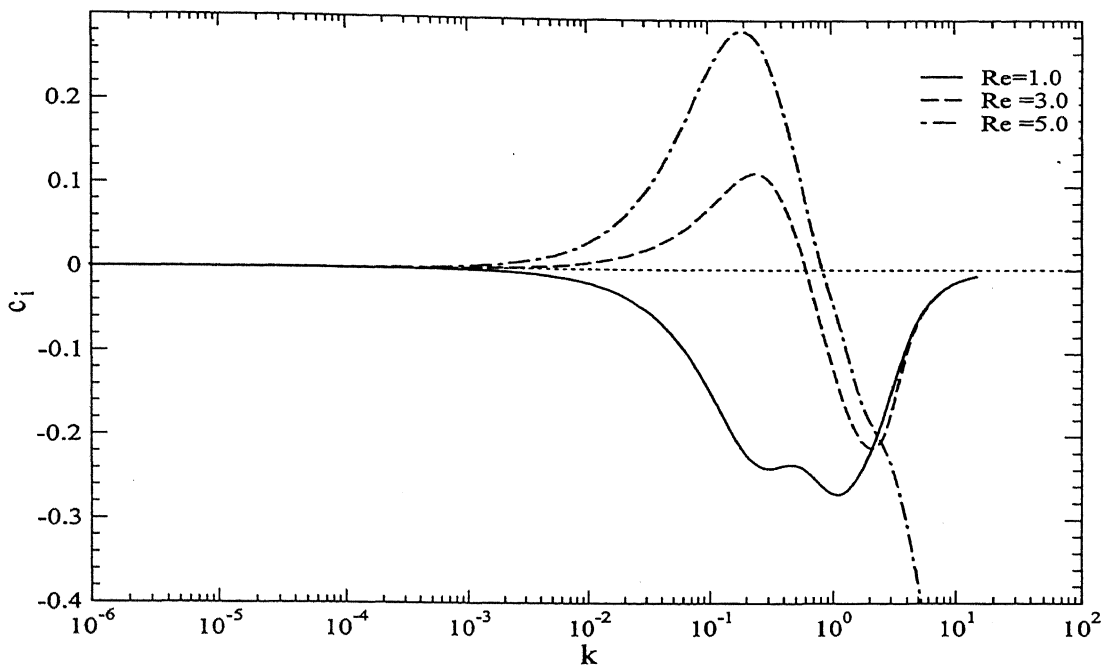


Figure 2.9 Effect of Reynolds number on c_i vs k for $H=2, \Gamma=0.1, \eta_r=0, \Sigma=0$ and $\theta=45^\circ$.

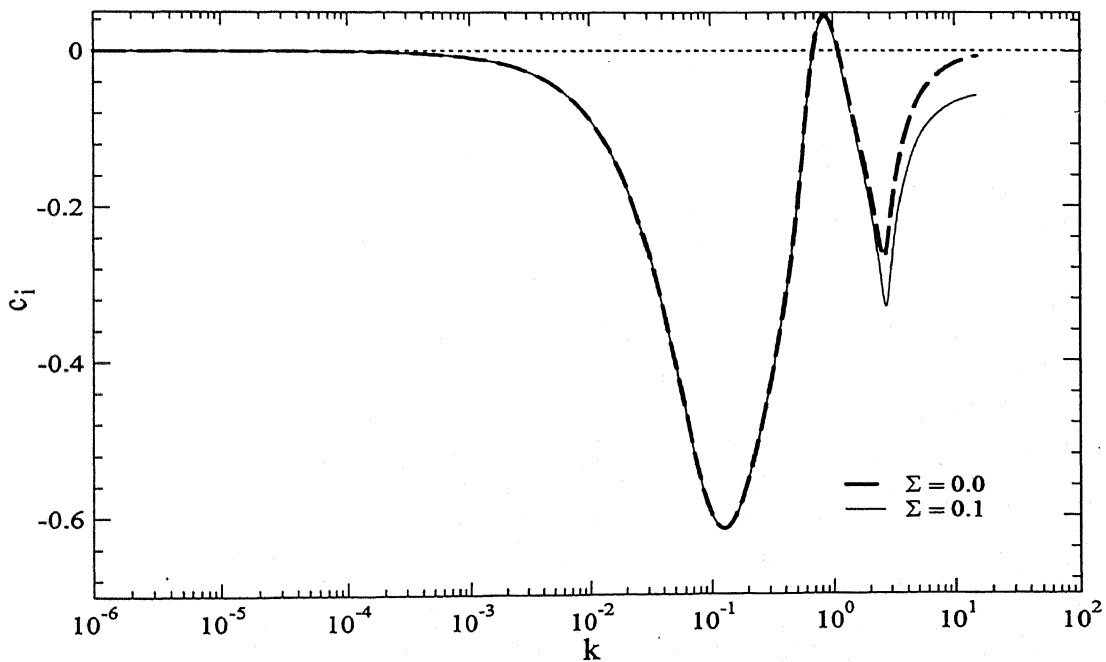


Figure 2.10 Effect of nonzero gas-liquid interfacial tension on c_i vs k for $H=2, Re=1, \Gamma=0.5, \eta_r=0$ and $\theta=45^\circ$.

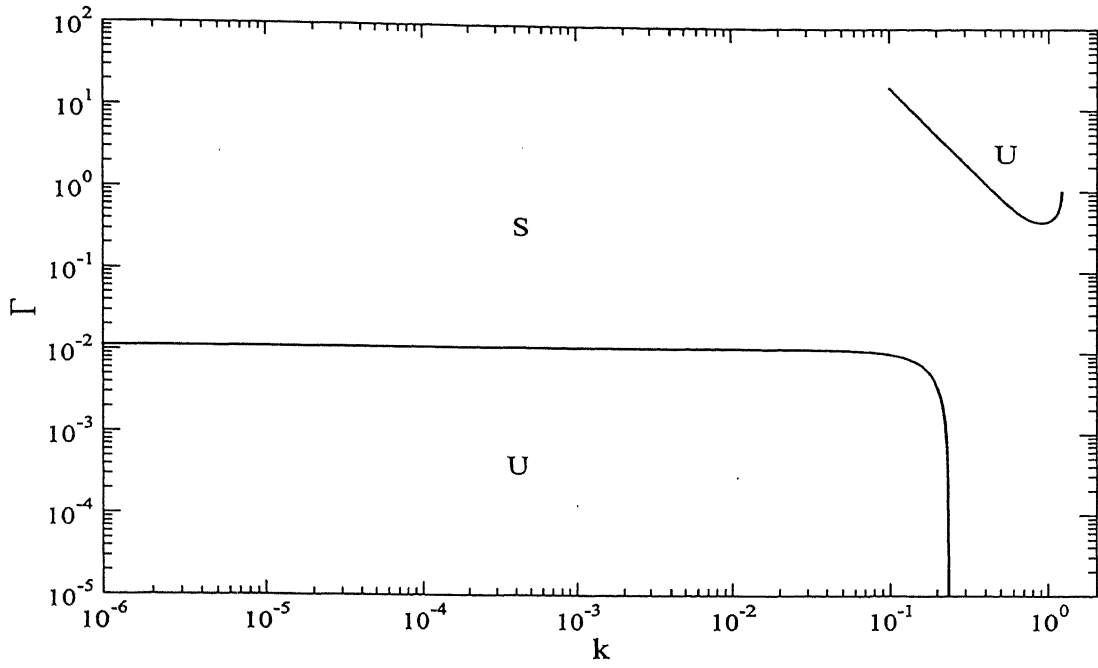


Figure 2.11 Neutral stability curves: Γ vs k for $H=2$, $Re=1$, $\eta_r=0$, $\Sigma=0$ and $\theta=45^\circ$. Stable regions are denoted by S, unstable regions by U.

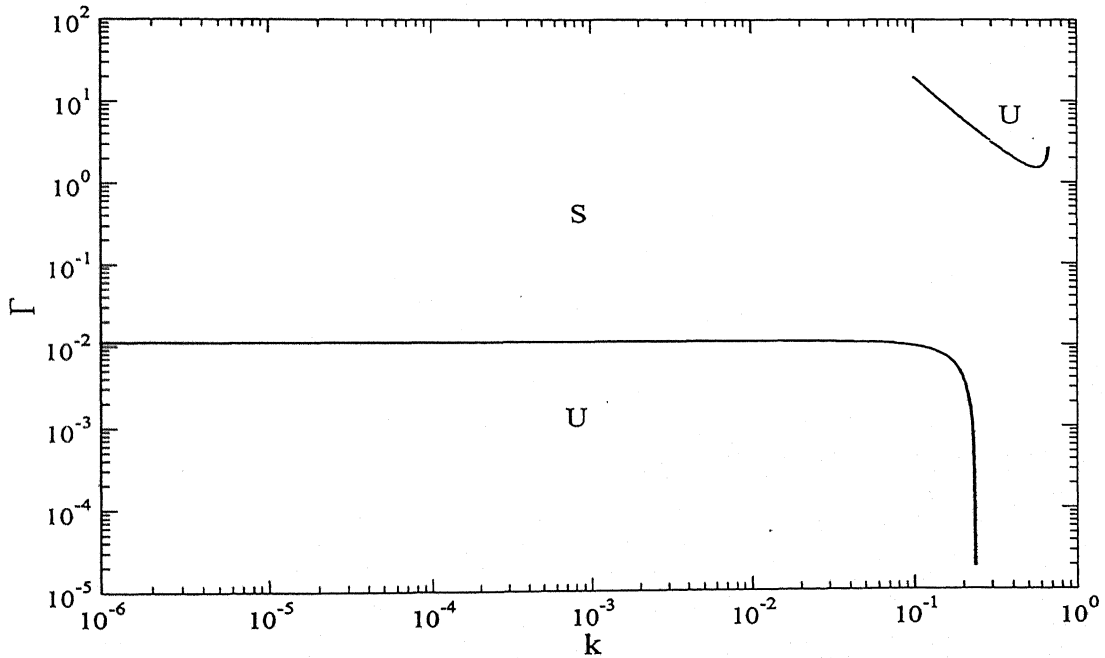


Figure 2.12 Neutral stability curves: Γ vs k for $H=2$, $Re=1$, $\eta_r=0.5$, $\Sigma=0$ and $\theta=45^\circ$. Stable regions are denoted by S, unstable regions by U.

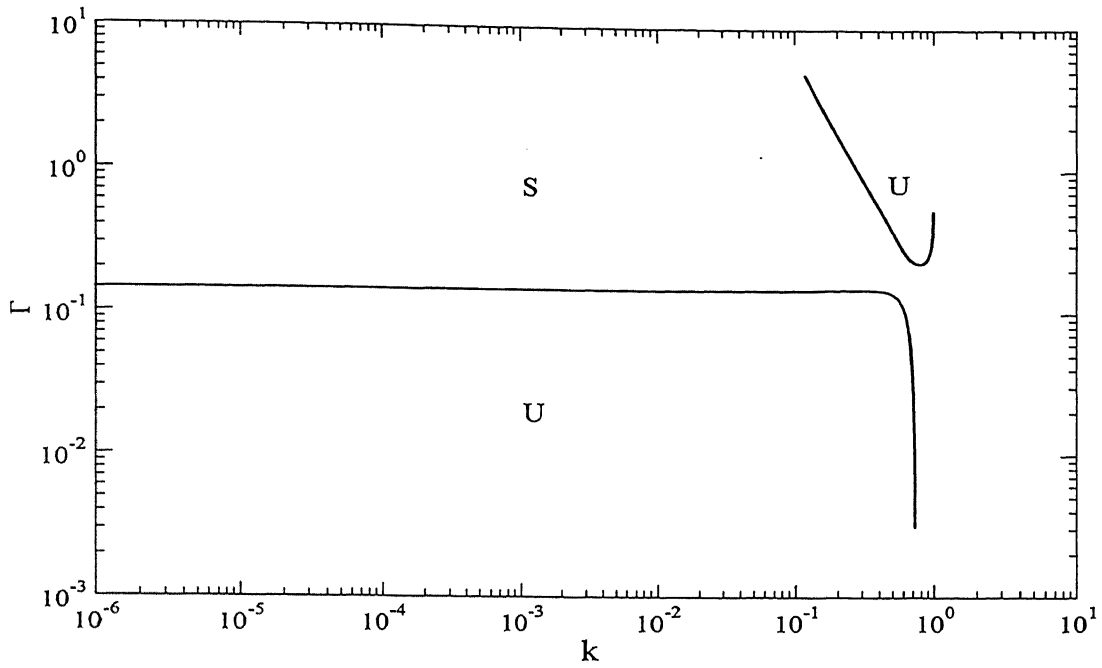


Figure 2.13 Neutral stability curves: Γ vs k for $H=2$, $Re=3$, $\eta_r=0$, $\Sigma=0$ and $\theta=45^\circ$. Stable regions are denoted by S, unstable regions by U.

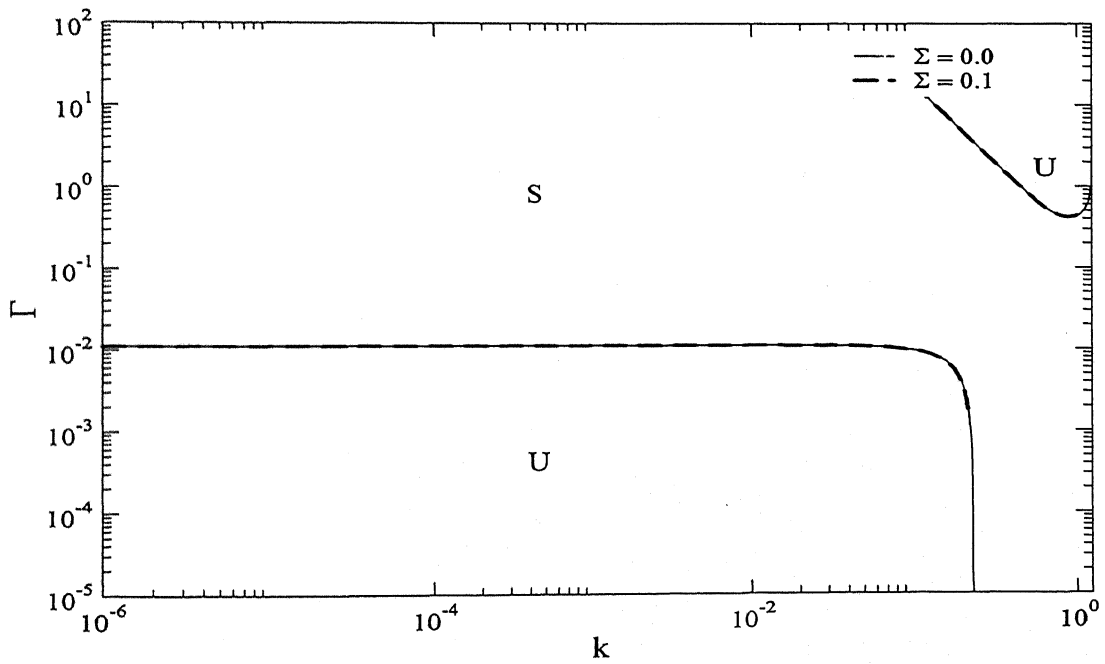


Figure 2.14 Neutral stability curves: Γ vs k for $H=2$, $Re=1$, $\eta_r=0$ and $\theta=45^\circ$. Stable regions are denoted by S, unstable regions by U.

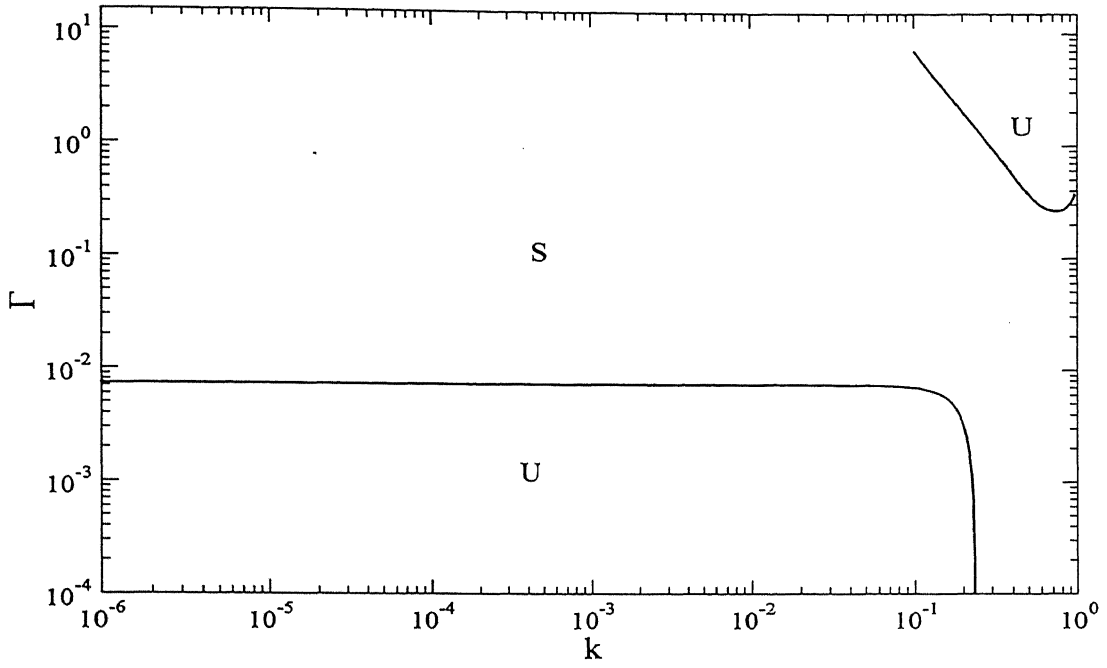


Figure 2.15 Neutral stability curves: Γ vs k for $H=3$, $Re=1$, $\eta_r=0$, $\Sigma=0$ and $\theta=45^\circ$. Stable regions are denoted by S, unstable regions by U.

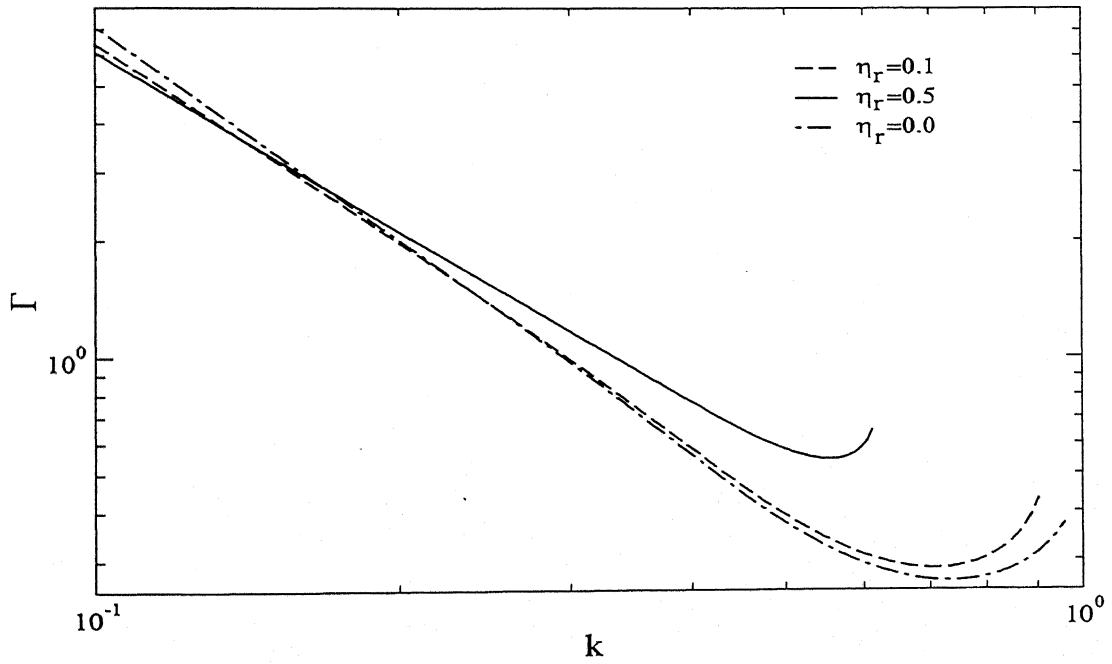


Figure 2.16 Effect of viscosity of soft solid layer on Γ vs k for $Re=1$, $\theta=45^\circ$, $\Sigma=0$ and $H=3$.

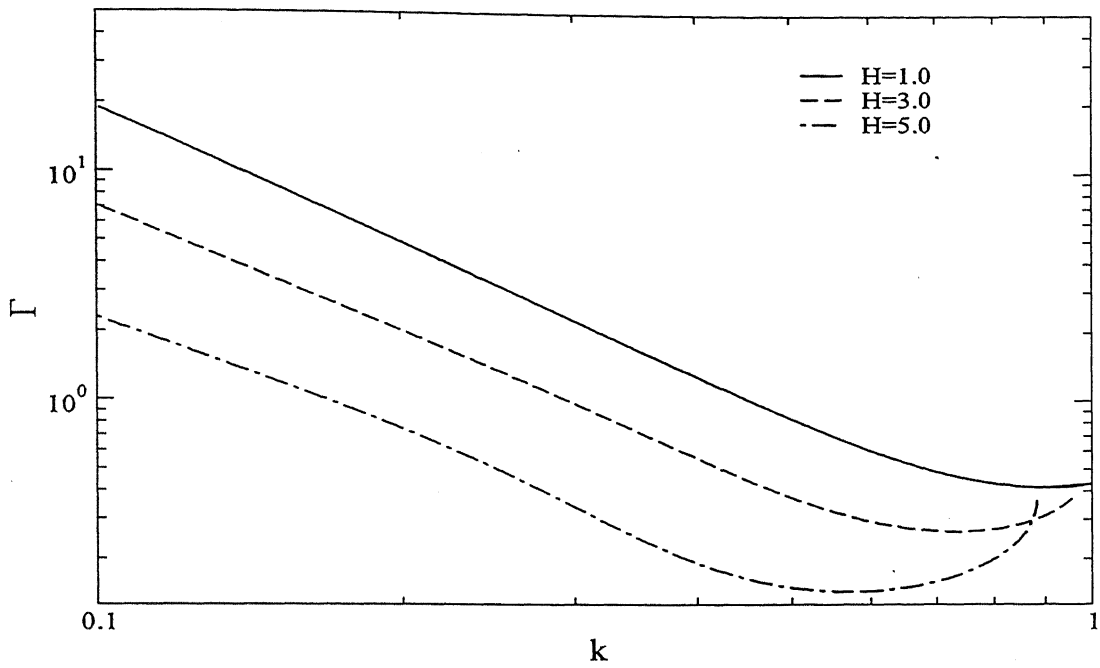


Figure 2.17 Effect of thickness of soft solid layer on Γ vs k for $Re=1, \theta=45^\circ, \eta_r=0$ and $\Sigma=0$.

Chapter 3

Stability of Pressure-driven Two-Layer Plane Poiseuille Flow in a Channel Lined with Soft Solid Layer

In this chapter, we consider the stability of pressure-driven two-layer plane Poiseuille flow of Newtonian fluids in a channel lined with soft solid layer. Multilayer flows of immiscible liquids are involved in several engineering application such as in multilayer extrusion of plastic films, in multilayer coating and in the transportation of oil. At certain processing conditions, wavy interfaces are observed in these multilayer flows and this is known as “interfacial instability”. In the present study we consider plane Poiseuille flow of two layers of Newtonian fluid having different physical properties and study the effect of soft solid layer on the interfacial instability.

This chapter is structured as follows: The governing equations, base state and the linearized stability analysis are presented in Sec. 3.1. In Sec. 3.2, we present the low wavenumber asymptotic results. In Sec. 3.3, we briefly discuss the numerical method used to study finite wavenumber perturbations, and in Sec. 3.4 we provide representative results for the complex wavespeed as a function of the wavenumber, and neutral stability diagrams in appropriate parameter space. Conclusions are given in Sec. 3.5.

3.1 Problem Formulation

The system under consideration (shown in Figure 3.1) consists of two layers of linear viscoelastic solid of thickness H_1R and H_2R , shear modulus E_1 and E_2 , and viscosity $\mu_g^{(1)}$ and $\mu_g^{(2)}$ fixed onto rigid surfaces at $z = -H_1R$ and $z = (1+H_2)R$ respectively, a layer of Newtonian fluid (fluid B) of thickness βR in the region $0 < z < \beta R$ with viscosity μ_b , and another Newtonian fluid (fluid A) of thickness $(1-\beta)R$ in the region $\beta R < z < R$ with viscosity μ_a . We have assumed that the densities of the fluids are equal ($\rho_a = \rho_b = \rho$), in order to exclusively focus on the instability of the two-fluid interface due to viscosity stratification. The soft solid layer is modeled as an incompressible linear viscoelastic solid, similar to that used in the previous chapter as well as in the previous studies [13]. The base flow consists of two parabolic profiles. Similar to the previous problem, small perturbations to the flow are induced by spontaneous fluctuations, and we study the effect of walls deformability on the stability of these perturbations.

3.1.1 Dimensional Governing Equations

The governing equations for fluid and solid layer are same as in Chapter 2.

Equation of continuity

$$\partial_i v_i^\alpha = 0. \quad (3.1)$$

Equation of motion [Navier-Stokes equation]

$$\rho(\partial_t + v_j^\alpha \partial_j) v_i^\alpha = -\partial_i p_f^\alpha + \mu^\alpha \partial_j^2 v_i^\alpha. \quad (3.2)$$

Here $\alpha = a$ and b represents the upper and lower fluid respectively. The soft solid layer is considered to be incompressible, so that the displacement field satisfies the following incompressibility condition

$$\partial_i u_i^\varphi = 0. \quad (3.3)$$

Equation of motion [Linear viscoelastic model]

$$\rho_g (\partial_t^2 u_i^\varphi) = -\partial_i p_g^\varphi + E^\varphi \partial_j^2 u_i^\varphi + \mu_g^\varphi \partial_i \partial_j^2 u_j^\varphi. \quad (3.4)$$

Here $\varphi = 1$ and 2 are indices for soft solid layers at top and bottom plates respectively. In these equations $v_i^\alpha, u_i^\varphi, p_f^\alpha$ and p_g^φ characterizes the velocity field in the fluid layers, displacement field of solid layers, pressure field in fluid and the pressure in viscoelastic solid layers respectively. The soft solid layer (1) is fixed onto a rigid surface and it satisfies the no slip condition at $z = -H_1 R$

$$u_i^{(1)} = 0 \quad (3.5)$$

The continuity of velocities and stresses at fluid-fluid and fluid-solid interfaces give rise to following equations

at fluid-solid interface ($z = 0$) continuity of velocities and stresses

$$\partial_i u_i^{(1)} = v_i^b, \quad (3.6)$$

$$\Pi_{ij}^{(1)} n_j = T_{ij}^b n_j, \quad (3.7)$$

at fluid-fluid interface ($z = \beta R$) continuity of velocities and stresses

$$v_i^b = v_i^a \quad (3.8)$$

$$T_{ij}^b n_j = T_{ij}^a n_j \quad (3.9)$$

at fluid-solid interface ($z = R$) continuity of velocities and stresses

$$v_i^\alpha = \partial_i u_i^{(2)} \quad (3.10)$$

$$T_{ij}^\alpha n_j = \Pi_{ij}^{(2)} n_j \quad (3.11)$$

The soft solid layer (2) satisfies no slip condition at $z = (1 + H_2)R$

$$u_i^{(2)} = 0. \quad (3.12)$$

The dimensional total stress tensor T_{ij}^α in the two fluids is given by

$$T_{ij}^\alpha = -p_f^\alpha \delta_{ij} + \tau_{ij}^\alpha, \quad (3.13)$$

$$\tau_{ij}^\alpha = \mu^\alpha (\partial_i v_j^\alpha + \partial_j v_i^\alpha), \quad (3.14)$$

where τ_{ij}^α is the deviatoric stress tensor in the fluid α and p_f^α is pressure in the fluid α .

The nondimensional total stress tensor Π_{ij}^α in solid layers is given by

$$\Pi_{ij}^\varphi = -p_g^\varphi \delta_{ij} + \sigma_{ij}^\varphi, \quad (3.15)$$

$$\sigma_{ij}^\varphi = (E^\varphi + \mu_g^\varphi \partial_i) (\partial_i u_j^\varphi + \partial_j u_i^\varphi), \quad (3.16)$$

where σ_{ij}^φ is the deviatoric stress tensor in the soft solid layer φ .

3.1.2 Nondimensional Governing Equations

The scales used to nondimensionalize various physical quantities are as follows: R for

lengths and displacement, $v_c = \frac{-GR^2}{2\mu_b}$ for the velocities where G is constant pressure

gradient, $\frac{R}{v_c}$ for time, and $\frac{\mu_b v_c}{R}$ for stresses and pressure. H_1 and H_2 , therefore, are

nondimensional thickness of solid layers, while $(1 - \beta)$ and β are, respectively, the

nondimensional thickness of fluid A and B . From this point onwards, all the variables are nondimensional unless it is explicitly stated that they are dimensional.

The Nondimensional governing equations in the two fluids are, respectively, the Navier-Stokes continuity and momentum equation:

$$\partial_i v_i^\alpha = 0 \quad (3.17)$$

$$Re(\partial_i + v_j^\alpha \partial_j) v_i^\alpha = -\partial_i p_f^\alpha + \mu_r^\alpha \partial_j^2 v_i^\alpha \quad (3.18)$$

Here, $Re = \frac{Rv_c \rho}{\mu_b}$ is the Reynolds number based on viscosity of fluid B , and

$\mu_r^a \equiv \mu_r = \frac{\mu_a}{\mu_b}, \mu_r^b = \frac{\mu_b}{\mu_b} = 1$ are the viscosity ratios. The nondimensional total stress tensor

T_{ij}^α in the two fluids is given by

$$T_{ij}^\alpha = -p_f^\alpha \delta_{ij} + \tau_{ij}^\alpha, \quad (3.19)$$

$$\tau_{ij}^\alpha = \mu_r^\alpha (\partial_i v_j^\alpha + \partial_j v_i^\alpha), \quad (3.20)$$

The nondimensional governing equations for soft solid layers are same as in Chapter 2. The displacement field satisfies the continuity.

$$\partial_i u_i^\varphi = 0 \quad (3.21)$$

The momentum conservation equation is given by

$$Re(\partial_i^2 u_i^\varphi) = \partial_j \Pi_{ij}^\varphi, \quad (3.22)$$

The nondimensional total stress tensor Π_{ij}^α in solid layers is given by

$$\Pi_{ij}^\varphi = -p_g^\varphi \delta_{ij} + \sigma_{ij}^\varphi \quad (3.23)$$

$$\sigma_{ij}^\varphi = \left(\frac{1}{\Gamma_\varphi} + \eta_r^\varphi \partial_i \right) (\partial_j u_i^\varphi + \partial_i u_j^\varphi) \quad (3.24)$$

Nondimensional boundary conditions are:

at $z = -H_1$ [bottom rigid plate]

$$\bar{u}_x^{(1)} = 0, \quad \bar{u}_z^{(1)} = 0 \quad (3.25)$$

at $z = 0$ [Fluid B -Solid (1) interface]

$$v_z^b = \partial_t u_z^{(1)} \quad (3.26)$$

$$v_x^b = \partial_t u_x^{(1)} \quad (3.27)$$

$$T_{zx}^b = \Pi_{zx}^{(1)} \quad (3.28)$$

$$T_{zz}^b = \Pi_{zz}^{(1)} \quad (3.29)$$

at $z = \beta$ [fluid A -Fluid B interface]

$$v_z^a = v_z^b \quad (3.30)$$

$$v_x^a = v_x^b \quad (3.31)$$

$$T_{zx}^a = T_{zx}^b \quad (3.32)$$

$$T_{zz}^a = T_{zz}^b \quad (3.33)$$

at $z = 1$ [Solid (2)-Fluid A interface]

$$v_z^a = \partial_t u_z^{(2)} \quad (3.34)$$

$$v_x^a = \partial_t u_x^{(2)} \quad (3.35)$$

$$T_{zx}^a = \Pi_{zx}^{(2)} \quad (3.36)$$

$$T_{zz}^a = \Pi_{zz}^{(2)} \quad (3.37)$$

at $z = 1 + H_2$ [top rigid plate]

$$\bar{u}_x^{(2)} = 0, \quad \bar{u}_z^{(2)} = 0 \quad (3.38)$$

3.1.3 Base State

The steady velocity profiles in the two fluids are simply the Poiseuille flow velocity profiles:

$$\bar{v}_x^b = -z^2 + \phi z, \quad (3.39)$$

$$\bar{v}_x^a = \frac{1}{\mu_r} (1 - z^2 + \phi(z-1)), \quad (3.40)$$

where $\phi = \frac{\beta^2(\mu_r - 1) + 1}{\beta(\mu_r - 1)}$.

3.1.4 Linear Stability Analysis

In this section, the stability problem is formulated by the method of normal modes [3]. The velocity and other dynamical quantities in the two fluids and the solid layers are decomposed into two parts, the base fields and infinitesimal perturbations:

$$v_i^\alpha = \bar{v}_i^\alpha + v_i^{\alpha'}, \quad u_i^\varphi = \bar{u}_i^\varphi + u_i^{\varphi'}. \quad (3.41)$$

All the perturbation quantities are expanded in the forms of Fourier modes in the x - direction, and with an exponential dependence in time:

$$v_i^{\alpha'} = \tilde{v}_i^\alpha(z) \exp[ik(x - ct)], \quad u_i^{\varphi'} = \tilde{u}_i^\varphi(z) \exp[ik(x - ct)], \quad (3.42)$$

where k is wave number, c is wave speed and $\tilde{v}_i^\alpha(z)$ and $\tilde{u}_i^\varphi(z)$ are the eigenfunctions, determined by solving the conservation equation. For simplicity only two dimensional perturbations are considered. Substituting Eqs. (3.41) and (3.42) in the conservation equation for the fluid, Eqs. (3.17) and (3.18), we get the linearized equation for the fluid as:

$$d_z \tilde{v}_i^\alpha + ik \tilde{v}_i^\alpha = 0 \quad (3.43)$$

$$Re\{ik(\bar{v}_x^\alpha - c)\tilde{v}_x^\alpha + (d_z \bar{v}_x^\alpha)\tilde{v}_z^\alpha\} = -ik\tilde{P}_f^\alpha + \mu_r^\alpha[d_z^2 - k^2]\tilde{v}_x^\alpha \quad (3.44)$$

$$Re\{ik(\bar{v}_x^\alpha - c)\tilde{v}_z^\alpha\} = -d_z \tilde{P}_f^\alpha + \mu_r^\alpha[d_z^2 - k^2]\tilde{v}_z^\alpha \quad (3.45)$$

The above equations can be combined to give a single fourth-order, Orr-Sommerfeld-like equation for \tilde{v}_z :

$$ik Re\{(\bar{v}_x^\alpha - c)[d_z^2 - k^2] + (d_z^2 \bar{v}_x^\alpha)\}\tilde{v}_z^\alpha = \mu_r^\alpha[d_z^2 - k^2]^2 \tilde{v}_z^\alpha \quad (3.46)$$

The linearized equations for the soft solid layer are obtained by inserting (3.41) and (3.42) in (3.21) and (3.22):

$$d_z \tilde{u}_z^\varphi + ik \tilde{u}_x^\varphi = 0 \quad (3.47)$$

$$-Re k^2 c^2 \tilde{u}_x^\varphi = -ik \tilde{p}_g^\varphi + \left(\frac{1}{\Gamma_\varphi} - \eta_r^\varphi ikc\right)[d_z^2 - k^2] \tilde{u}_x^\varphi \quad (3.48)$$

$$-Re k^2 c^2 \tilde{u}_z^\varphi = -d_z \tilde{p}_g^\varphi + \left(\frac{1}{\Gamma_\varphi} - \eta_r^\varphi ikc\right)[d_z^2 - k^2] \tilde{u}_z^\varphi \quad (3.49)$$

These equations can be reduced to a single fourth-order differential equation for \tilde{u}_z^α :

$$Re k^2 c^2 [d_z^2 - k^2] \tilde{u}_z^\varphi + \left(\frac{1}{\Gamma_\varphi} - \eta_r^\varphi ikc\right)[d_z^2 - k^2]^2 \tilde{u}_z^\varphi = 0 \quad (3.50)$$

The linearized equations for perturbations to stress fields in the fluid and soft solid layer are derived from (3.19) and (3.23):

$$\tilde{T}_{zx}^\alpha = \mu_r^\alpha (d_z \tilde{v}_x^\alpha + ik \tilde{v}_z^\alpha), \quad \tilde{T}_{zz}^\alpha = -\tilde{p}_f^\alpha + 2\mu_r^\alpha d_z \tilde{v}_z^\alpha, \quad (3.51)$$

$$\tilde{\Pi}_{zx}^\varphi = \left(\frac{1}{\Gamma_\varphi} - ikc\eta_r^\varphi\right)(d_z \tilde{u}_x^\varphi + ik \tilde{u}_z^\varphi), \quad \tilde{\Pi}_{zz}^\varphi = -\tilde{p}_g^\varphi + \left(\frac{1}{\Gamma_\varphi} - ikc\eta_r^\varphi\right)2d_z \tilde{u}_z^\varphi \quad (3.52)$$

The linearized boundary conditions at the unperturbed interface position $z = 0$ between fluid B and the solid layer B are obtained by Taylor expanding about the flat interface position in the base state. These become

$$\tilde{v}_z^b = -ikc\tilde{u}_z^{(1)}, \quad (3.53)$$

$$\tilde{v}_x^b + (d_z \bar{v}_x^b)_{z=0} \tilde{u}_z^{(1)} = -ikc\tilde{u}_x^{(1)}, \quad (3.54)$$

$$\tilde{T}_{zx}^b = \tilde{\Pi}_{zx}^{(1)}, \quad (3.55)$$

$$\tilde{T}_{zz}^b = \tilde{\Pi}_{zz}^{(1)}. \quad (3.56)$$

In these equations, the height of interface, $h_1(x)$, is approximated by $\tilde{u}_z^{(1)}$ at $z=0$; this approximation is valid for small perturbations. The second term in left side of equation (3.54) represents the nontrivial contribution that arises as a result of the Taylor expansion of mean flow quantities about the unperturbed fluid-solid interface. This additional term is responsible for the instability of interface between the fluid and deformable solid wall.

Similarly, the linearized boundary conditions at the unperturbed interface position at $z = \beta$ between the two fluids A and B are given by

$$\tilde{v}_z^a = \tilde{v}_z^b, \quad (3.57)$$

$$\tilde{v}_x^a + [d_z \bar{v}_x^a]_{z=\beta} \tilde{g} = \tilde{v}_x^b + [d_z \bar{v}_x^b]_{z=\beta} \tilde{g}, \quad (3.58)$$

$$\tilde{T}_{zx}^a = \tilde{T}_{zx}^b, \quad (3.59)$$

$$\tilde{T}_{zz}^a - \Sigma k^2 \tilde{g} = \tilde{T}_{zz}^b, \quad (3.60)$$

where \tilde{g} is the Fourier expansion coefficient for the interface position

$g = \tilde{g} \exp[ik(x-ct)]$, and $\Sigma = \frac{\gamma}{\mu_b \nu_c}$ is the nondimensional interfacial tension between

fluids A and B . The linearized kinematic condition at $z = \beta$ between the two fluids is given by

$$ik \left[\bar{v}_x^a \Big|_{z=\beta} - c \right] \tilde{g} = \tilde{v}_z^a. \quad (3.61)$$

The linearized boundary conditions at the unperturbed interface position at $z = 1$ between the fluid A and solid layer A , similar to (3.53)-(3.56), are given by

$$\tilde{v}_z^a = -ikc\tilde{u}_z^{(2)}, \quad (3.62)$$

$$\tilde{v}_x^a + (d_z \tilde{v}_x^a)_{z=1} \tilde{u}_z^{(2)} = -ikc\tilde{u}_x^{(2)}, \quad (3.63)$$

$$\tilde{T}_{zx}^a = \tilde{\Pi}_{zx}^{(2)}, \quad (3.64)$$

$$\tilde{T}_{zz}^a = \tilde{\Pi}_{zz}^{(2)}. \quad (3.65)$$

The boundary conditions at $z = (1 + H_2)$ are simply

$$\tilde{u}_z^{(2)} = 0, \quad \tilde{u}_x^{(2)} = 0, \quad (3.66)$$

While the boundary conditions at $z = -H_1$ are

$$\tilde{u}_z^{(1)} = 0, \quad \tilde{u}_x^{(1)} = 0. \quad (3.67)$$

Differential equations (3.46) and (3.50) along with boundary conditions (3.53)-(3.67) completely specify the stability problem of interest in this study.

The complex wavespeed c is a function of $\Gamma_\phi, \eta_r^\phi, Re, \Sigma, \beta, k, H_\phi$ and μ_r . For arbitrary Re and k , there are no closed form solutions to the fourth-order differential equation (3.49), and so a numerical method must be used to solve the stability problem in general. However, when we consider very long waves, i.e., $k \ll 1$, an asymptotic analysis in the small parameter k is possible, similar to the analysis of Yih [17], which yields an analytical expression for the wavespeed as an asymptotic series in k . In the following section, we briefly discuss the low wavenumber asymptotic results carried out by Shankar [12]. These low- k results are then used as starting guesses for a complete numerical treatment of the stability problem.

3.2 Asymptotic Results

The asymptotic analysis carried out by Shankar [12] gives an analytical expression for complex wave speed, but is valid only for long-waves ($k \ll 1$):

$$c = c^0 + kc^1, \quad (3.68)$$

where leading order c^0 is purely real and first correction c^1 is purely imaginary. The asymptotic analysis shows that at in the $k \rightarrow 0$ limit, the parameter Σ (interfacial tension) and η_r^ϕ do not appear in c^0 and c^1 . The analytical expression for c^1 is very complicated when remaining parameters $\Gamma_\phi, \eta_r^\phi, Re, \Sigma, \beta, k, H_\alpha$ and μ_r are left unspecified. However, when only β and μ_r are specified, it is possible to obtain analytical expressions for c^1 with the other parameters left unspecified. First we consider two layers of fluid with single soft solid layer fixed onto bottom plate. For $\mu_r = 2$ and $\beta = 0.6$, the results for c^0 and c^1 are

$$c^0 = 0.168052, \quad (3.69)$$

$$c^1 = i \left\{ -0.00283 \Gamma_1 (H_1 - 1.2368) H_1 (H_1 + 0.01897) + 0.00001792 Re \right\}. \quad (3.70)$$

The first correction c^1 , has two contributions: the term proportional to Re is destabilizing. However, there is another term proportional to Γ_1 and H_1 which appears due to the presence of the solid layer placed at bottom plate. This soft solid layer contribution gets change by changing the arrangement of solid layer. Since c^0 is independent from Γ_ϕ and H_ϕ and depends only on β and μ_r , for same values of β and μ_r but solid layer at top plate value of c^0 is same. The analytical expression for first correction c^1 is very different and is given by

$$c^1 = i \left\{ -0.01536 \Gamma H_2 - 0.01119 \Gamma_2 H_2^2 - 0.00283 \Gamma H_2^3 + 0.00001792 Re \right\} \quad (3.71)$$

On comparing Eq. (3.70) with (3.71), we find that for $\beta = 0.6$ and $\mu_r = 2$ if we place the solid layer on bottom plate then solid layer is stabilizing only when nondimensional thickness H is greater than 1.2368 while in the case of solid layer fixed onto top plate, it is always stabilizing irrespective of values of H .

Now we consider the configuration where $\mu_r = 0.25 (< 1)$. First we consider two layers of fluid with single soft solid layer fixed onto bottom plate. For $\mu_r = 0.25$ and $\beta = 0.4$, the results are

$$c^0 = 0.458211 \quad (3.72)$$

$$c^1 = i \left\{ -0.1701 \Gamma_1 H_1 - 0.1574 \Gamma H_1^2 - 0.0461 \Gamma H_1^3 + 0.0008859 Re \right\} \quad (3.73)$$

For same values of β and μ_r , but solid layer at top plate, the analytical expression for first correction c^1 is

$$c^1 = i \left\{ -0.04610 \Gamma_2 (H_2 - 0.6318) H_2 (H_2 + 0.2176) + 0.0008859 Re \right\} \quad (3.74)$$

In this case where μ_r is less than 1 it is advantageous to fix the solid layer onto bottom plate because it is stabilizing for all values of H_1 , while it is destabilizing if $H_2 < 0.6318$ when it is placed with the top plate.

In general, therefore, the asymptotic results can be expressed as follows:

$$c = c^0 + k i \left[\Gamma_\phi H_\phi F(H_\phi) + Re C_1 \right], \quad (3.75)$$

where c^0 is purely real, $F(H_\phi)$ is a real valued function of H_ϕ (which can be positive or negative depending upon H_ϕ) that represents the effect of solid layer, and C_1 is a real constant that represents the contribution due to viscosity stratification between the two

fluids. A few representative results for $F(H_\phi)$ and C_1 are summarized for different values of μ_r (>1 as well as <1) and β in Tables 3.1 - 3.6. From these results (and from the results for other values of μ_r and β which are not presented here), the general trend appears to be that when the two fluid layers are arranged so that they undergo the long-wave two-layer viscosity stratification instability, the solid layer usually has a stabilizing effect in the long-wave limit. The stabilization due to presence of solid layer depends on placement of solid layer, if it is placed next to more viscous fluid then its thickness has no qualitative effect on stabilization, while if it is placed near to less viscous fluid then stabilization occurs only when nondimensional thickness H_ϕ exceeds a critical value and this critical value depends on thickness ratio of fluids (β). On the other hand, when the two fluid layers are arranged so that the interface is stable in the long-wave limit, then the solid layer usually has a destabilizing effect, but this destabilization is also affected by placement of solid layer. If solid layer is next to more viscous fluid then it is destabilizing irrespective of thickness H_ϕ in the long-wave limit, while it could be stabilizing for certain values of H_ϕ if it is placed near to less viscous fluid.

For example, the result for $\mu_r = 2$ and $\beta = 0.6$ (see Table 3.1) shows that the solid layer placed at top plate has a stabilizing effect for all values of H_2 while solid layer at bottom plate is stabilizing for $H_1 > 1.2368$. In the same table for $\beta = 0.2$, solid layer at bottom plate is destabilizing for all values of H_1 and solid layer at top plate is stabilizing for $H_2 < 0.9922$.

The asymptotic results when solid layers are placed on both the plates for $\mu_r = 2$ and $\beta = 0.6$ is obtained simply by adding the contributions from top and bottom solid layers. This is possible owing to the linearity of the problem.

$$c^0 = 0.168052 \quad (3.76)$$

$$c^1 = i \left\{ \begin{array}{l} -0.00283 \Gamma_1 (H_1 - 1.2368) H_1 (H_1 + 0.01897) \\ -0.01536 \Gamma_2 H_2 - 0.01119 \Gamma_2 H_2^2 - 0.00283 \Gamma_2 H_2^3 \\ + 0.00001792 Re \end{array} \right\} \quad (3.77)$$

In Eq. (3.77) first two negative terms corresponds to lower and upper soft solid layer contribution and third term is inertial contribution. This asymptotic result is obtained by simply the addition of all the contribution known in Eq. (3.70) and (3.71).

The above asymptotic results, however, are applicable only in the low- k limit. In order to determine whether the predicted stabilization extends to perturbations with finite and high- k , it is necessary to solve the governing stability equations and boundary conditions numerically. In addition, at finite- k , the interfacial mode at the fluid B -solid (1) and fluid A -solid (2) interface can become unstable when elasticity parameter Γ_φ is increased beyond a critical value. In the following section, we use the numerical solution to determine regions in the Γ_φ - k plane where the two-fluid interfacial modes is stable.

3.3 Numerical Method

The asymptotic results fails to predict the results when wavelength of a disturbance is of $O(1)$. To obtain the stability results over a wide range of wavelengths, a

numerical solution of Orr-Sommerfeld equations is undertaken. We use the same method which has been used in the previous studies [13,14] as well as to solve the stability problem of liquid flow down an inclined plane. We use a fourth-order Runge-Kutta integrator with adaptive step size control to obtain numerical representations of the linearly independent solutions to the fourth-order ODEs. We recast the fourth order ODE in each layer as a system of first-order differential equations for the variables $[\tilde{u}_z^{(1)}, d_z \tilde{u}_z^{(1)}, d_z^2 \tilde{u}_z^{(1)}, d_z^3 \tilde{u}_z^{(1)}]$. For solid layer (1), this system of equation can be integrated from $z = -H_1$ to $z = 0$, provided the values of $\tilde{u}_z^{(1)}$ and its first three derivatives are known at $z = -H_1$. The soft solid layer B satisfies the boundary conditions $\tilde{u}_z^{(1)} = 0$, and $\tilde{u}_z^{(1)} = \frac{i}{k} d_z \tilde{u}_z^{(1)} = 0$ at $z = -H_1$. We use two different sets of higher derivatives $d_z^2 \tilde{u}_z^{(1)}$ and $d_z^3 \tilde{u}_z^{(1)}$ at $z = -H_1$ that are consistent with the boundary conditions at $z = -H_1$, which will yield the two linearly independent solutions to the displacement field in soft solid layer B :

$$\tilde{u}_z^{(1)} = 0, d_z \tilde{u}_z^{(1)} = 0, d_z^2 \tilde{u}_z^{(1)} = 1, d_z^3 \tilde{u}_z^{(1)} = 0, \quad (3.78)$$

$$\tilde{u}_z^{(1)} = 0, d_z \tilde{u}_z^{(1)} = 0, d_z^2 \tilde{u}_z^{(1)} = 0, d_z^3 \tilde{u}_z^{(1)} = 1. \quad (3.79)$$

Using these conditions at $z = -H_1$, we use the Runge-Kutta method to integrate the ODE [Eq. (3.50)] in solid layer B up to $z = 0$. The displacement field in soft solid is then obtained as a linear combination of these two solutions.

$$\tilde{u}_z^{(1)} = A_1 \tilde{u}_z^{(1)I} + A_2 \tilde{u}_z^{(1)II}, \quad (3.80)$$

$$d_z \tilde{u}_z^{(1)} = A_1 d_z \tilde{u}_z^{(1)I} + A_2 d_z \tilde{u}_z^{(1)II}, \quad (3.81)$$

$$d_z^2 \tilde{u}_z^{(1)} = A_1 d_z^2 \tilde{u}_z^{(1)I} + A_2 d_z^2 \tilde{u}_z^{(1)II}, \quad (3.82)$$

$$d_z^3 \tilde{u}_z^{(1)} = A_1 d_z^3 \tilde{u}_z^{(1)I} + A_2 d_z^3 \tilde{u}_z^{(1)II}, \quad (3.83)$$

here A_1 and A_2 are constants which have to be determined by the boundary conditions.

Now we evaluate the velocity field \tilde{v}_z^b of fluid B , and its higher derivatives, in terms of same constants A_1 and A_2 with the help of boundary conditions at fluid B -solid B interface i.e. Eqs. (3.53)-(3.56). Using these two set of values at $z=0$, we integrate the ODE [Eq.(3.46)] in fluid B up to $z=\beta$ and the velocity field \tilde{v}_z^b in the fluid is then obtained as a linear combination of these two set of solutions.

The soft solid layer (2) displacement field $\tilde{u}_z^{(2)}$ satisfies

$$\tilde{u}_z^{(2)} = 0, \text{ and } \tilde{u}_x^{(2)} = \frac{i}{k} d_z \tilde{u}_z^{(2)} = 0 \text{ at } z=1+H_2. \text{ Therefore, we choose the following initial}$$

conditions at $z=1+H_2$ consistent with the boundary conditions for the displacement field

$$\tilde{u}_z^{(2)} = 0, d_z \tilde{u}_z^{(2)} = 0, d_z^2 \tilde{u}_z^{(2)} = 1, d_z^3 \tilde{u}_z^{(2)} = 0, \quad (3.84)$$

$$\tilde{u}_z^{(2)} = 0, d_z \tilde{u}_z^{(2)} = 0, d_z^2 \tilde{u}_z^{(2)} = 0, d_z^3 \tilde{u}_z^{(2)} = 1. \quad (3.85)$$

Using these conditions at $z=1+H_2$, we integrate the ODE [Eq. (3.50)] in solid layer A up to $z=1$. The displacement field in soft solid A is then obtained as a linear combination of these two solutions.

$$\tilde{u}_z^{(2)} = A_3 \tilde{u}_z^{(2)I} + A_4 \tilde{u}_z^{(2)II} \quad (3.86)$$

here A_3 and A_4 are constants which have to be determined by the boundary conditions.

Now similar to previous steps we evaluate the velocity field \tilde{v}_z^a of fluid A , and its higher derivatives, in terms of same constants A_3 and A_4 with the help of boundary conditions

at fluid A -solid A interface i.e. Eqs. (3.62)-(3.65). Using these two set of values at $z = 1$, we integrate the ODE [Eq.(3.46)] in fluid A up to $z = \beta$ and the velocity field \tilde{v}_z^a in the fluid is then obtained as a linear combination of these two set of solutions.

At $z = \beta$ fluids velocity field \tilde{v}_z^a and \tilde{v}_z^b must satisfy the boundary conditions (3.57)-(3.60). We can write the equations in matrix form as:

$$\begin{bmatrix} \tilde{v}_z^{aI} & \tilde{v}_z^{aII} & \tilde{v}_z^{bI} & \tilde{v}_z^{bII} \\ \tilde{v}_x^{aI} + d_z \tilde{v}_x^{aI} \tilde{g}^I & \tilde{v}_x^{aII} + d_z \tilde{v}_x^{aII} \tilde{g}^{II} & \tilde{v}_x^{bI} + d_z \tilde{v}_x^{bI} \tilde{g}^I & \tilde{v}_x^{b(2)} + d_z \tilde{v}_x^{bI} \tilde{g}^{II} \\ \tilde{T}_{xz}^{aI} & \tilde{T}_{xz}^{aII} & \tilde{T}_{xz}^{bI} & \tilde{T}_{xz}^{bII} \\ \tilde{T}_{zz}^{aI} & \tilde{T}_{zz}^{aII} & \tilde{T}_{zz}^{bI} & \tilde{T}_{zz}^{bII} \end{bmatrix} \begin{bmatrix} A_1 \\ A_2 \\ A_3 \\ A_4 \end{bmatrix} = 0 \quad (3.87)$$

In this matrix, the subscripts I and II over the quantities refer to the solutions for the velocity and stress field at two-fluid interface calculated using the first and second set of boundary conditions respectively. For nontrivial solutions of A_1, A_2, A_3 and A_4 , determinant of matrix is set to be zero, which gives the characteristic equation. The characteristic equation is non-linear in c , so it is not possible to solve for c analytically. A Newton-Raphson iteration technique is used to solve the characteristic equation and obtain the complex wave speed, for specified values of $\Gamma_1, \Gamma_2, \eta_r^{(1)}, \eta_r^{(2)}, Re, \Sigma, \beta, k, H_1$ and H_2 .

3.4 Results and Discussion

We first briefly recapitulate the results of Yih [17]. Linear stability of two superposed fluids in shear flow was first studied theoretically by Yih [17], who derived the general expression for the complex wavespeed in the low wavenumber limit for two-layer Couette flow and showed the interfacial instability depends on geometrical and

physical parameters of flow system (β and μ_r) and it exists if the thickness of more viscous liquid is smaller than that of the less viscous liquid ($\mu_r > 1$ & $\beta > 0.5$ or $\mu_r < 1$ & $\beta < 0.5$). For the opposite case, viz., when the thickness of less viscous liquid is smaller than that of the more viscous liquid ($\mu_r < 1$ & $\beta > 0.5$ or $\mu_r > 1$ & $\beta < 0.5$), the interface is stable ("thin layer effect" [4]). These results are presented in Figure 3.2 in the form of neutral stability diagram. For plane Poiseuille flow, Yih [17] did not discuss explicitly how the interfacial instability depends on these parameters and gave numerical results only for the case $\beta = 0.5$. Yiantsios and Higgins [16] extended the Yih's [17] result for two-layer plane Poiseuille flow and showed that the interfacial mode is neutrally stable when $\mu_r = \frac{(1-\beta)^2}{\beta^2}$. Neutral stability diagram (μ_r vs β) for two-layer plane Poiseuille flow in rigid-walled channel is given in Figure 3.3.

The results of the asymptotic analysis carried out by Shankar [12] are valid only in the low wavenumber limit. Using numerical procedure described in the previous section, we obtain the results at finite wavenumber. The results of the low wavenumber asymptotic analysis are used as starting guess for these numerical solutions. First we represent the numerical results for flow in rigid-walled channel. Figure 3.4(a) and (b) shows that the interfacial instability exists in the case of flow through rigid-walled channel if the geometrical and physical parameters (β and μ_r) lie in the unstable region shown in Figure 3.3. In Figure 3.4(a) and (b) interfacial instability at finite k is stabilized by nonzero Σ . In the following discussion we consider the parameters (β and μ_r) where

the interfacial instability exists in the flow through rigid-walled channel and we study the effect of soft solid layer on the interfacial instability.

Now we present the results for the two-layer flow system with soft solid layer which is placed either on bottom plate or on top plate or on both the plates. In the Sec. 3.3 we have already discussed how the placement of solid layer affects the instability. Effect of thickness of solid layer when it is placed only on the bottom plate is presented in Figure 3.5. For $\beta = 0.4, \mu_r = 0.25$ soft solid layer is stabilizing for all values of H_1 and is shown in Figure 3.5(a). For $\beta = 0.6, \mu_r = 2$ soft solid layer is destabilizing in low wavenumber limit for $H_1 = 1.1$ which agrees with the asymptotic results [Eq.(3.70)] while for $H_1 = 2$ soft solid layer's stabilizing contribution is enough to overcome the destabilizing inertial contribution. Now we shift the position of solid layer from bottom plate to top plate and results are given in Figure 3.6. Here also we found agreement of numerical results with asymptotic results. In Figure 3.6(a) for $\beta = 0.4, \mu_r = 0.25$ solid layer is destabilizing for $H_2 = 0.5$ while it stabilizes the interface in low wavenumber limit when H_2 become 2.5. For $\beta = 0.6, \mu_r = 2$ solid layer is stabilizing for all values of H_2 in the low wavenumber limit. If we compare the results for the flow system with solid layer and without solid layer (rigid-walled channel) we find that solid layer stabilizes the interface in low wavenumber limit while it destabilizes the flow at finite- k . Now we move on to explore the effect of elasticity parameter (Γ_ϕ) on interfacial instability. Figure 3.7 and Figure 3.8 represents the results when solid layer is placed only on bottom plate and only on top plate respectively. Here we have considered sufficient thickness of solid layer so in all the cases c_i values are negative in low wavenumber

limit. From both the figures we conclude that increase in parameter Γ_ϕ decreases the c_i in low wavenumber limit but it amplifies the disturbances at finite- k .

Now we discuss the flow systems with solid layer placed on both the plates. Figure 3.9 simply present stabilized two-fluid interface in the low wavenumber limit by placing solid layers on the walls of channel where the interfacial instability exists in rigid channel. In Figure 3.10 we present the effect of interfacial tension on the instability when both of walls are deformable. Similar to previous studies [13] in the case of two-layer plane Poiseuille flow presence of strong nonzero interfacial tension can only stabilize the short wave instability. Effect of Reynolds number is given in Figure 3.11. Increase in Reynolds Number increases the growth rate at all k , thus it is always destabilizing. Figure 3.12 shows the effect of viscosity of solid layers on the instability for two different set of parameter. Qualitatively the viscosity of solid layers has no significant effect and quantitatively it has very little effect. So we can conclude that the viscosity of solid layers has no significant effect in interfacial instability. Up to now we have discussed the stability of two-fluid interfacial mode only there are two more fluid-solid interfacial modes are present. Kumaran *et al* [5,14] showed that to excite these modes elasticity parameter Γ should be $O(1)$. In the present study we have considered very small values of parameter Γ $[O(10^{-2})]$, so here the other two modes will not be excited.

It is useful to construct neutral stability curves demarcating stable and unstable regions in the $\Gamma_\phi - k$ plane, for fixed values of $\eta_r^\phi, Re, \Sigma, \beta$ and H_ϕ . Such plots allow us to select the parameter Γ_ϕ (i.e. the shear modulus of the solid layer), for complete stabilization at all wavelengths. We present the neutral stability curve for the flow system

where both of the walls of channel are deformable. So we have two elasticity parameter Γ_1 and Γ_2 and we are fixing the elasticity parameter of one solid to get Γ_ϕ vs k plots. Neutral curves are provided in Figure 3.13-Figure 3.15. The general trend appears to be when Γ_ϕ is increased beyond the neutral curve, there is transition from unstable to stable perturbations. In Figure 3.13(a) for $\beta = 0.4, \mu_r = 0.25$ when Γ_1 exceeds the value 0.00067 the fluid-fluid interface becomes stable in the low wavenumber limit from an unstable interface. Similarly in Figure 3.13(b) for $\beta = 0.6, \mu_r = 2$ when Γ_2 is increased beyond 0.00085 there is transition from unstable to stable perturbations but in the low wavenumber limit only. In both the figures perturbations at finite- k are still unstable which can be stabilized only by the presence of interfacial tension and is presented in Figure 3.14. Effect of Reynolds number on neutral stability curve is shown in Figure 3.15. This figure shows that increase in Reynolds number increases the unstable region in $\Gamma_\phi - k$ plane.

3.5 Conclusion

In conclusion, the present study concerning the stability of two-layer plane Poiseuille flow through a channel where walls of the channel are lined by soft solid layer shows that solid layer has a profound effect on the interfacial mode due to viscosity stratification between the two fluids. Shankar's [12] low wavenumber asymptotic analysis shows that the effect of solid layer appears at same order $[O(k)]$ as the destabilizing effect due to fluid inertia in the asymptotic expression for the complex wavespeed c . Both these contributions could be stabilizing or destabilizing, depending on

the fluid viscosity ratio μ_r , relative thickness of the fluid layers β , and the parameters characterizing the solid layers (Γ_ϕ, H_ϕ) . When the two fluids are arranged so that they undergo a low- k instability in rigid channels due to viscosity stratification, the solid layer invariably has a stabilizing effect on fluid-fluid interfacial mode. and in the present study we are interested only in the stabilizing behavior of solid layer. When the two fluids are arranged such that the two-fluid interfacial mode is stable, the solid layer could have both destabilizing and stabilizing effects, depending on its thickness. In the present study we explore only the stabilizing characteristics of solid layer. The placement of solid layer also affects the stabilization. When solid layer is placed next to more viscous fluid it exhibits stabilizing behavior irrespective of its thickness, while the placement of solid layer near to less viscous fluid can be destabilizing if its thickness is less than a critical value and this critical value depends on thickness ratio of fluids. The nondimensional parameter Γ_ϕ required to achieve the stabilization of two-fluid interfacial mode is typically very small compared to unity in the limit of low k . Kumaran *et al.*[5,14] showed that when $\Gamma_\phi \sim O(1)$, the interfacial mode between fluid and solid layer also become unstable. In the present study we have considered $\Gamma_\phi \sim O(10^{-2})$ so the interfacial mode between fluid and solid layer will not be excited. The results of the low wavenumber asymptotic analysis were continued to finite and higher values of k using a numerical solution of the governing stability equations. Numerical solutions showed that the solid layer has a destabilizing effect on two-fluid interfacial mode at finite and large k . These finite and short wavelength unstable perturbations can be stabilized only by the presence of a nonzero interfacial tension between the two fluids. Neutral stability curves were

TABLE 3.1 Summary of results from low wavenumber analysis when solid layer is placed at bottom plate for $\mu_r = 2.0$

β	$F(H_1)$	C_1
0.1	$9.52 \times 10^{-3} + 1.05 \times 10^{-2} H_1 + 3.59 \times 10^{-3} H_1^2$	-1.66424×10^{-6}
0.2	$1.05 \times 10^{-2} + 9.61 \times 10^{-3} H_1 + 2.61 \times 10^{-3} H_1^2$	-6.0140×10^{-6}
0.3	$5.39 \times 10^{-3} + 3.33 \times 10^{-3} H_1 + 5.93 \times 10^{-4} H_1^2$	-8.0559×10^{-6}
0.4	$4.56 \times 10^{-4} + 5.02 \times 10^{-5} H_1 + 1.41 \times 10^{-6} H_1^2$	-1.6275×10^{-6}
0.5	$-3.25 \times 10^{-4} (-3.1328 + H_1) (-1.1172 + H_1)$	1.1011×10^{-5}
0.6	$-2.84 \times 10^{-3} (-1.2368 + H_1) (0.01897 + H_1)$	1.7927×10^{-5}
0.7	$-6.89 \times 10^{-3} (-0.6221 + H_1) (0.3029 + H_1)$	1.3369×10^{-5}
0.8	$-7.79 \times 10^{-3} (-0.3110 + H_1) (0.4153 + H_1)$	6.6255×10^{-6}
0.9	$-3.52 \times 10^{-3} (-0.1230 + H_1) (0.4692 + H_1)$	2.9082×10^{-6}

TABLE 3.2 Summary of results from low wavenumber analysis when solid layer is placed at top plate for $\mu_r = 2.0$

β	$F(H_2)$	C_1
0.1	$3.59 \times 10^{-3} (-0.4079 + H_2) (0.4839 + H_2)$	-1.66424×10^{-6}
0.2	$2.61 \times 10^{-3} (-0.9922 + H_2) (0.3208 + H_2)$	-6.0140×10^{-6}
0.3	$5.94 \times 10^{-4} (-2.3457 + H_2) (-0.31912 + H_2)$	-8.0559×10^{-6}
0.4	$1.4119 (-19.4078 + H_2) (-13.1494 + H_2)$	-1.6275×10^{-6}
0.5	$-3.24 \times 10^{-4} ((3.625 - 1.3635 i) + H_2)((3.625 + 1.3635 i) + H_2)$	1.1011×10^{-5}
0.6	$-2.84 \times 10^{-3} ((2.10 - 0.98 i) + H_2)((2.10 + 0.98 i) + H_2)$	1.7927×10^{-5}
0.7	$-6.88 \times 10^{-3} ((1.65 - 0.83 i) + H_2)((1.65 + 0.83 i) + H_2)$	1.3369×10^{-5}
0.8	$-7.79 \times 10^{-3} ((1.44 - 0.75 i) + H_2)((1.44 + 0.75 i) + H_2)$	6.6255×10^{-6}
0.9	$-3.53 \times 10^{-3} ((1.33 - 0.70 i) + H_2)((1.33 + 0.70 i) + H_2)$	2.9082×10^{-6}

TABLE 3.3 Summary of results from low wavenumber analysis when solid layer is placed at bottom plate for $\mu_r = 0.25$

β	$F(H_1)$	C_1
0.1	$-0.01440 ((1.30 - 0.69 i) + H_1)((1.30 + 0.69 i) + H_1)$	1.9614×10^{-4}
0.2	$-0.0463 ((1.37 - 0.73 i) + H_1)((1.37 + 0.73 i) + H_1)$	4.0866×10^{-4}
0.3	$-0.0638 ((1.49 - 0.79 i) + H_1)((1.49 + 0.79 i) + H_1)$	5.5680×10^{-4}
0.4	$-0.0461 ((1.70 - 0.88 i) + H_1)((1.70 + 0.88 i) + H_1)$	8.8859×10^{-4}
0.5	$-0.0151 ((2.19 - 1.05 i) + H_1)((2.19 + 1.05 i) + H_1)$	9.2418×10^{-4}
0.6	$-9.90 \times 10^{-4} ((4.17 - 1.56 i) + H_1)((4.17 + 1.56 i) + H_1)$	3.6217×10^{-4}
0.7	$1.021 \times 10^{-4} (-7.8911 + H_1) (-3.7832 + H_1)$	-1.1989×10^{-4}
0.8	$4.55 \times 10^{-3} (-1.7711 + H_1) (0.0878 + H_1)$	-1.9493×10^{-4}
0.9	$1.31 \times 10^{-2} (-0.6925 + H_1) (0.4732 + H_1)$	-6.8955×10^{-5}

TABLE 3.4 Summary of results from low wavenumber analysis when solid layer is placed at top plate for $\mu_r = 0.25$

β	$F(H_2)$	C_1
0.1	$-1.44 \times 10^{-1} (-0.0643 + H_2) (0.4614 + H_2)$	1.9614×10^{-4}
0.2	$-3.33 \times 10^{-2} (-0.1673 + H_2) (0.4157 + H_2)$	4.0866×10^{-4}
0.3	$-6.38 \times 10^{-2} (-0.3353 + H_2) (0.3476 + H_2)$	5.5680×10^{-4}
0.4	$-4.61 \times 10^{-2} (-0.6319 + H_2) (0.2176 + H_2)$	8.8859×10^{-4}
0.5	$-1.52 \times 10^{-2} (-1.2696 + H_2) (-0.1138 + H_2)$	9.2418×10^{-4}
0.6	$-9.90 \times 10^{-4} (-3.6684 + H_2) (-1.6835 + H_2)$	3.6217×10^{-4}
0.7	$5.72 \times 10^{-3} + 1.49 \times 10^{-3} H_2 + 1.02 \times 10^{-4} H_2^2$	-1.1989×10^{-4}
0.8	$2.83 \times 10^{-2} + 2.13 \times 10^{-2} H_2 + 4.54 \times 10^{-3} H_2^2$	-1.9493×10^{-4}
0.9	$4.08 \times 10^{-2} + 4.22 \times 10^{-2} H_2 + 1.31 \times 10^{-2} H_2^2$	-6.8955×10^{-5}

TABLE 3.5 Summary of results from low wavenumber analysis when solid layer is placed at bottom plate for $\mu_r = 4.0$

β	$F(H_1)$	C_1
0.1	$1.02 \times 10^{-2} + 1.05 \times 10^{-2} H_1 + 3.28 \times 10^{-3} H_1^2$	-1.07×10^{-6}
0.2	$7.07 \times 10^{-3} + 5.33 \times 10^{-3} H_1 + 1.14 \times 10^{-3} H_1^2$	-3.04×10^{-6}
0.3	$1.43 \times 10^{-3} + 3.74 \times 10^{-4} H_1 + 2.55 \times 10^{-5} H_1^2$	-1.87×10^{-6}
0.4	$-2.47 \times 10^{-4} (H_1 - 3.6684)(H_1 - 1.6835)$	5.87×10^{-6}
0.5	$-3.78 \times 10^{-3} (-1.2695 + H_1) (-0.1137 + H_1)$	1.44×10^{-5}
0.6	$-1.152 \times 10^{-2} (-0.6318 + H_1) (0.2176 + H_1)$	1.38×10^{-5}
0.7	$-1.59 \times 10^{-2} (-0.3352 + H_1)(0.3476 + H_1)$	8.7×10^{-6}
0.8	$-1.15 \times 10^{-2} (-0.1674 + H_1)(0.4157 + H_1)$	6.38×10^{-6}
0.9	$-3.60 \times 10^{-3} (-0.0643 + H_1)(0.4614 + H_1)$	3.06×10^{-6}

TABLE 3.6 Summary of results from low wavenumber analysis when solid layer is placed at top plate for $\mu_r = 4.0$

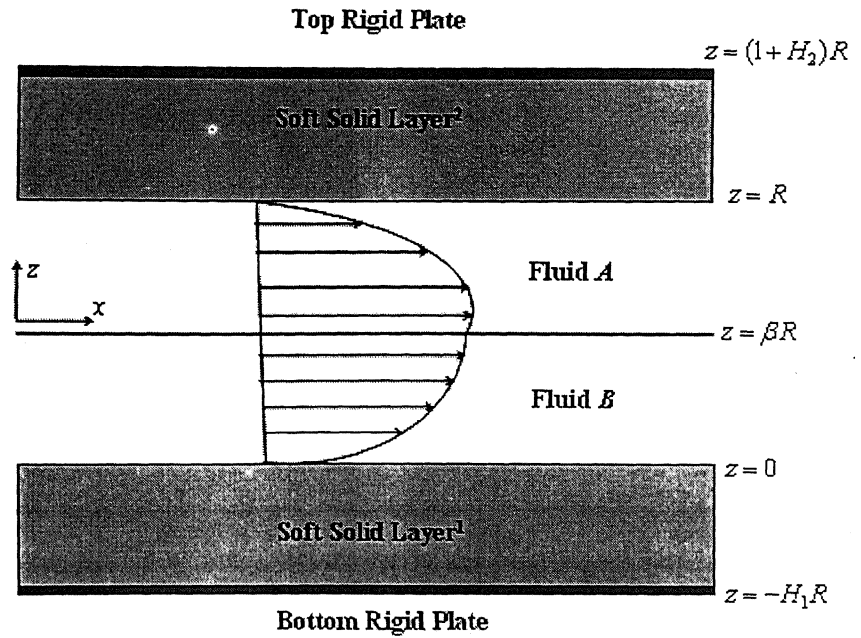
β	$F(H_2)$	C_1
0.1	$3.28 \times 10^{-3} (-0.6925 + H_2) (0.4731 + H_2)$	-1.07×10^{-6}
0.2	$1.11 \times 10^{-3} (-1.7711 + H_2) (0.0878 + H_2)$	-3.04×10^{-6}
0.3	$2.55 \times 10^{-5} (-7.8911 + H_2) (-3.7832 + H_2)$	-1.87×10^{-6}
0.4	$-3.78 \times 10^{-3} ((4.1759 - 1.5624 i) + H_2)((4.1759 + 1.5624 i) + H_2)$	5.87×10^{-6}
0.5	$-3.78 \times 10^{-3} ((2.1917 - 1.0524 i) + H_2)((2.1917 + 1.0524 i) + H_2)$	1.44×10^{-5}
0.6	$-1.11 \times 10^{-2} ((1.7071 - 0.8813 i) + H_2)((1.7071 + 0.8813 i) + H_2)$	1.38×10^{-5}
0.7	$-1.59 \times 10^{-2} ((1.4938 - 0.7919 i) + H_2)((1.4938 + 0.7919 i) + H_2)$	8.7×10^{-6}
0.8	$-1.11 \times 10^{-2} ((1.3758 - 0.7354 i) + H_2)((1.3758 + 0.7354 i) + H_2)$	6.38×10^{-6}
0.9	$-3.60 \times 10^{-3} ((1.3014 - 0.6945 i) + H_2)((1.3014 + 0.6945 i) + H_2)$	3.06×10^{-6}

TABLE 3.7 ummary of results from low wavenumber analysis when solid layer is placed only at bottom plate for $\mu_r = 0.5$

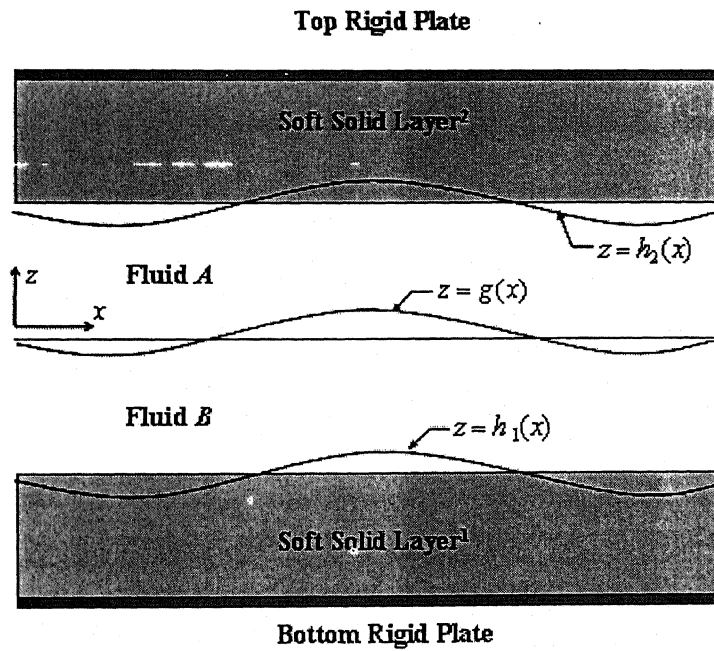
β	$F(H_1)$	C_1
0.1	$-7.05 \times 10^{-3} ((1.32 - 0.69 i) + H_1)((1.30 + 0.69 i) + H_1)$	2.326×10^{-5}
0.2	$-1.55 \times 10^{-2} ((1.44 - 0.75 i) + H_1)((1.37 + 0.73 i) + H_1)$	5.3×10^{-5}
0.3	$-1.37 \times 10^{-2} ((1.65 - 0.83 i) + H_1)((1.65 + 0.83 i) + H_1)$	1.069×10^{-4}
0.4	$-5.678 \times 10^{-3} ((2.10 - 0.98 i) + H_1)((2.10 + 0.98 i) + H_1)$	1.434×10^{-4}
0.5	$-6.49 \times 10^{-4} ((3.62 - 1.36 i) + H_1)((3.62 + 1.36 i) + H_1)$	8.88×10^{-5}
0.6	$2.82 \times 10^{-6} (-19.4078 + H_1) (-13.1494 + H_1)$	-1.30×10^{-5}
0.7	$1.118 \times 10^{-3} (-2.3457 + H_1) (-0.3191 + H_1)$	-6.44×10^{-5}
0.8	$5.23 \times 10^{-3} (-0.9922 + H_1) (0.3208 + H_1)$	-4.88×10^{-5}
0.9	$7.18 \times 10^{-3} (-0.4079 + H_1) (0.4839 + H_1)$	-1.33×10^{-5}

TABLE 3.8 Summary of results from low wavenumber analysis when solid layer is placed only at top plate for $\mu_r = 0.5$

β	$F(H_2)$	C_1
0.1	$-7.05 \times 10^{-3} (-0.1230 + H_2) (0.4692 + H_2)$	2.326×10^{-5}
0.2	$-1.55 \times 10^{-2} (-0.3110 + H_2) (0.4153 + H_2)$	5.3×10^{-5}
0.3	$-1.37 \times 10^{-3} (-0.6221 + H_2) (0.3029 + H_2)$	1.069×10^{-4}
0.4	$-5.67 \times 10^{-3} (-1.2368 + H_2) (0.01897 + H_2)$	1.434×10^{-4}
0.5	$-6.49 \times 10^{-4} (-3.1328 + H_2) (-0.1172 + H_2)$	8.88×10^{-5}
0.6	$8.91 \times 10^{-4} + 1.004 \times 10^{-4} H_2 + 2.82 \times 10^{-6} H_2^2$	-1.30×10^{-5}
0.7	$1.06 \times 10^{-2} + 6.72 \times 10^{-3} H_2 + 1.18 \times 10^{-3} H_2^2$	-6.44×10^{-5}
0.8	$2.10 \times 10^{-2} + 1.92 \times 10^{-2} H_2 + 5.2 \times 10^{-3} H_2^2$	-4.88×10^{-5}
0.9	$1.90 \times 10^{-2} + 2.1 \times 10^{-2} H_2 + 7.18 \times 10^{-3} H_2^2$	-1.33×10^{-5}



(a) Base State



(b) Perturbed state

Figure 3.1 Schematic diagram of two-layer plane Poiseuille flow in a channel lined with soft solid layers.

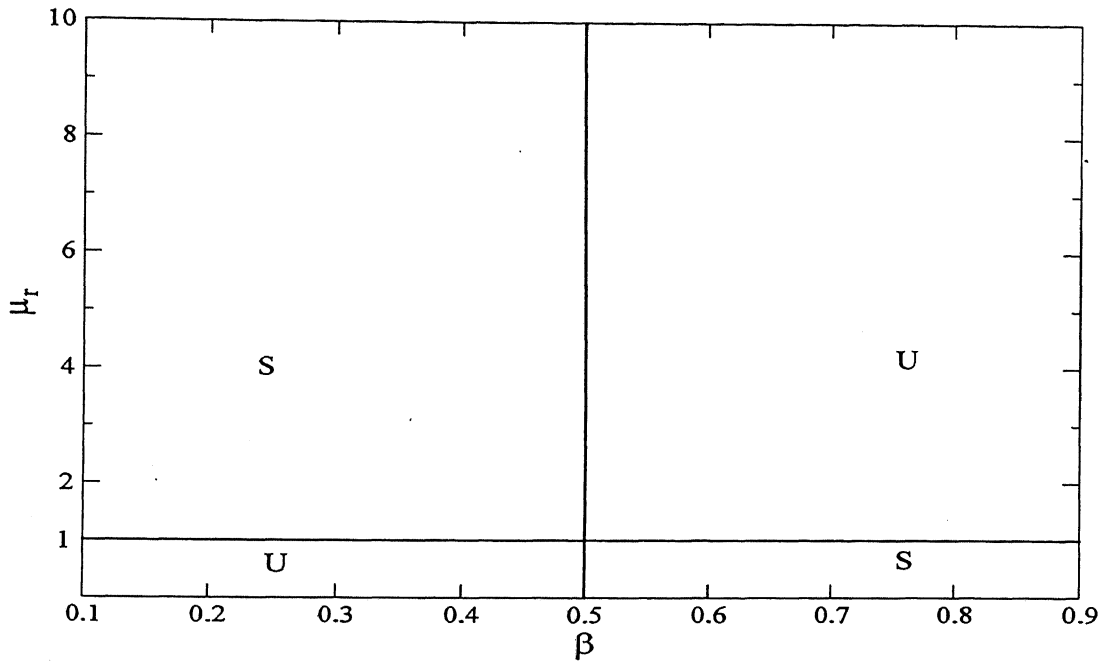


Figure 3.2 Neutral stability diagram for two-layer Plane Couette flow for long-wavelength disturbances. Stable regions are denoted by S, unstable regions by U.

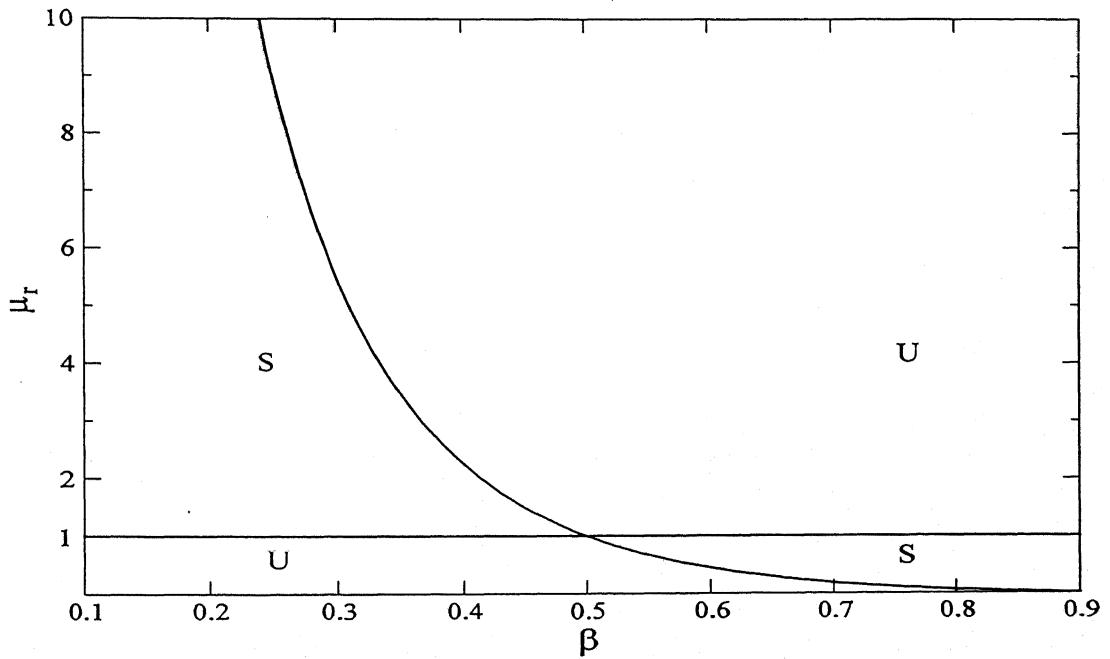
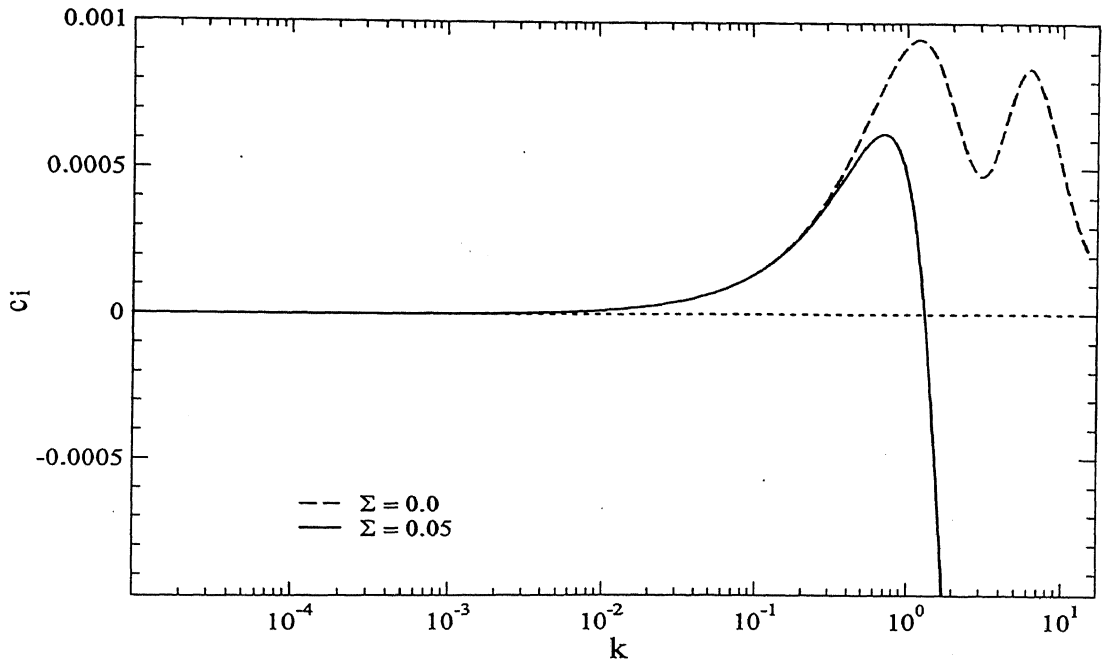
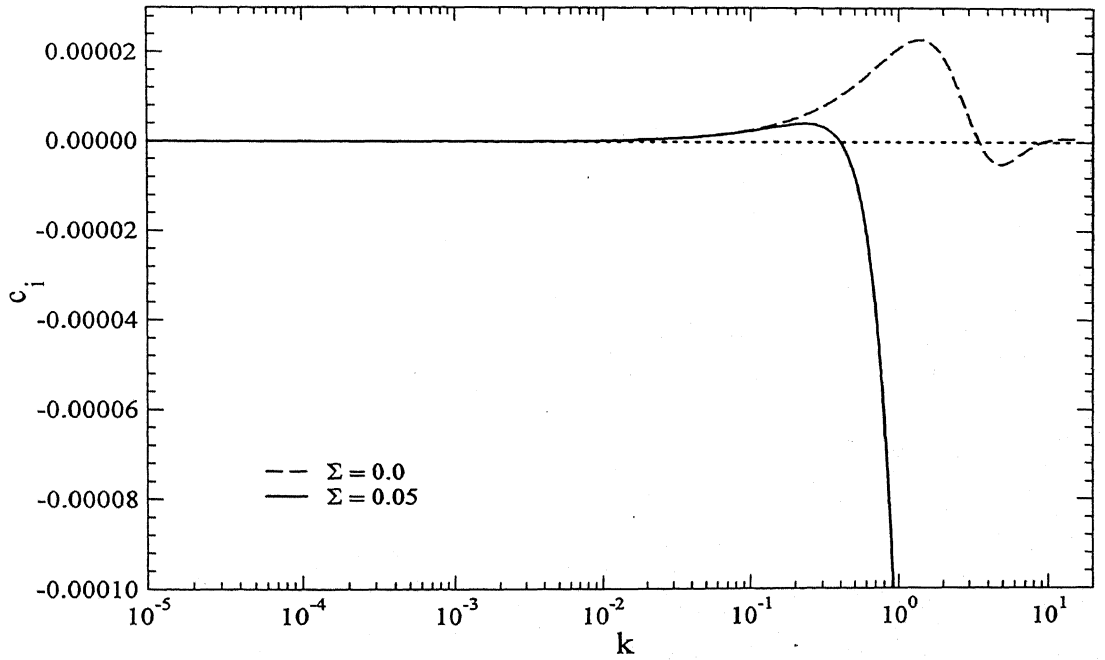


Figure 3.3 Neutral stability diagram for two-layer Plane Poiseuille flow for long-wavelength disturbances. Stable regions are denoted by S, unstable regions by U.

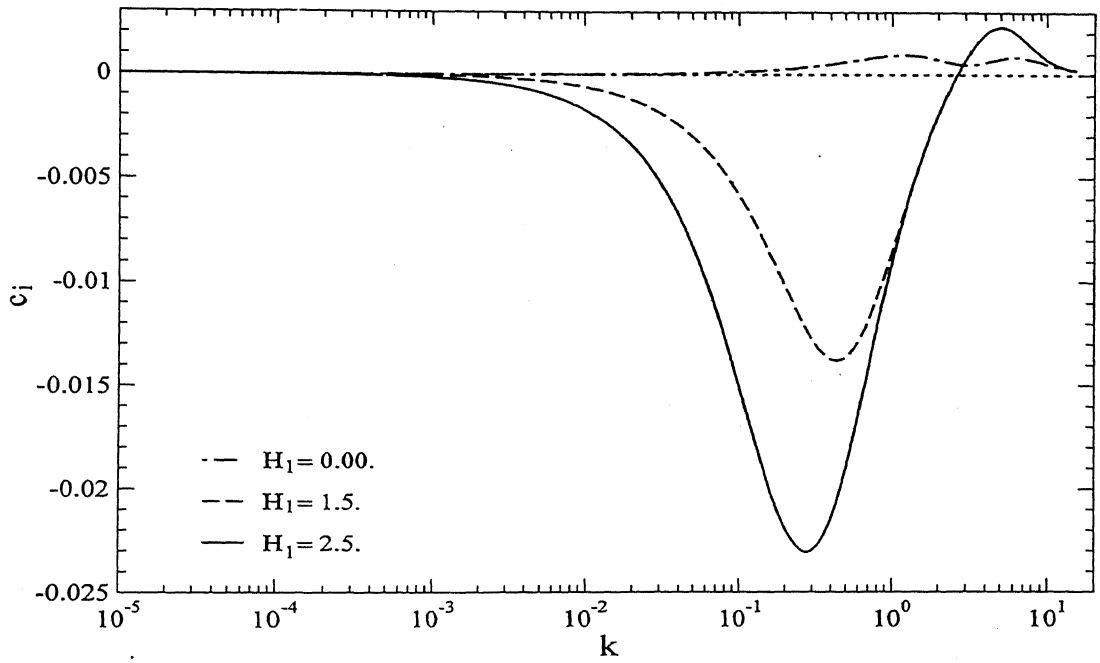


(a) $\beta = 0.4, \mu_r = 0.25$ and $Re = 1.5$.

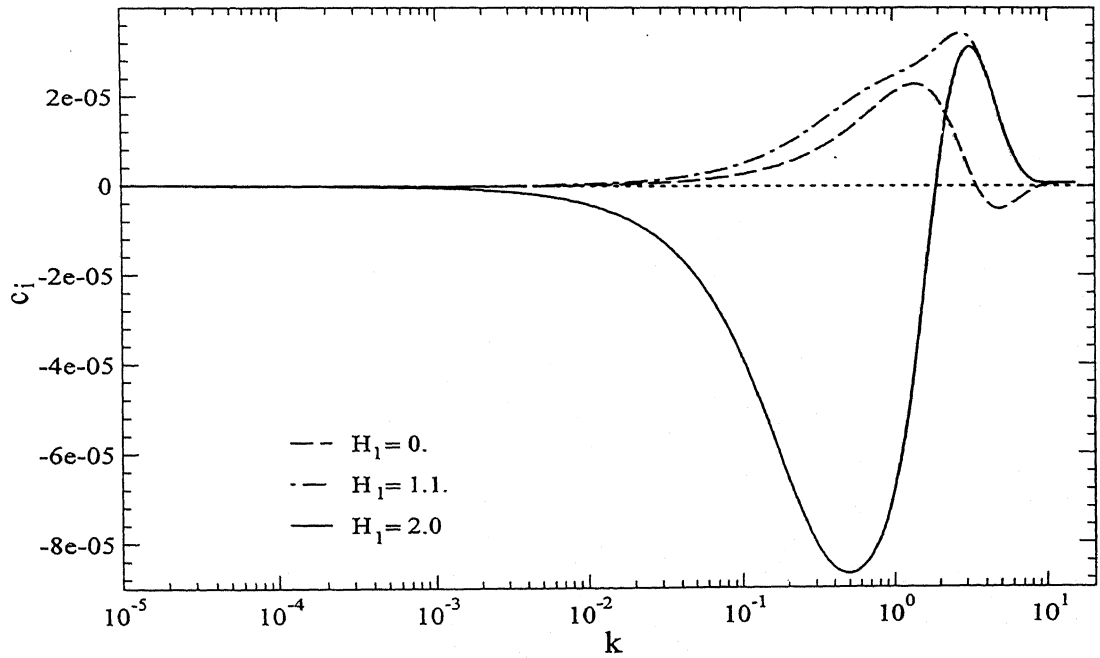


(b) $\beta = 0.6, \mu_r = 2$ and $Re = 1.5$.

Figure 3.4 Interfacial instability in the rigid channels: variation of imaginary part of wavespeed c with wavenumber k for two-layer Plane Poiseuille flow in rigid channels ($\Gamma_1 = 0$ and $\Gamma_2 = 0$).

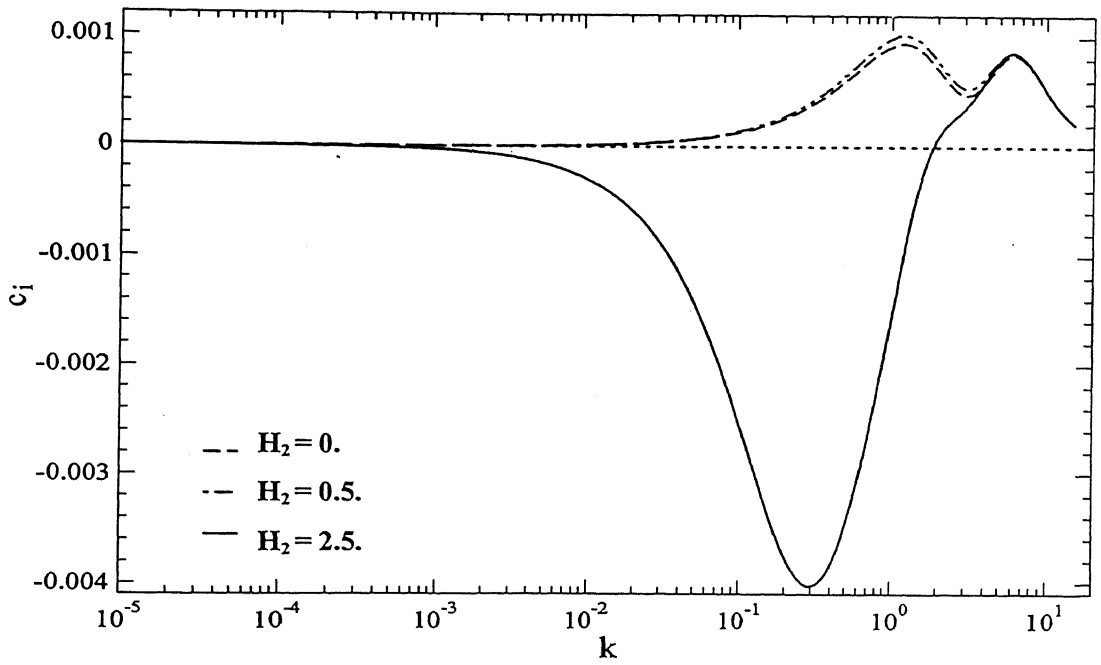


(a) $\beta = 0.4, \mu_r = 0.25, \Gamma_1 = 0.08, Re = 1.5, \Sigma = 0, \Gamma_2 = 0, H_2 = 0$.

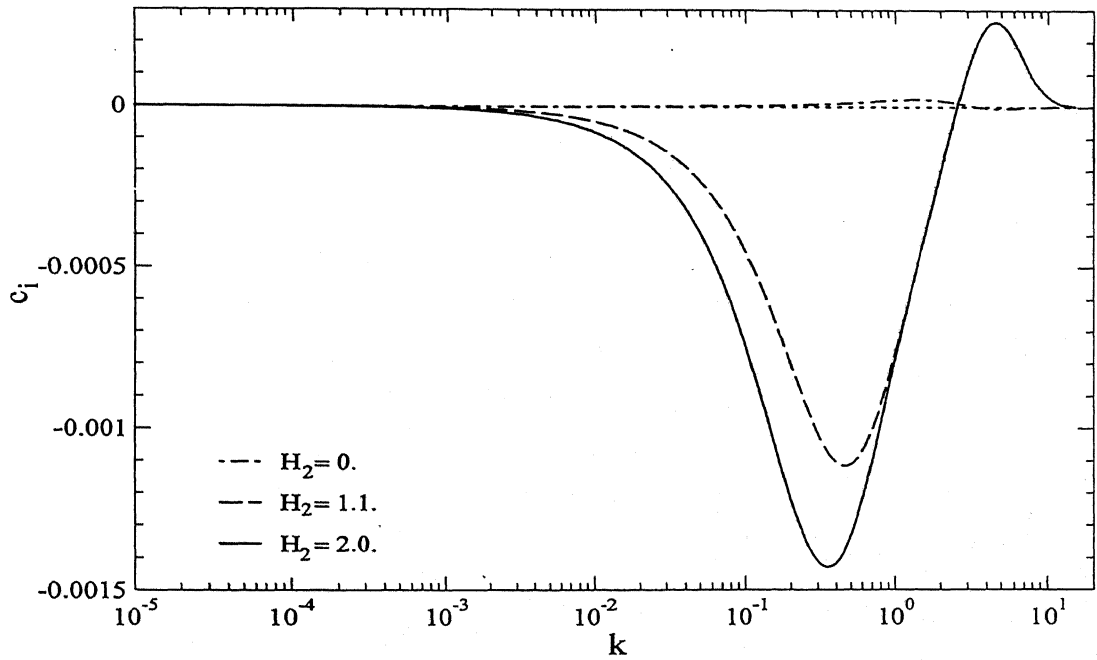


(b) $\beta = 0.6, \mu_r = 2, \Gamma_1 = 0.05, Re = 1.5, \Sigma = 0, \Gamma_2 = 0, H_2 = 0$.

Figure 3.5 Effect of solid layer deformability on fluid-fluid interfacial mode: variation of c_i with k for different values of thickness H_1 when the solid layer is placed only at bottom plate.

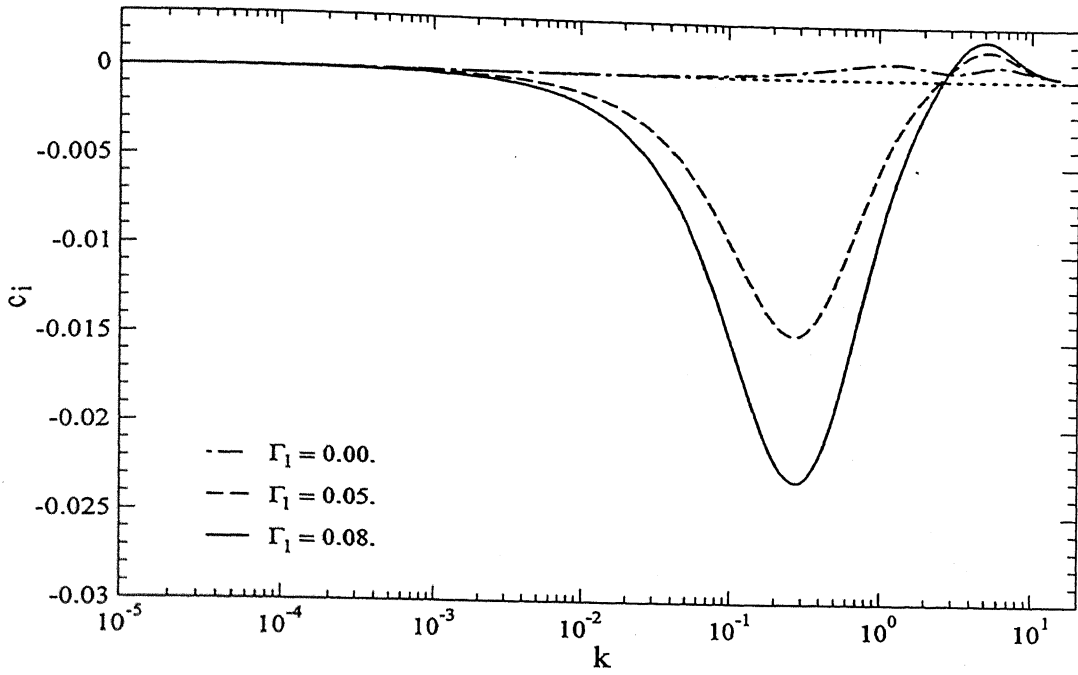


(a) $\beta = 0.4, \mu_r = 0.25, \Gamma_2 = 0.05, Re = 1.5, \Sigma = 0, \Gamma_1 = 0, H_1 = 0$.

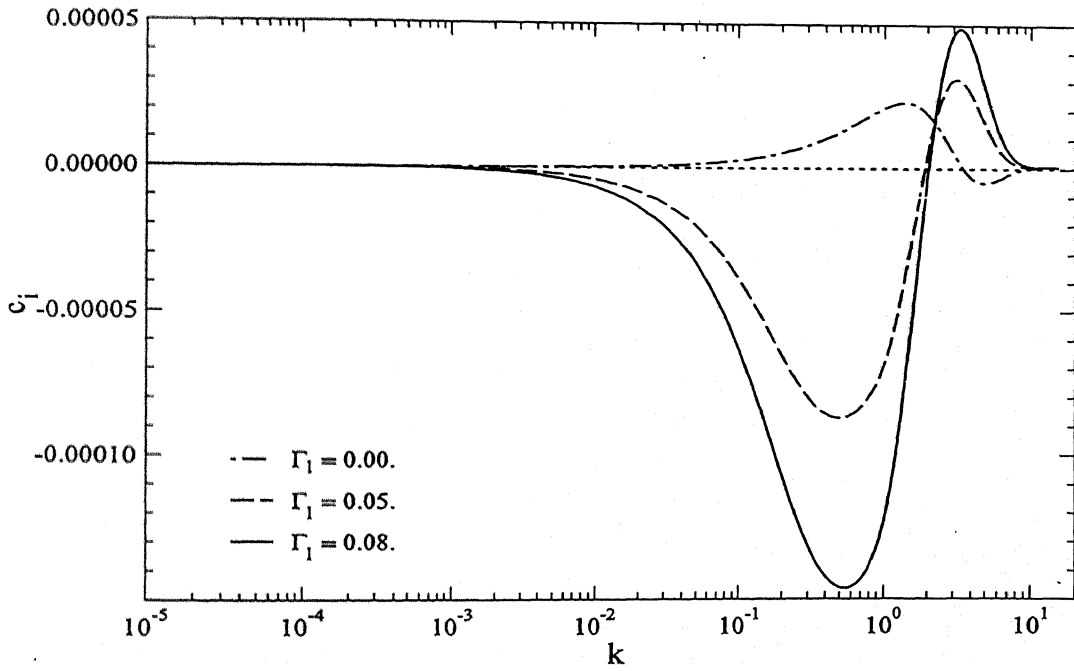


(b) $\beta = 0.6, \mu_r = 2, \Gamma_2 = 0.08, Re = 1.5, \Sigma = 0, \Gamma_1 = 0, H_1 = 0$.

Figure 3.6 Effect of solid layer deformability on fluid-fluid interfacial mode: variation of c_i with k for different values of thickness H_2 when the solid layer is placed only at top plate.

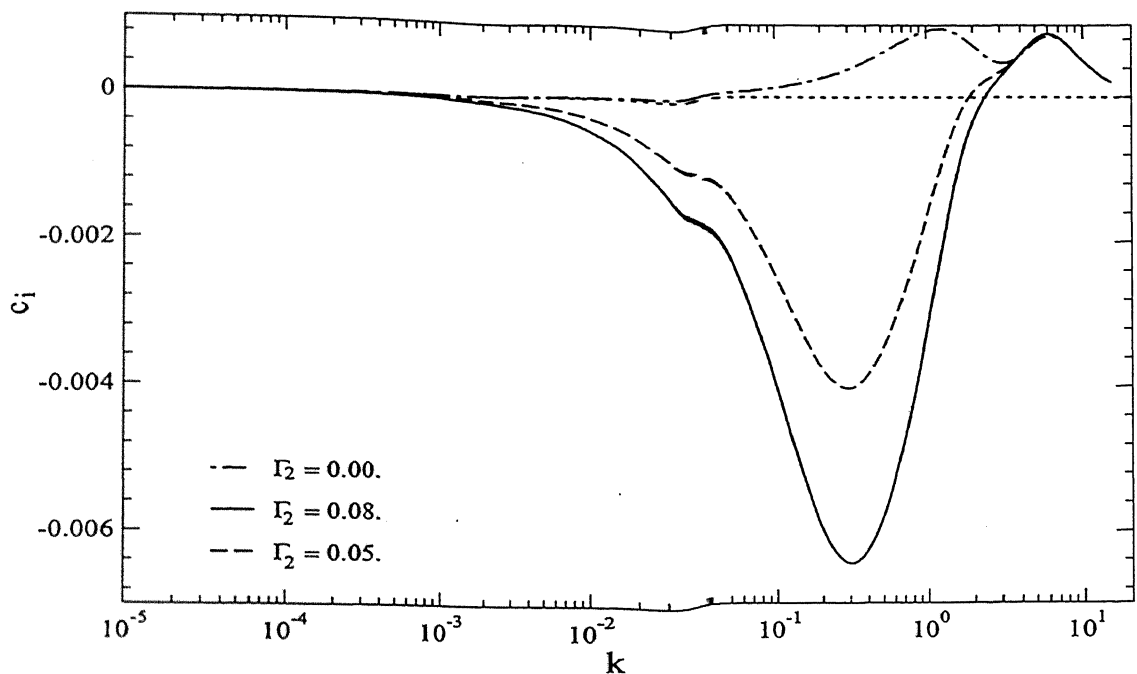


(a) $\beta = 0.4, \mu_r = 0.25, H_1 = 2.5, Re = 1.5, \Sigma = 0, \Gamma_2 = 0, H_2 = 0$.

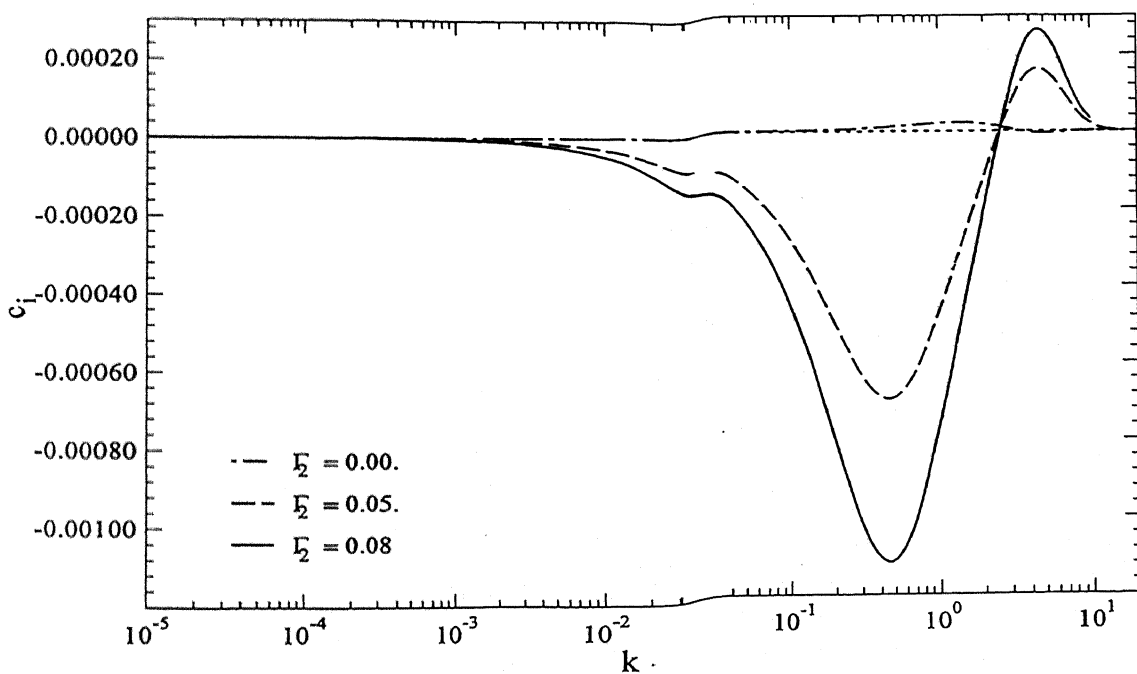


(b) $\beta = 0.6, \mu_r = 2, H_1 = 2.0, Re = 1.5, \Sigma = 0, \Gamma_2 = 0, H_2 = 0$.

Figure 3.7 Effect of solid layer deformability on fluid-fluid interfacial mode: variation of c_i with k for different values of parameter Γ_1 when the solid layer is placed only at bottom plate.

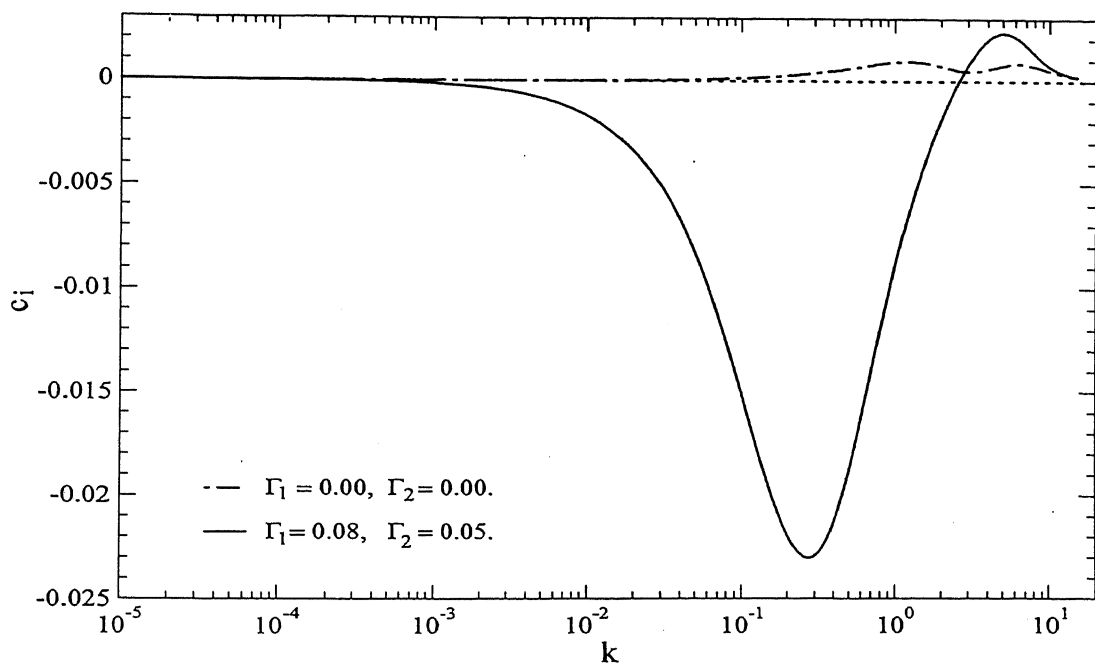


(a) $\beta = 0.4, \mu_r = 0.25, H_2 = 2.5, Re = 1.5, \Sigma = 0, \Gamma_1 = 0, H_1 = 0$.

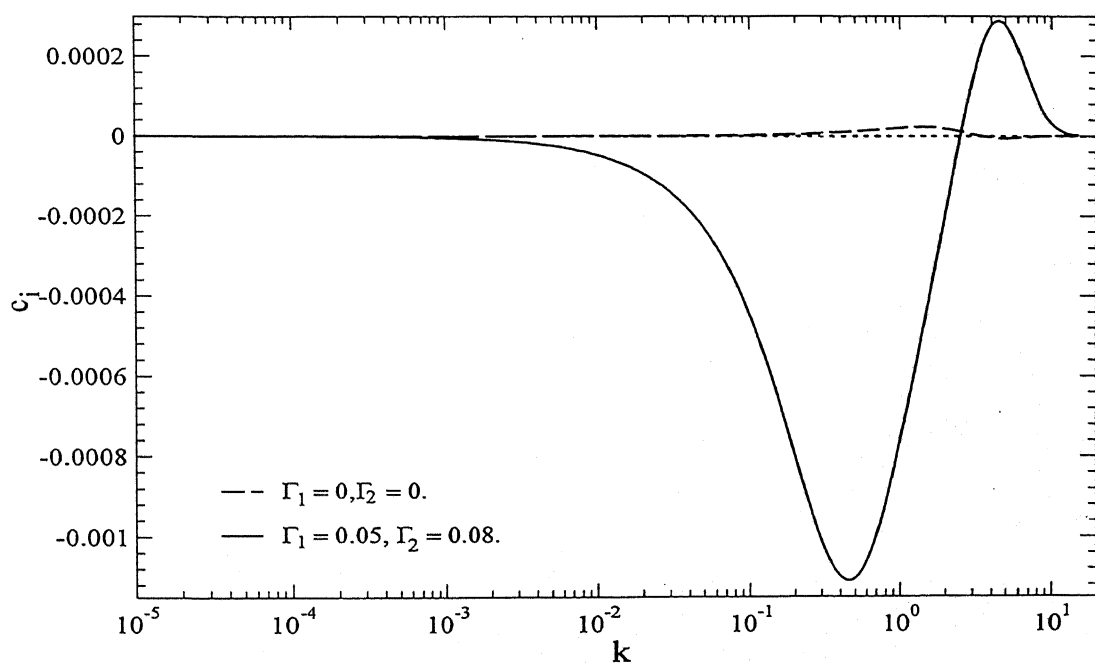


(b) $\beta = 0.6, \mu_r = 2, H_2 = 1.5, Re = 1.5, \Sigma = 0, \Gamma_1 = 0, H_1 = 0$.

Figure 3.8 Effect of solid layer deformability on fluid-fluid interfacial mode: variation of c_i with k for different values of thickness Γ_2 when the solid layer is placed only at top plate.

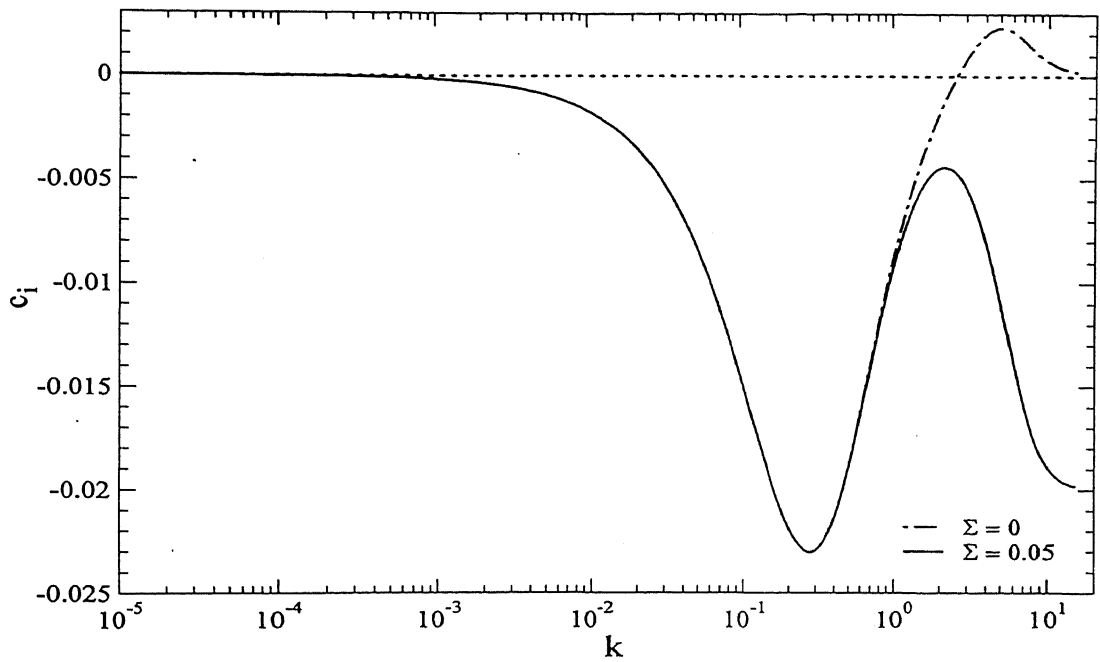


(a) $\beta = 0.4, \mu_r = 0.25, H_1 = 2.5, H_2 = 0.5, Re = 1.5, \Sigma = 0, \eta_r^{(1)} = 0, \eta_r^{(2)} = 0.$

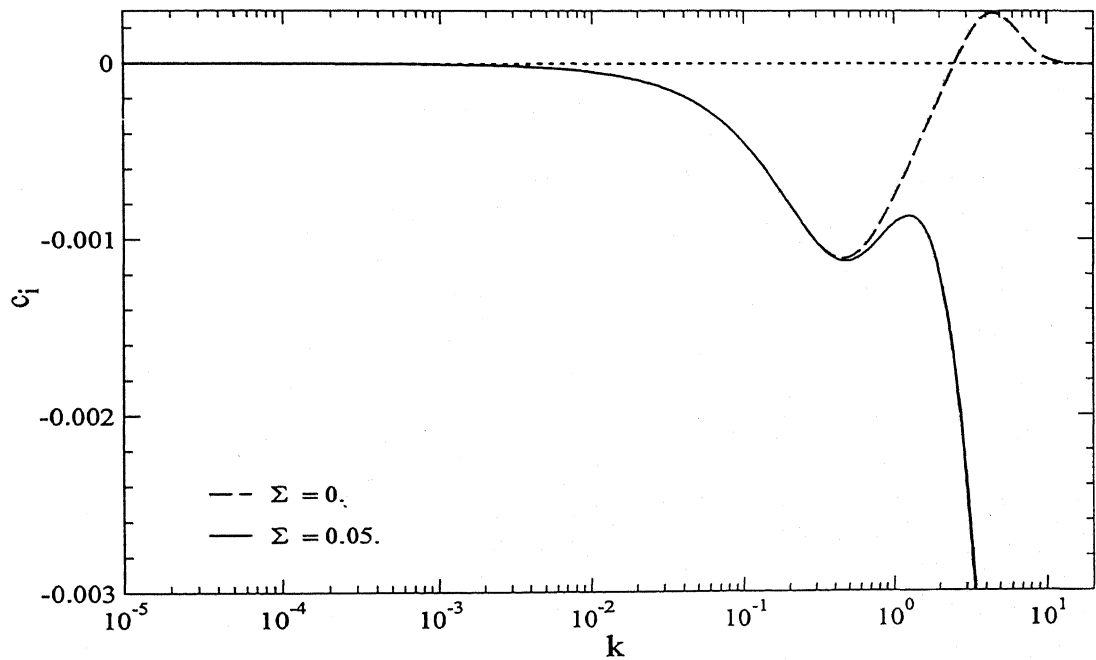


(b) $\beta = 0.6, \mu_r = 2, H_1 = 1.1, H_2 = 1.5, Re = 1.5, \Sigma = 0, \eta_r^{(1)} = 0, \eta_r^{(2)} = 0.$

Figure 3.9 Effect of solid layer deformability on fluid-fluid interfacial mode: variation of c_i with k when the solid layer is placed at both plates.

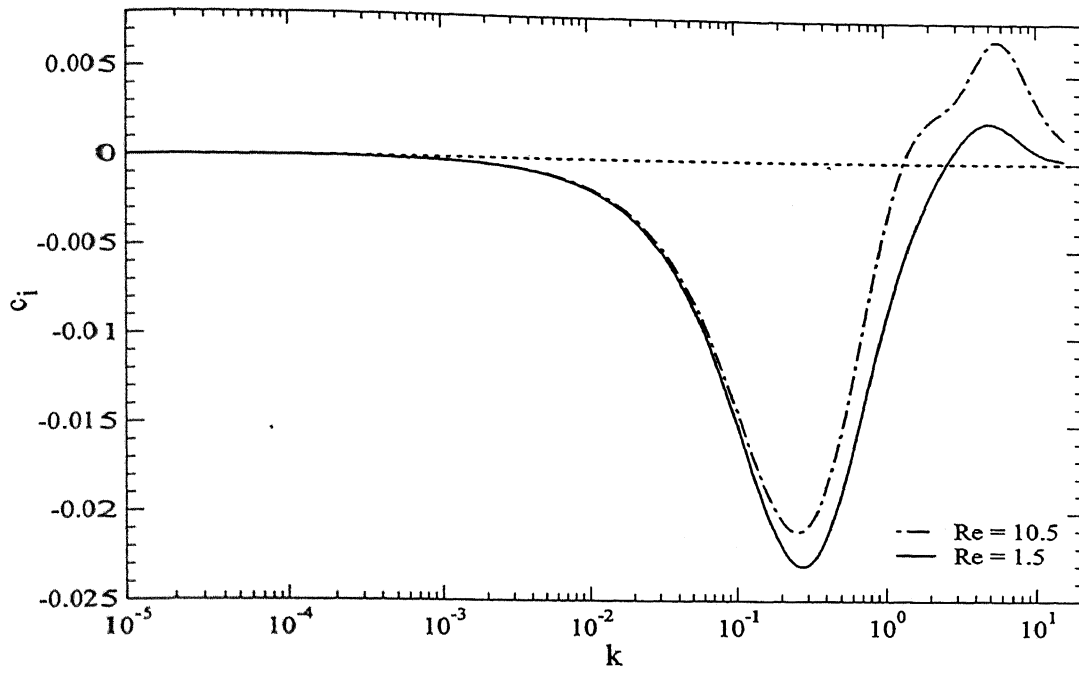


(a) $\beta = 0.4, \mu_r = 0.25, H_1 = 2.5, \Gamma_1 = 0.08, H_2 = 0.5, \Gamma_2 = 0.05, Re = 1.5, \eta_r^{(1)} = 0, \eta_r^{(2)} = 0$.

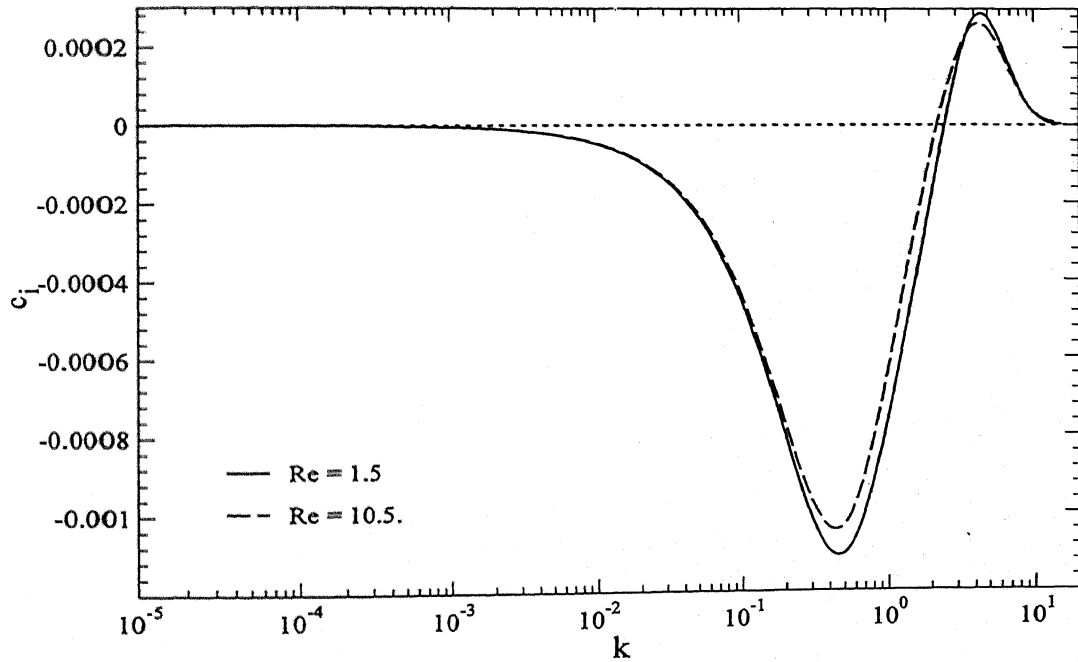


(b) $\beta = 0.6, \mu_r = 2, H_1 = 1.1, H_2 = 1.5, \Gamma_1 = 0.05, \Gamma_2 = 0.08, Re = 1.5, \eta_r^{(1)} = 0, \eta_r^{(2)} = 0$.

Figure 3.10 Effect of interfacial tension when solid layers are placed on both the plates.

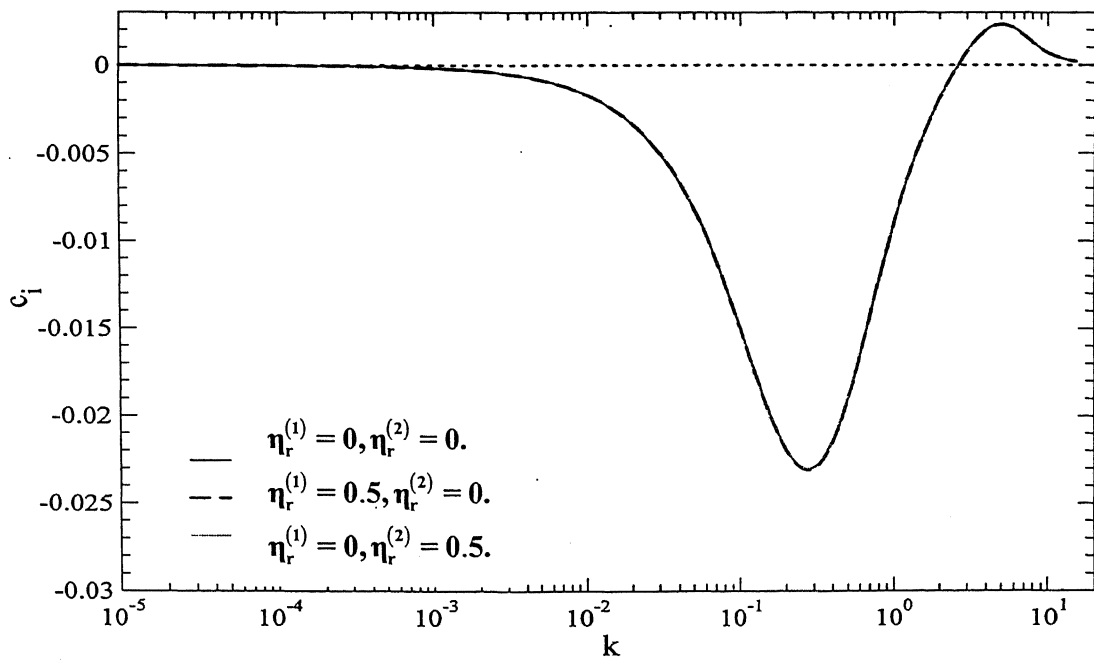


(a) $\beta = 0.4, \mu_r = 0.25, H_1 = 2.5, \Gamma_1 = 0.08, H_2 = 0.5, \Gamma_2 = 0.05, \Sigma = 0, \eta_r^{(1)} = 0, \eta_r^{(2)} = 0$.

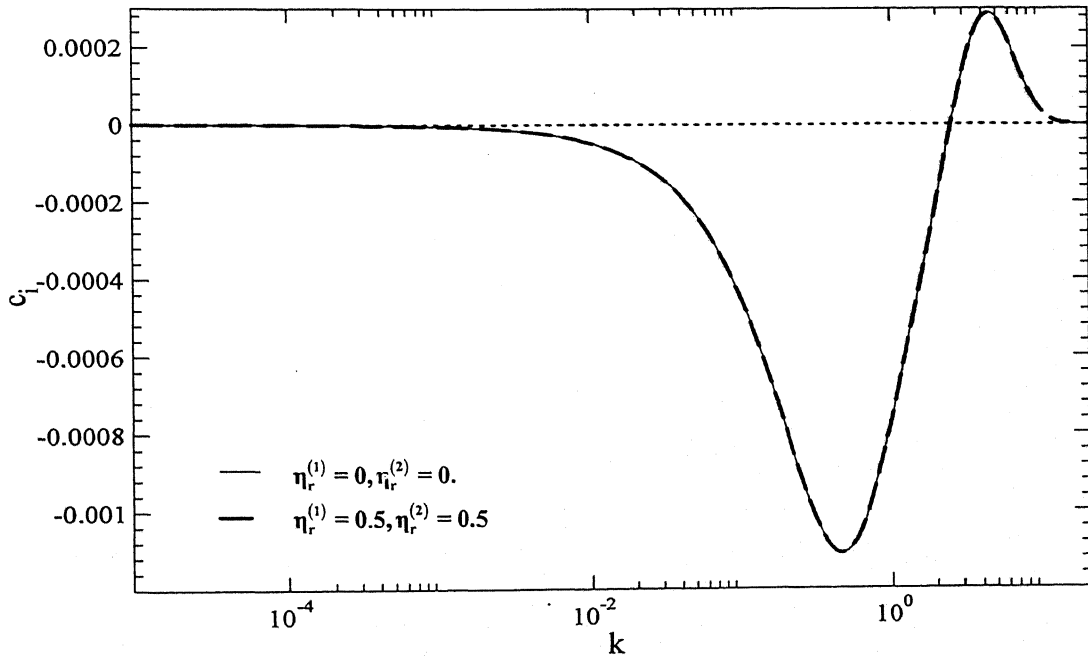


(b) $\beta = 0.6, \mu_r = 2, H_1 = 1.1, H_2 = 1.5, \Gamma_1 = 0.05, \Gamma_2 = 0.08, \Sigma = 0, \eta_r^{(1)} = 0, \eta_r^{(2)} = 0$.

Figure 3.11 Effect of Reynolds number when solid layers are placed on both the plates.

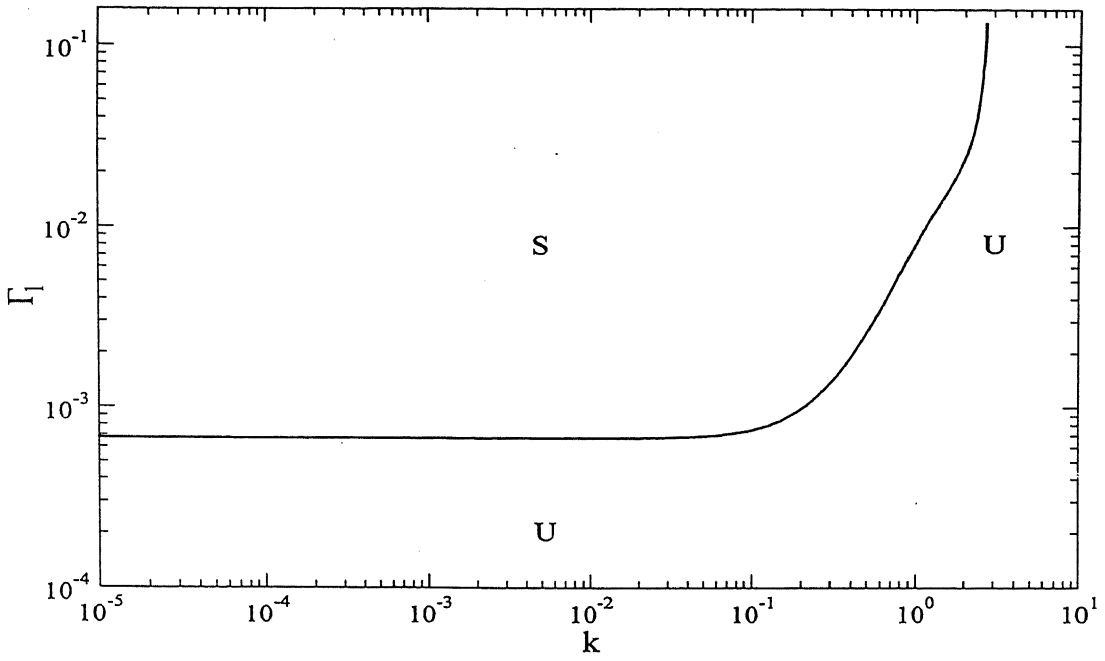


(a) $\beta = 0.4, \mu_r = 0.25, H_1 = 2.5, \Gamma_1 = 0.08, H_2 = 0.5, \Gamma_2 = 0.05, Re = 1.5, \Sigma = 0$.

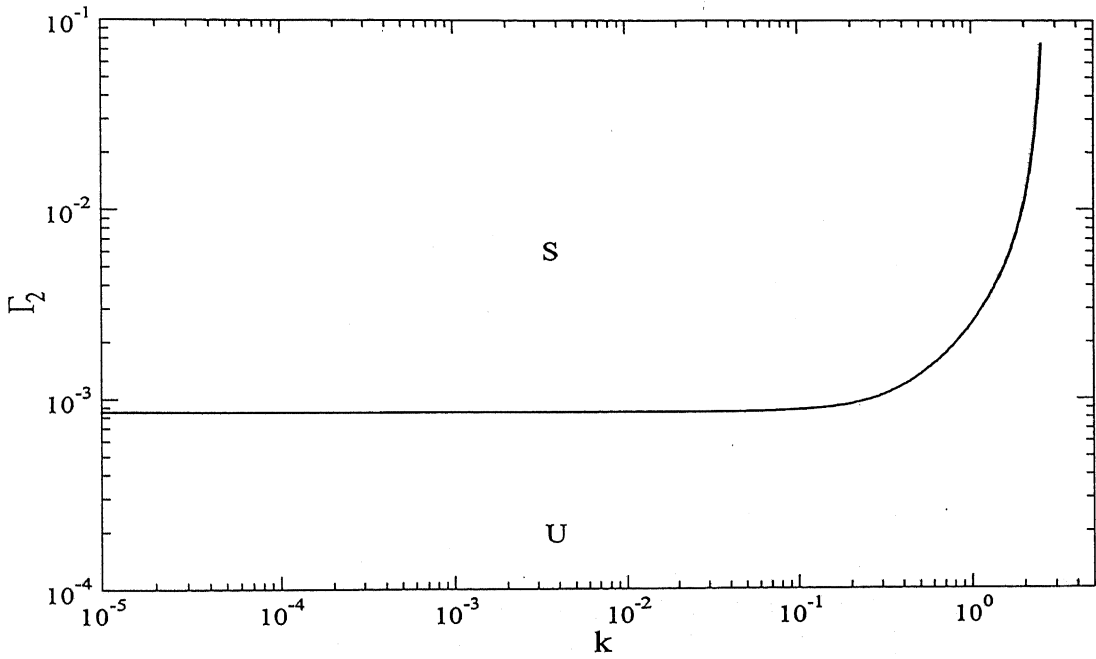


(b) $\beta = 0.6, \mu_r = 2, H_1 = 1.1, H_2 = 1.5, \Gamma_1 = 0.05, \Gamma_2 = 0.08, Re = 1.5, \Sigma = 0$.

Figure 3.12 Effect of viscosity of solid layers when solid layers are placed on both the plates.

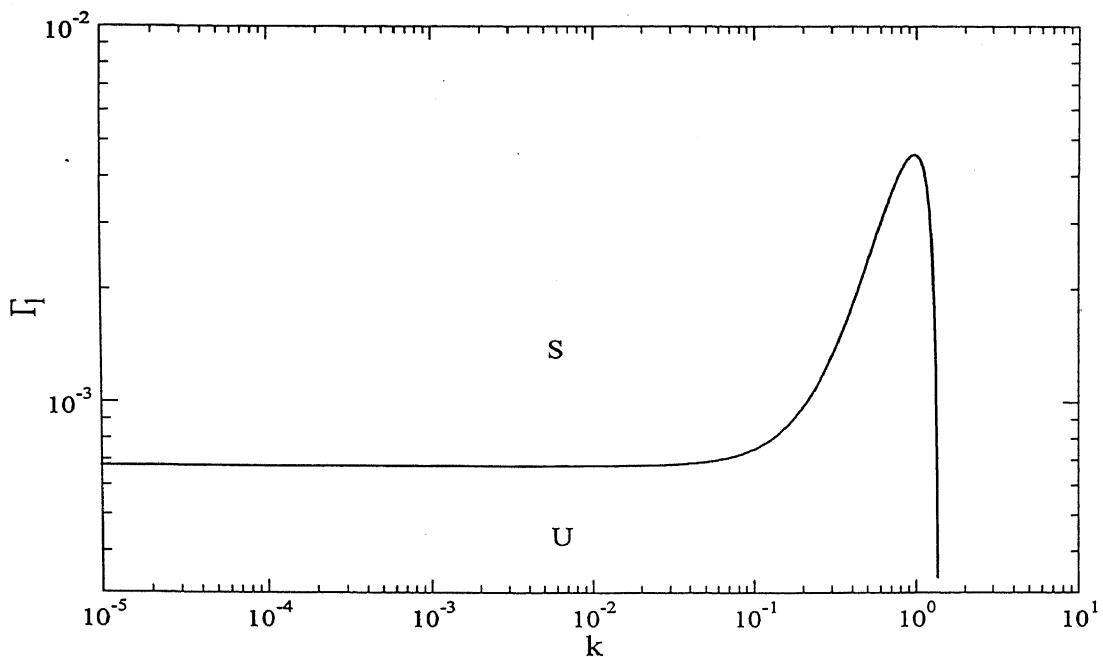


(a) $\beta = 0.4, \mu_r = 0.25, H_1 = 2.5, H_2 = 0.5, \Gamma_2 = 0.05, \text{Re} = 1.5, \Sigma = 0, \eta_r^{(1)} = 0, \eta_r^{(2)} = 0$.

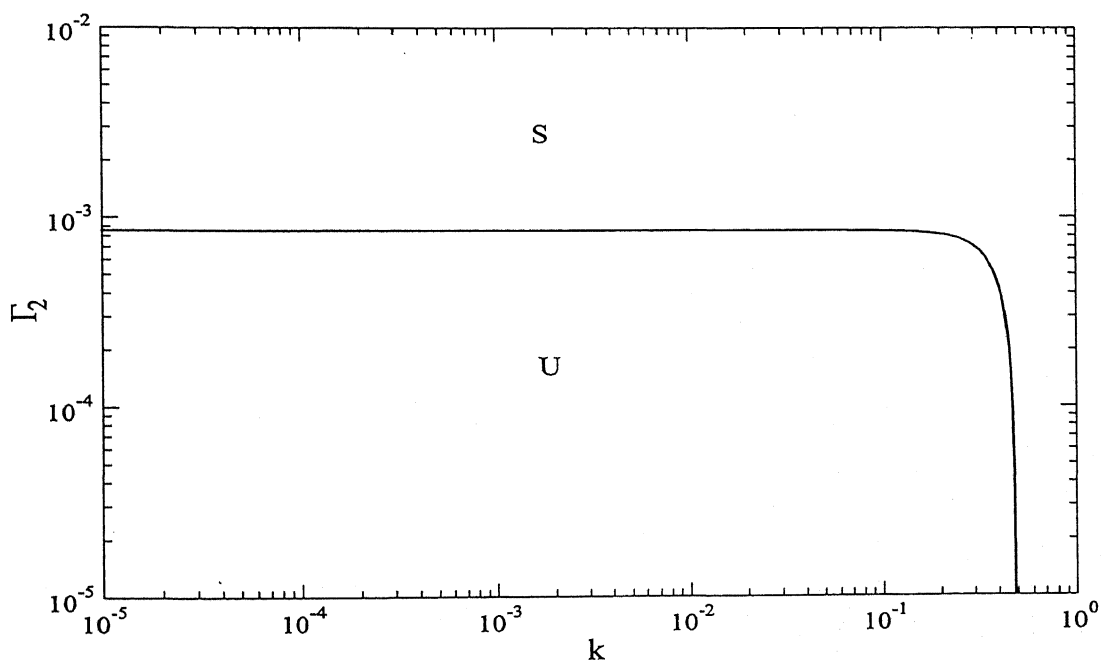


(b) $\beta = 0.6, \mu_r = 2, H_1 = 1.1, H_2 = 1.5, \Gamma_1 = 0.05, \text{Re} = 1.5, \Sigma = 0, \eta_r^{(1)} = 0, \eta_r^{(2)} = 0$.

Figure 3.13 Neutral stability curves for fluid-fluid interfacial mode: variation of Γ with k . Stable region is denoted by S, unstable region by U.

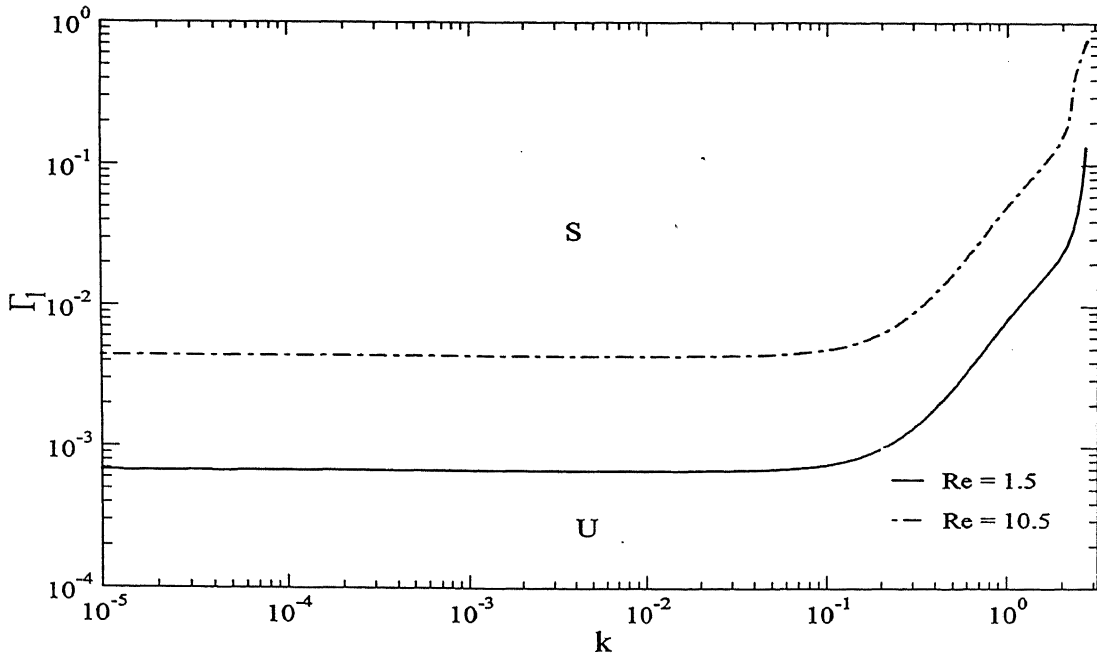


(a) $\beta = 0.4, \mu_r = 0.25, H_1 = 2.5, H_2 = 0.5, \Gamma_2 = 0.05, \text{Re} = 1.5, \Sigma = 0.05, \eta_r^{(1)} = 0, \eta_r^{(2)} = 0$.

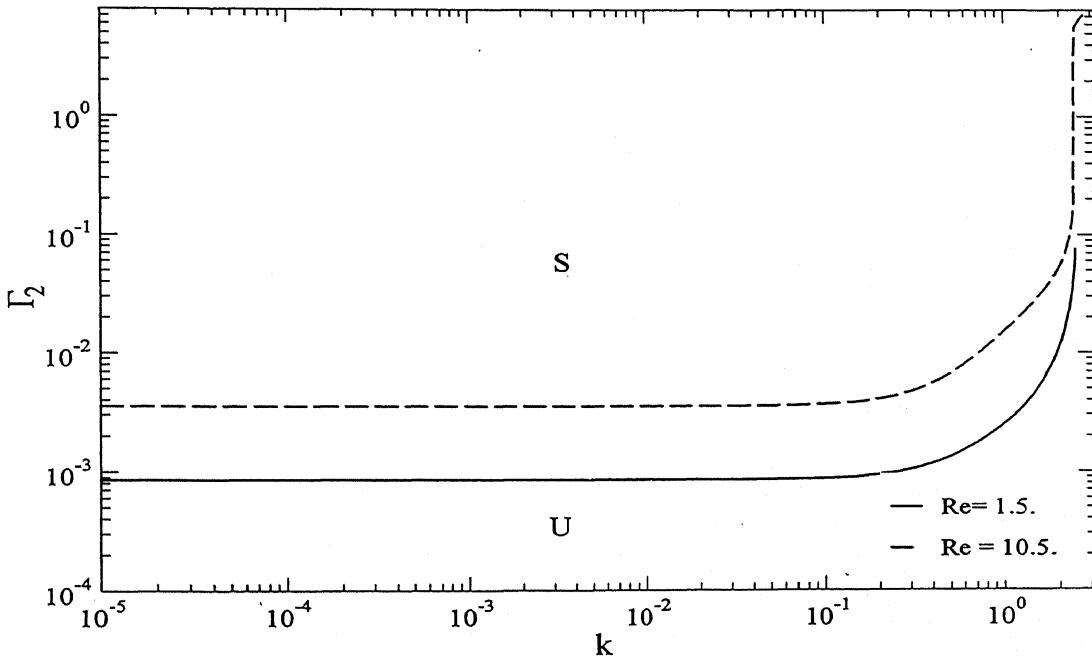


(b) $\beta = 0.6, \mu_r = 2, H_1 = 1.1, H_2 = 1.5, \Gamma_1 = 0.05, \text{Re} = 1.5, \Sigma = 0.05, \eta_r^{(1)} = 0, \eta_r^{(2)} = 0$.

Figure 3.14 Effect of interfacial tension on neutral stability curves for fluid-fluid interfacial mode: variation of Γ with k . Stable regions is denoted by S, unstable region by U.



(a) $\beta = 0.4, \mu_r = 0.25, H_1 = 2.5, H_2 = 0.5, \Gamma_2 = 0.05, \Sigma = 0, \eta_r^{(1)} = 0, \eta_r^{(2)} = 0$.



(b) $\beta = 0.6, \mu_r = 2, H_1 = 1.1, H_2 = 1.5, \Gamma_1 = 0.05, \Sigma = 0, \eta_r^{(1)} = 0, \eta_r^{(2)} = 0$.

Figure 3.15 Effect of Reynolds number on neutral stability curves for fluid-fluid interfacial mode: variation of Γ with k . Stable regions is denoted by S, unstable region by U.

Chapter 4

Conclusion and Scope for Future Work

A linear stability analysis of single layer and two-layer flow of Newtonian fluid to two-dimensional perturbations has been conducted. The numerical solutions are computed for a wide range of wavenumber with the help of the initial guess from solutions of low wavenumber asymptotic analysis.

The present study concerning the stability of gravity flow of a Newtonian fluid past a soft solid layer which is fixed onto a inclined plane shows that solid layer has a profound effect on the free surface flow instability. The soft solid layer has a stabilizing effect in the low wavenumber limit while it is destabilizing at finite- k when the solid layer is sufficiently soft. Disturbances at large- k are stable regardless of soft solid layer coating. In the case of two-layer plane Poiseuille flow soft solid layer has a stabilizing effect when the rigid-walled channel exhibits the interfacial instability.

In the present work we have considered the stability of Newtonian fluids. However in practical application, we may encounter the non-Newtonian fluids as well. For example, many biological fluids, fluids in industrial applications etc are viscoelastic. In this study we have considered single layer and two-layer of fluids but industries may deal with multilayer flow like in manufacturing of plastic films, manufacturing of photographic films, multilayer extrusion, multilayer coatings etc. In all these applications interfacial instabilities are detrimental to product quality. Since soft solid layer has stabilizing effect on two-layer interfacial instability, it is instructive to perform the same

analysis for multilayer non-Newtonian fluids in order to extend the present results to more realistic system.

References

- [1] Benjamin T. B., "Waves formation of laminar flow down an inclined plane," *J. Fluid Mech.* **554**, 505 (1957).
- [2] Chao-Tsai Huang and Bamin Khomami "The instability mechanism of single and multilayer Newtonian and viscoelastic flows down an inclined plane," *Rheologica Acta* **40**, 467 (2001).
- [3] Drazin P. G., Introduction to Hydrodynamic Stability (*Cambridge University Press, Cambridge*, 2002).
- [4] Joseph D. and Renardy Y., Fundamentals of Two-Fluid Dynamics: Part 1, Mathematical theory and applications, (*Springer-Verlag, New York*, 1993).
- [5] Kumaran V., Fredrickson G. H., and Pincus P., "Flow induced instability of the interface between a fluid and a gel at low Reynolds number," *J. Phys. II* **4**, 893 (1994).
- [6] Kumaran V. and Muralikrishnan R., "Spontaneous growth of fluctuations in the viscous flow of a fluid past a soft interface," *Phys. Rev. Lett* **84**, 3310 (2000).
- [7] Lin S. P., Chen J. N., and Woods D. R. "Suppression of instability in a liquid film flow," *Phys. Fluids* **8** (12), 3247 (1996).
- [8] Lin S. P. and Jiang W. Y., "Enhancement or suppression of instability in a two-layered liquid film flow," *Phys. Fluids* **17**, 54105 (2005).
- [9] Muralikrishnan R. and Kumaran V., "Experimental study of the instability of viscous flow past a flexible surface," *Phys. Fluids* **14**, 775 (2002).

- [10] Papanastasiou T.C., Anturkar N.R., Wilkes J.O., "Linear stability analysis of multilayer plane Poiseuille flow," *Phys. Fluids* **2**, 530 (1990).
- [11] Pinarbasi A., "Interface stabilization in two-layer channel flow by surface heating or cooling," *European Journal of Mechanics B/Fluids* **21**, 225 (2002).
- [12] Shankar V., (2005), *Personal communication*.
- [13] Shankar V. and Kumar L., "Stability of two-layer Newtonian plane Couette flow past a deformable solid layer," *Phys Fluids* **16**, 4426 (2004)
- [14] Srivatsan L. and Kumaran V., "Flow induced instability of the interface between a fluid and a gel," *J. Phys. II (France)* **7**, 947, (1997).
- [15] Weinstein S. J. and Kurz M. R., "Long-wavelength instabilities in three-layer flow down an incline," *Phys. Fluids A* **3**, 2680 (1991).
- [16] Yiantsios S. G. and Higgins B. G. "Linear stability of plane Poiseuille flow of two superposed fluids," *Phys Fluids* **31**, 3225 (1988).
- [17] Yih C. S., "Instability due to viscosity stratification," *J. Fluid Mech.* **27**, 337 (1967).
- [18] Yih C. S., "Stability of liquid flow down an inclined plane," *Phys Fluids* **6**, 321 (1963).